

Copyright  
by  
Randy Michael Drevland  
2009

**The Dissertation Committee for Randy Michael Drevland Certifies that this is the  
approved version of the following dissertation:**

**Coenzyme B, Amino Acid, and Iron-Sulfur Cluster Biosynthesis in  
Methanogenic Archaea**

**Committee:**

---

David E. Graham, Supervisor

---

Walter L. Fast

---

Kenneth A. Johnson

---

Hung-wen Liu

---

Jon D. Robertus

**Coenzyme B, Amino Acid, and Iron-Sulfur Cluster Biosynthesis in  
Methanogenic Archaea**

**by**

**Randy Michael Drevland, B.S.**

**Dissertation**

Presented to the Faculty of the Graduate School of

The University of Texas at Austin

in Partial Fulfillment

of the Requirements

for the Degree of

**Doctor of Philosophy**

**The University of Texas at Austin**

**August, 2009**

## **Dedication**

To Ellie

## **Acknowledgements**

I would like to thank the following: Dr. David Graham, for his guidance and support throughout my graduate career; my family, for supporting my educational pursuits; my father, for providing a comforting voice during times of stress as well as financial backing in times of need; my Nan, whose Sunday night phone calls I always looked forward to; Lisa Alexander, for her love, support, and afternoon coffee breaks; Eric Ritschdorff, for his friendship, good times, paying half of the rent, and upgrades; Dr. Brett Spain, for the roadtrip, Dunkin donuts, wings, and Honey Brown; Tom Curtin, for a long friendship based on childish humor; Cody Rotwein, for his love, support, and friendship; Luz Carrillo, for helping out with my qualifiers and teaching me Spanish; Lakshmi Krishnamoorthy, for helping out with my qualifiers and for her ability to take a joke; the Marist College Department of Science faculty, for providing an extraordinary learning experience and for their continued support; Seema Namboori, Dr. Teresa Giles, Conor Smith, Nikolaos Simeon, Rachel Wolf, and Stephanie Taylor, for making lab life more enjoyable; my Ellie, whose life meant more to me than I can express in words.

# **Coenzyme B, Amino Acid, and Iron-Sulfur Cluster Biosynthesis in Methanogenic Archaea**

Publication No. \_\_\_\_\_

Randy Michael Drevland, Ph.D  
The University of Texas at Austin, 2009

Supervisor: David E. Graham

Methane is a greenhouse gas and a major contributor to climate change. Methanogenic Archaea produce more than 1 billion tons of this gas each year through methanogenesis, the anaerobic reduction of CO<sub>2</sub> to methane. Coenzyme B (CoB) is one of eight coenzymes required for methanogenesis and it is unique to methanogens. Therefore, this coenzyme is a potential target for inhibiting methanogenesis. To further elucidate the CoB biosynthetic pathway, genes from *Methanocaldococcus jannaschii* were cloned and expressed in an effort to identify the CoB homoaconitase. From this study, the MJ0499-MJ1277 pair of proteins was identified as the methanogen isopropylmalate isomerase involved in leucine and isoleucine biosynthesis. The MJ1003-MJ1271 pair of proteins was characterized as the homoaconitase required for CoB biosynthesis. This enzyme exhibited broad substrate specificity, catalyzing the isomerization of *cis*-unsaturated tri-carboxylates with  $\gamma$ -chains of 1-5 methylenes in length. Previously characterized homoaconitases only catalyzed half of the predicted reactions in the isomerization of homocitrate. The MJ1003-MJ1271 proteins function as

the first homoaconitase described to catalyze the full isomerization of homocitrate to homoisocitrate. Also, the CoB homoaconitase was identified as specific for (*R*)-homocitrate and *cis*-unsaturated intermediates, contrary to a previous study that suggested the substrate specificity of this enzyme included (*S*)-homocitrate and *trans*-homoaconitate. The *M. jannaschii* isopropylmalate isomerase and homoaconitase share more than 50% sequence identity and catalyze analogous reactions. Site directed mutagenesis of the MJ1271 protein was used to identify residues involved in substrate specificity. Arg26 of MJ1271 was critical for the specificity of the CoB homoaconitase. Mutation of this residue to the analogous residue in the *M. jannaschii* isopropylmalate isomerase, Val28, altered the substrate specificity of the homoaconitase to include the substrates of isopropylmalate isomerase. These homologs of aconitase require a [4Fe-4S] cluster for coordinating their respective substrates at the enzyme active site. However, methanogens lack most of the proteins required for iron-sulfur cluster assembly. Therefore, genes homologous to the *Salmonella enterica* ApbC iron-sulfur scaffold protein were characterized from methanogens. The MMP0704, MJ0283, and SSO0460 proteins from *Methanococcus maripaludis*, *M. jannaschii*, and *Solfolobus solfataricus*, respectively, were identified as scaffold proteins involved in methanogen iron-sulfur cluster biosynthesis.

## Table of Contents

List of Tables.....	xii
List of Figures .....	xiii
Chapter 1 Introduction.....	1
1.1. Methane as a greenhouse gas and biofuel .....	1
1.2. Methanogenesis.....	3
1.3. Coenzyme B.....	7
1.3.1. Identification and Structure .....	7
1.3.2. CoB in the mechanism of methyl-coenzyme M reductase.....	8
1.3.3. Elucidation of the biosynthetic pathway .....	13
1.3.4. 2-Oxoacid chain elongation pathway .....	17
1.4. Identification of methanogen homoaconitase, isopropylmalate isomerase, and proteins involved in iron-sulfur cluster biosynthesis..	20
1.4.1. The genome sequence of <i>M. jannaschii</i> .....	20
1.4.2. MJ0499-MJ1277 functions as the <i>M. jannaschii</i> IPMI .....	23
1.4.3. MJ1003-MJ1271 functions as the <i>M. jannaschii</i> HACN .....	23
1.4.4. Structure and function of MJ1271 and MJ1277 .....	24
1.4.5. Archaeal iron-sulfur cluster biosynthesis .....	24
Chapter 2 Isoleucine and leucine biosynthesis-isopropylmalate isomerase.....	41
2.1. Introduction.....	25
2.2. Materials and methods.....	25
2.2.1. Chemicals.....	32
2.2.2. Cloning of MJ0499-MJ1277, MJ1003-MJ1277, and MJ0720..	32
2.2.3. Protein expression and purification .....	35
2.2.4. Protein purification.....	35
2.2.5. Analytical size exclusion chromatography .....	37
2.2.6. Reconstitution of Fe-S centers .....	37
2.2.7. Measurement of hydrolyase activities .....	37



2.2.8. Measurement of oxidative decarboxylation activities .....	38
2.2.9. Coupled assay of dehydratase activity .....	39
2.2.10. Identification of dehydratase reaction products .....	39
2.2.11. Stereochemical analysis of malate product .....	41
2.3 Results .....	42
2.3.1. Protein expression, purification, and subunit interaction .....	42
2.3.2. Reconstitution of iron-sulfur clusters .....	46
2.3.3. Identification of the citramalate/isopropylmalate isomerase .....	46
2.3.4. Characterizing isopropylmalate/ $\beta$ -methylmalate dehydrogenase .....	50
2.3.5. Coupled assay for $\beta$ -methylmalate oxidative decarboxylation. ....	53
2.4. Discussion .....	58
Chapter 3 Enzymology of the <i>M. jannaschii</i> homoaconitase involved in coenzyme B biosynthesis .....	61
3.1. Introduction .....	61
3.2. Materials and methods .....	68
3.2.1. Chemicals and reagents .....	68
3.2.2. Protein expression and purification .....	68
3.2.3. Reconstitution of the iron-sulfur center .....	69
3.2.4. Determination of iron-sulfur content .....	69
3.2.5. Measurement of hydrolyase activities .....	70
3.2.6. Coupled assay of hydratase activity .....	70
3.2.7. HPLC analysis of reaction products .....	71
3.2.8. LC-MS analysis of enzyme reaction products .....	72
3.3. Results .....	73
3.3.1. Protein purification and subunit interaction .....	73
3.3.2. Hydrolyase activity of the MJ1003/MJ1271 proteins .....	76
3.3.3. Coupled activity of HACN and HICDH .....	82
3.3.4. Dehydration reaction and stereospecificity of HACN .....	87
3.3.5. Inhibitors of HACN .....	89

3.4. Discussion .....	89
Chapter 4 Crystallography and mutational analysis of the <i>Methanocaldococcus jannaschii</i> homoaconise small subunit-insight into structural determinants for substrate recognition.....	94
4.1. Introduction .....	94
4.2. Materials and Methods .....	100
4.2.1. Cloning and molecular biology .....	100
4.2.2. Protein expression and purification .....	102
4.2.3. Analytical size exclusion chromatography .....	103
4.2.4. Reconstitution of the iron-sulfur center.....	103
4.2.5. Measurement of hydrolyase activities .....	103
4.2.6. Homology modeling and structure representation.....	103
4.3. Results .....	104
4.3.1. Structure of MJ1277 homology model .....	104
4.3.2. Expression and subunit interaction of MJ1003 and MJ1271 variants .....	106
4.3.3. MJ1003-MJ1271 Arg26Val and Arg26Lys .....	106
4.3.4. MJ1003-MJ1271 Thr27Ala .....	108
4.3.5. MJ1003-MJ1271 Arg26Val/Thr27Tyr.....	109
4.3.6. MJ1003-MJ1271/1277 chimera .....	109
4.3.7. Loop replacement: MJ1003-MJ1271/LysU .....	110
4.4. Discussion .....	110
Chapter 5 Archaeal iron-sulfur cluster biosynthesis .....	120
5.1. Introduction .....	120
5.2. Materials and methods.....	124
5.2.1. Cloning of MJ0283 and MMP0704 .....	124
5.2.2. Protein expression and purification .....	125
5.2.3. Reconstitution of the protein iron-sulfur centers and determination of iron-sulfur content.....	125
5.2.4. Size exclusion chromatography .....	126

5.3. Results.....	126
5.3.1. Expression and purification of methanogen ApbC/Nbp35 proteins.....	126
5.3.2. Reconstitution of the protein iron-sulfur centers .....	128
5.3.3. MMP0704 proteins interact in a complex dynamic equilibrium .....	130
5.4. Discussion .....	133
Chapter 6 Summary and future directions .....	141
6.1. Overview .....	141
6.2. Methanogen leucine and isoleucine biosynthesis .....	142
6.3. Methanogen coenzyme B biosynthesis .....	143
6.4. HACN <sub>MJ</sub> and IPMI <sub>MJ</sub> structural study .....	144
6.5. Iron-sulfur cluster biosynthesis in archaea.....	146
Bibliography.....	148
Vita.....	160

## List of Tables

Table 2.1:	Oligodeoxyribonucleotide primers used for PCR .....	33
Table 2.2:	List of plasmids and microorganisms .....	34
Table 2.3:	Steady-state kinetic parameters for MJ0499-MJ1277 .....	50
Table 2.4:	Kinetic parameters for IPMDH homologs .....	53
Table 3.1:	Steady-state kinetic parameters for the direct assay of hydrolyase activity.....	80
Table 3.2:	Kinetic parameters for the coupled assay of HACN hydrolyase activity with HICDH .....	85
Table 4.1:	List of plasmids and microorganisms.....	101
Table 4.2:	Oligonucleotide primers used to construct MJ1271 mutations .....	102
Table 4.3:	Steady-state kinetic values for the MJ1003-MJ1271 variant enzymes compared to WT IPMI <sub>MJ</sub> .....	107
Table 4.4:	Steady-state kinetic values for the MJ1003-MJ1271 variant enzymes compared to WT HACN <sub>MJ</sub> .....	108
Table 5.1:	Archaeal ApbC/Npb35 homologs can function in place of <i>S. enterica</i> ApbC <i>in vivo</i> .....	135

## List of Figures

Figure 1.1: Methanogenesis.....	6
Figure 1.2: The structure of UDP-GlcNAc-ManNAcA-CoB.....	8
Figure 1.3: The active site of MCR .....	10
Figure 1.4: Proposed mechanisms for methyl-coenzyme M reductase.....	12
Figure 1.5: Proposed pathway for coenzyme B biosynthesis.....	16
Figure 1.6: Analogous chain elongation reactions.....	19
Figure 1.7: Sequence alignment of the homologous HACN/IPMI large and small subunits from <i>Methanocaldococcus jannaschii</i> .....	22
Figure 2.1: Isoleucine biosynthesis using a threonine dehydratase for the production of 2-oxobutyrate.....	26
Figure 2.2: Analogous chain elongation pathways .....	29
Figure 2.3: Sequence alignment of hydrolyase small subunits .....	31
Figure 2.4: Purified IPMDH <sub>MJ</sub> and combinations of large and small subunits of the hydrolyase apoenzymes .....	44
Figure 2.5: MJ0499-MJ1277 and MJ1003-MJ1277 subunit interaction .....	45
Figure 2.6: Representative of the steady-state kinetics of MJ0499-MJ1277 .....	48
Figure 2.7: Representative of the steady-state kinetics of MJ0720 .....	52
Figure 2.8: MJ0499-MJ1277 and IPMI <sub>MJ</sub> coupled assay optimization: MgCl <sub>2</sub> and KCl .....	55
Figure 2.9: MJ0499-MJ1277 and IPMI <sub>MJ</sub> coupled assay optimization: buffer, pH, and temperature.....	56
Figure 2.10: Representative of the steady-state kinetics of MJ0499-MJ1277 and IPMDH <sub>MJ</sub> .....	57

Figure 3.1: Initially proposed 2-oxoacid chain elongation pathway for coenzyme B biosynthesis .....	63
Figure 3.2: Reactions involved in lysine biosynthesis and propionate metabolism .....	66
Figure 3.3: Purified HACN <sub>MJ</sub> .....	74
Figure 3.4: MJ1003-MJ1271 subunit interaction.....	75
Figure 3.5: MJ1003-MJ1271 direct assay optimization.....	77
Figure 3.6: Steady-state kinetics of MJ1003-MJ1271 .....	79
Figure 3.7: HACN catalyzed the hydration of cis-unsaturated tricarboxylic acids to produce hydroxyacids.....	81
Figure 3.8: MJ1003-MJ1271 and HICDH <sub>MJ</sub> coupled assay optimization.....	83
Figure 3.9: Steady-state kinetics of the MJ1003-MJ1271 and HICDH <sub>MJ</sub> .....	84
Figure 3.10: HACN and HICDH hydrated <i>cis</i> -homoaconitate analogs and catalyzed their oxidative decarboxylation to prouce the corresponding 2-oxoacids .....	86
Figure 3.11: Homoaconitase and homoisocitrate dehydrogenase specifically converted ( <i>R</i> )-homocitrate to 2-oxoadipate in a coupled reaction. ...	88
Figure 3.12: The proposed 2-oxoacid chain elongation pathway for methanogen coenzyme B biosynthesis.....	92
Figure 4.1: Reactions catalyzed by members of the aconitase superfamily.....	95
Figure 4.2: A multiple sequence alignment of proteins homologous to the <i>Methanocaldococcus jannaschii</i> HACN small subunit, MJ1271, using the ClustalW program (version 1.83) .....	98
Figure 4.3: Homology model of the <i>M. jannaschii</i> small subunit, MJ1277 .....	105

Figure 4.4: Structure of the <i>M. jannaschii</i> HACN small subunit, MJ1271 (PDB 2PKP).....	112
Figure 4.5: Structural alignment of the mACN domain 4 (blue; PDB1 AMJ) and <i>M. jannaschii</i> HACN small subunit, MJ1271 (green; 2PKP) .	113
Figure 4.6: Structural alignment of MJ1271 (PDB 2PKP) with domain 4 of mACN in the relaxed (PDB 1AMI) and tense states (PDB 1AMJ) .....	115
Figure 4.7: Structural alignment of the MJ1271 loop regions proposed to function in substrate specificity and catalysis with the corresponding loop regions of mACN .....	117
Figure 5.1: A protein sequence alignment of bacterial, archaeal, and eukaryotic ApbC/Npb35 homologs was constructed using the ClustalW program (version 1.83).....	123
Figure 5.2: Sodium dodecyl sulfate-polyacrylamide gel electrophoresis analysis of an overloaded, Coomassie blue-stained gel shows the purities and solubilities of heterologously expressed MMP0704 and MJ0283 proteins (10 µg each).....	127
Figure 5.3: UV-visible absorption spectra of reconstituted MMP0704-His <sub>6</sub> and MMP0704(20-289)-His <sub>6</sub> holoproteins.....	129
Figure 5.4: Analytical size exclusion chromatography of the MMP0704(20-289)-His <sub>6</sub> protein .....	131
Figure 5.5: Analytical size exclusion chromatography of the MMP0704-His <sub>6</sub> protein .....	132
Figure 5.6: Model for iron-sulfur cluster biosynthesis in <i>M. jannaschii</i> with MJ0283 .....	139

Figure 5.7: Model for iron-sulfur cluster biosynthesis in <i>M. jannaschii</i> with MJ0283 and MJ0034-MJ0035.....	140
--	-----



## **Chapter 1: Introduction**

Each year the energy metabolism of methanogenic archaea (methanogens), known as methanogenesis, produces over one billion tons of methane, approximately 400 million tons of which is emitted to the atmosphere [1,2]. Methane is a potent greenhouse gas, second in abundance after CO<sub>2</sub>, and plays a significant role in the chemistry of the atmosphere [1]. Therefore, understanding the biochemical pathway of methanogenesis may play a crucial role in identifying various means for controlling atmospheric concentrations of methane.

### **1.1. METHANE AS A GREENHOUSE GAS AND BIOFUEL**

Climate change, commonly referred to as “global warming,” results from energy imbalances between the Earth and space, measured as radiative forcings (W m<sup>-2</sup>), and is the current environmental issue posing a threat to the present and future global community [3]. The current crisis involves positive radiative forcing, i.e. alterations in the chemical composition of the atmosphere that affects the loss of long wavelength radiation to space and the redistribution of energy in the atmosphere, resulting in an increase in surface temperature [3]. These positive forcings are believed to be a result of increasing concentrations of greenhouse gases (GHGs; CO<sub>2</sub>, CH<sub>4</sub>, NO<sub>2</sub>, CFCs) in the troposphere and stratosphere. Measurements from 1861 until 2001 indicate an increase in the global average surface temperature of 0.6°C ± 0.2°C and palaeoclimate studies from ice cores indicate that present day levels of CO<sub>2</sub> are at concentrations that have not been exceeded in at least 450,000 years [3]. The growing consensus attributes at least part of

the climate change to increasing emissions of GHGs from the industrialized global community, most notably fossil fuel combustion and deforestation. Therefore, the positive radiative forcings are anthropogenic.

Methane plays a significant role in atmospheric chemistry. Increasing methane concentrations result in a reduction in the oxidative capacity of the troposphere by consuming hydroxyl radicals (a major sink for methane), sequestering  $\text{Cl}^\cdot$ , influencing stratospheric  $\text{H}_2\text{O}$ , affecting stratospheric and tropospheric ozone levels, as well as producing  $\text{CO}_2$ ,  $\text{CO}$ , and  $\text{H}_2$  [4]. Although controlling  $\text{CO}_2$  emissions is at the forefront of the climate change debate, due to its high positive forcing ( $1.4 \pm 0.2 \text{ W m}^{-2}$ ), concerted reduction of non- $\text{CO}_2$  GHGs, such as methane ( $0.7 \pm 0.2 \text{ W m}^{-2}$ ; lifetime of 8 years), is predicted to be a realistic and necessary measure in preventing near-term anthropogenic influence on the atmosphere [2,5]. Since 1750, the atmospheric concentration of methane has increased by 151% to approximately 1800 ppb [3]. While methane growth rates have slowly decreased in the 1990's and early 2000's (the cause for this decrease is unknown although deforestation is thought to play a role) the slowing effect is not expected to be permanent [4,6]. Therefore, efforts to reduce the anthropogenic methane emissions are predicted to provide a near-term negative radiative forcing necessary to compensate for  $\text{CO}_2$  emissions as "green" technology is developed.

Although methane is a GHG, there is a growing interest in harnessing methane gas for use as a biofuel in the movement away from fossil fuels. In agricultural and industrial waste streams, sewage sludge, and landfills, organic waste is converted to  $\text{CH}_4$  and  $\text{CO}_2$  by methanogens after hydrolysis of biopolymers and acetogenesis [7,8]. The methane produced from this anaerobic biodegradation can be captured for biofuel use, limiting the amount of methane emissions from these waste streams as well as reducing our dependency on fossil fuels and therefore reducing  $\text{CO}_2$  emissions [7]. Methanogens

also play a key role, albeit a negative one, in bioethanol and biobutanol production due to substrate competition [9]. Studies indicate increases in the production of these alternative energy sources by inhibition of methanogenesis [9].

The role of methane as a GHG and potential alternative energy source makes it a prominent constituent in preventing climate change. It would be desirable to inhibit anthropogenic methane production to limit influencing changes in atmospheric composition and to stimulate methane production in bioreactors for biofuel production. The main target for each of these endeavors is methanogenesis.

## 1.2. METHANOGENESIS

Methanogens are classified as members of the kingdom Euryarchaeota in the domain Archaea. Five orders of methanogens have been identified: *Methanococcales*, *Methanopyrales*, *Methanobacteriales*, *Methanosarcinales*, and *Methanomicrobiales* [10]. Several carbon sources are used to generate methane from methanogenesis, such as CO<sub>2</sub> (with electrons from H<sub>2</sub> or formate), acetate, methanol, methylamines, and methylthiols, although substrate specificity varies among the five orders [11,12]. Methanogenesis plays a significant role in the global carbon cycle, constituting the final step in the anaerobic biodegradation of complex organic compounds. These strictly anaerobic microbes (the presence of oxygen is detrimental to their survival) have been isolated from various anoxic environments, such as wetlands, swamps, rice paddies, landfills, hydrothermal vents, and the digestive tracts of ruminants and termites [11].

Eight enzymes and six coenzymes are required for methanogenesis from CO<sub>2</sub> and H<sub>2</sub> (Figure 1.1) [10,13]. This reductive pathway ( $4\text{ H}_2 + \text{CO}_2 \rightarrow \text{CH}_4 + 2\text{ H}_2\text{O}$ ;  $\Delta G'^{\circ} = -131\text{ kJ mol}^{-1}$ ) commences with the transfer of CO<sub>2</sub> to the first C1 carrier, methanofuran [10]. Formylmethanofuran dehydrogenase (EC

1.2.99.5), a molybdenum and iron-sulfur cluster-containing enzyme, catalyzes the formylation of the methanofuran amino group, producing formylmethanofuran ( $\Delta G'^{\circ} = +16 \text{ kJ mol}^{-1}$ ) [14,15]. The electrons required for the dehydrogenation reaction are derived from a membrane bound hydrogenase that oxidizes molecular hydrogen, a reaction that translocates  $\text{Na}^+$  ions into the cytoplasm [12]. Formylmethanofuran: $\text{H}_4\text{MPT}$  formyltransferase (EC 2.3.1.101) catalyzes the subsequent transfer of the formyl group to 5,6,7,8-tetrahydromethanopterin ( $\text{H}_4\text{MPT}$ ), a homolog of tetrahydrofolate, to give formyl- $\text{H}_4\text{MPT}$  ( $\Delta G'^{\circ} = -4.4 \text{ kJ mol}^{-1}$ ) [16]. Formyl- $\text{H}_4\text{MPT}$  is cyclized to *N*5, *N*10-methenyl- $\text{H}_4\text{MPT}$  by way of methenyl- $\text{H}_4\text{MPT}$  cyclohydrolase (EC 3.5.4.27;  $\Delta G'^{\circ} = -4.6 \text{ kJ mol}^{-1}$ ), followed by two reductive steps [17]. The first reductive step is catalyzed by one of two methylene- $\text{H}_4\text{MPT}$  dehydrogenases, depending on whether hydrogen is limiting, to produce *N*5, *N*10-methylene- $\text{H}_4\text{MPT}$  [10]. The first enzyme is an  $\text{F}_{420}$ -dependent methylene- $\text{H}_4\text{MPT}$  dehydrogenase (EC 1.5.99.9) that functions when hydrogen is limiting ( $\Delta G'^{\circ} = +5.5 \text{ kJ mol}^{-1}$ ) [18]. The coenzyme  $\text{F}_{420}$  is a deazaflavin derivative that can either accept or donate a hydride ion [13]. When hydrogen is not limiting, an  $\text{H}_2$ -dependent methylene- $\text{H}_4\text{MPT}$  dehydrogenase is responsible for reducing *N*5, *N*10-methenyl- $\text{H}_4\text{MPT}$  ( $\Delta G'^{\circ} = -5.5 \text{ kJ mol}^{-1}$ ) [19]. The subsequent reductive step is catalyzed by  $\text{F}_{420}$ -dependent methylene- $\text{H}_4\text{MPT}$  reductase (EC 1.5.99.11), producing *N*5,*N*10-methyl- $\text{H}_4\text{MPT}$  ( $\Delta G'^{\circ} = -6.2 \text{ kJ mol}^{-1}$ ) [20,21]. Methyl- $\text{H}_4\text{MPT}$ :coenzyme M methyltransferase (EC 2.1.1.86), a membrane protein containing a 5-hydroxybenzimidazolyl cobamide prosthetic group, transfers the methyl group from *N*5 of *N*5, *N*10-methyl- $\text{H}_4\text{MPT}$  to the thiol of coenzyme M (CoM; 2-mercaptoethanesulfonic acid) with a free energy ( $\Delta G'^{\circ}$ ) of  $-30 \text{ kJ mol}^{-1}$  [22]. This enzyme is also involved in energy conservation, pumping  $\text{Na}^+$  ions across the cytoplasmic membrane [12]. The  $\text{Na}^+$  ion gradient formed is thought to be the driving force for the initial oxidation of

molecular hydrogen as well as the production of ATP from ADP and inorganic phosphate. Methyl-coenzyme M reductase (MCR; EC 2.8.4.1) catalyzes the final step of methanogenesis: formation of a heterodisulfide bond between CoM and coenzyme B (CoB; 7-mercaptoheptanoyl-L-threonine phosphate), releasing methane ( $\Delta G'^{\circ} = -45 \text{ kJ mol}^{-1}$ ), by way of an active site nickel-tetrapyrrole cofactor ( $F_{430}$ ) [23,24]. Heterodisulfide reductase (EC 1.8.98.1) reductively cleaves the CoM-CoB disulfide ( $\Delta G'^{\circ} = -40 \text{ kJ mol}^{-1}$ ), releasing the coenzymes for further methane production [25]. The reduction of the CoM-CoB heterodisulfide is coupled to a  $\text{Na}^+$  or  $\text{H}^+$  gradient, depending on the organism, that drives ATP formation [12].

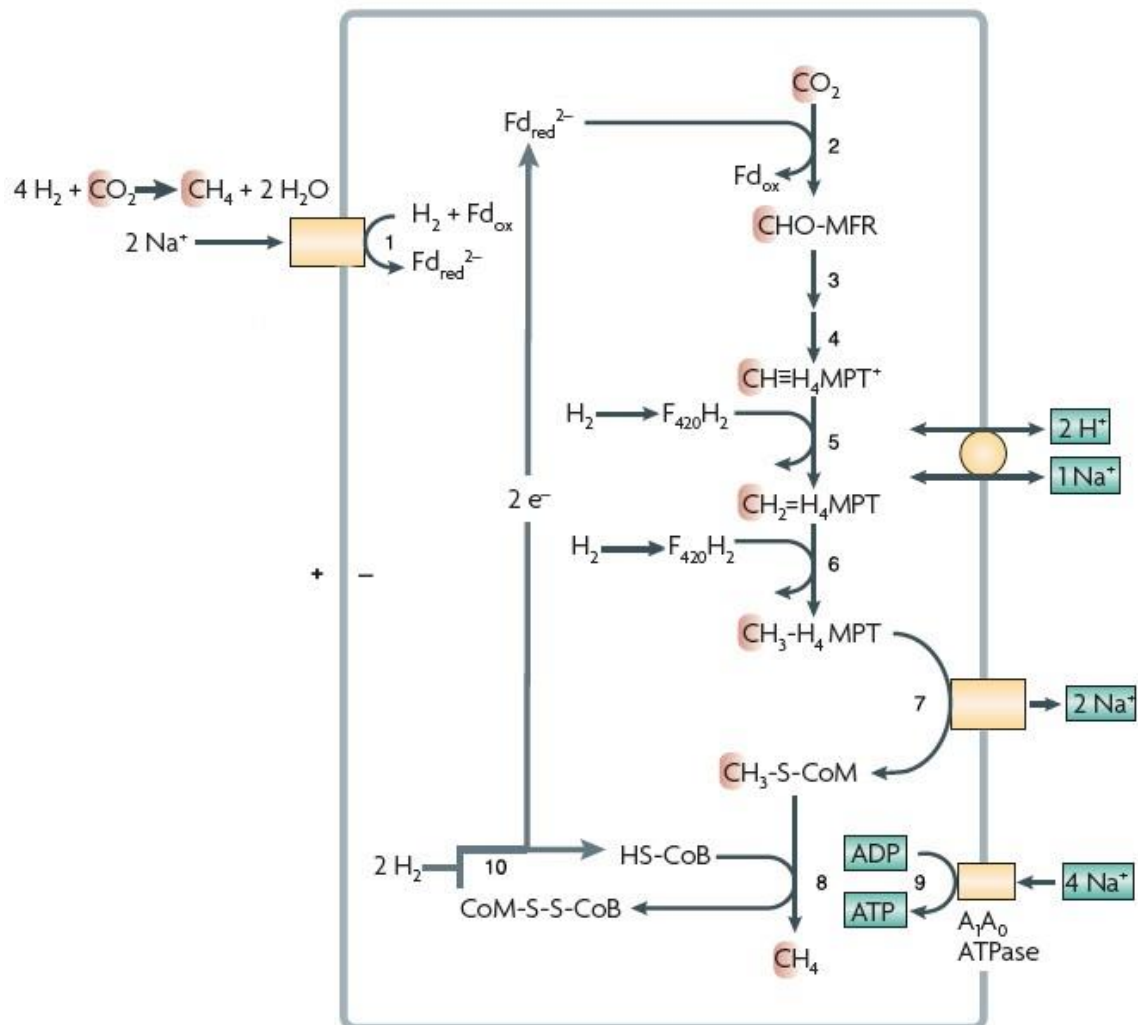


**Figure 1.1. Methanogenesis.** 1, [NiFe] hydrogenase; 2, Formylmethanofuran dehydrogenase; 3, Formylmethanofuran: $\text{H}_4\text{MPT}$  formyltransferase; 4, Methenyl- $\text{H}_4\text{MPT}$  cyclohydrolase; 5,  $\text{F}_{420}$ -dependent methylene- $\text{H}_4\text{MPT}$  dehydrogenase or  $\text{H}_2$ -dependent methylene- $\text{H}_4\text{MPT}$  dehydrogenase; 6,  $\text{F}_{420}$ -dependent methylene- $\text{H}_4\text{MPT}$  reductase; 7 Methyl- $\text{H}_4\text{MPT}$ :coenzyme M methyltransferase; 8, Methyl-coenzyme M reductase; 9,  $\text{A}_1\text{A}_0$  ATPase; 10, Heterodisulfide reductase. Adapted from [12].

### 1.3. COENZYME B

Although methanogenesis differs depending on the carbon source, the reaction catalyzed by MCR is common among methanogens for formation of the heterodisulfide and requires CoM, CoB, and F<sub>430</sub> for activity. Coenzyme B is considered to be unique to methanogens: the compound has not been identified in non-methanogenic organisms. Therefore, CoB is an attractive target for controlling methane output at the key step of methanogenesis.

#### 1.3.1. Identification and Structure

Coenzyme B was initially identified in 1980 by Gunsalus and Wolfe during experiments to elucidate the cellular components of *Methanobacterium thermoautotrophicum* required for MCR activity [23]. Isolation of the cytosolic fraction by ultracentrifugation and anion exchange chromatography revealed three components necessary for the reconstitution of MCR: components A, B, and C [23]. Component B was identified as a low molecular weight, heat-stable, oxygen-sensitive compound necessary for MCR activity but of unknown function[23]. Ultimately the structure of component B was determined by NMR and mass spectrometry, consisting of a thiol group linked to a phosphothreonine group via a C8 alkyl chain (C<sub>11</sub>H<sub>22</sub>NO<sub>7</sub>PS, 343.3 Da), and later renamed coenzyme B [26]. However, these initial studies also observed isolated cytosolic fractions containing a larger component (molecular weight greater than 1000 Da) that could stimulate MCR activity [27,28]. Therefore, the CoB identified was proposed to be the degradation product of a larger compound. Indeed, the works of Keltjens, Marsden, Sauer, and associates determined that the phosphothreonine headgroup of CoB is linked to a *N*-acetylmannosaminuronate (ManNAcA) ( $\beta$ -1 $\rightarrow$  4)

UDP-*N*-acetylglucosamine (GlcNAc) moiety (UDP-GlcNAc-ManNAcA-CoB) (Figure 1.2) [28,29,30,31].

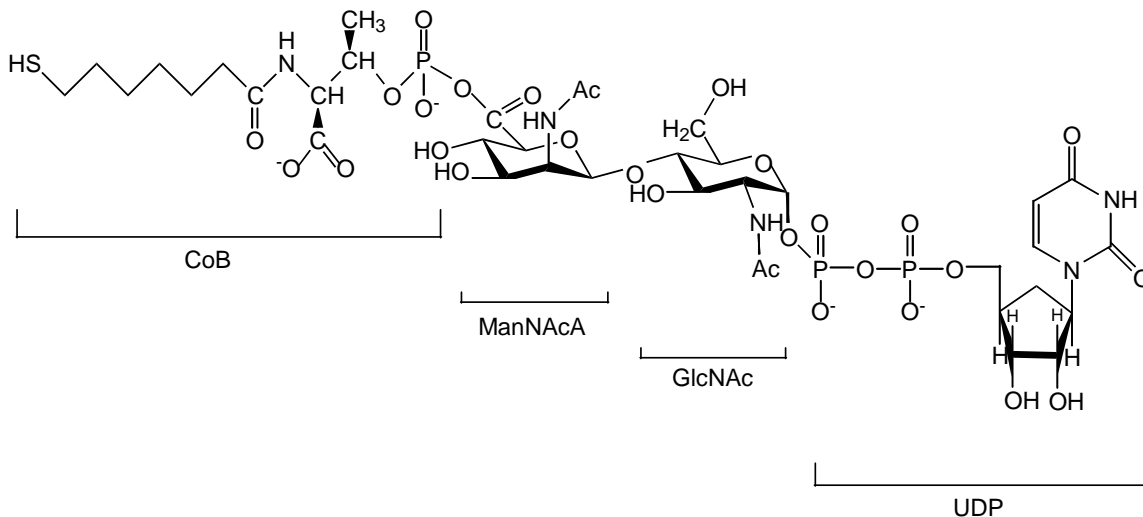


**Figure 1.2. The structure of UDP-GlcNAc-ManNAcA-CoB.**

### 1.3.2. CoB in the Mechanism of Methyl-Coenzyme M Reductase

CoB or UDP-GlcNAc-ManNAcA-CoB is essential for the mechanism of MCR, serving as the electron donor for the reduction of  $\text{CH}_3\text{-CoM}$ . The crystal structure of MCR from *M. thermoautotrophicum* was solved at 1.45 Å as a hexamer of  $\alpha_2\beta_2\gamma_2$  subunits with the three essential coenzymes bound: CoB, CoM, and  $\text{F}_{430}$  [32]. MCR has two identical active sites that are 5.1 nm apart with each site composed of a funnel-shaped channel from either  $\alpha'$ ,  $\alpha$ ,  $\beta$ ,  $\gamma$  or  $\alpha$ ,  $\alpha'$ ,  $\beta'$ ,  $\gamma'$ . Coenzyme  $\text{F}_{430}$  is located at the bottom of the active site channel and  $\text{CH}_3\text{-CoM}$  is bound in the channel by its sulfonate group above  $\text{F}_{430}$  in a parallel orientation to the tetrapyrrole ring [32]. The



phosphothreonine head group of CoB is bound at the top of the channel via salt bridges with five basic amino acids, essentially sealing the active site from solvent. The negatively charged phosphate and carboxylate of CoB interact with Arg <sup>$\alpha^{270}$</sup> , His <sup>$\beta^{379}$</sup> , Lys <sup>$\alpha^{256}$</sup> , methyl-His <sup>$\alpha^{257}$</sup> , and Arg <sup>$\alpha^{225}$</sup>  [32]. The thioheptanoyl chain extends through a narrow 8 Å diameter segment of the channel, making van der *Waals* contacts with several hydrophobic residues (Figure 1.3) [32,33]. The sulfhydryl group of CoB is positioned near CH<sub>3</sub>-CoM in the active site, interacting with Asn <sup>$\alpha^{481}$</sup> , Val <sup>$\alpha^{482}$</sup> , and a water molecule[32,33]. The UDP-disaccharide was not present in the MCR structure with CoB and the function of this sugar headgroup has not been determined.

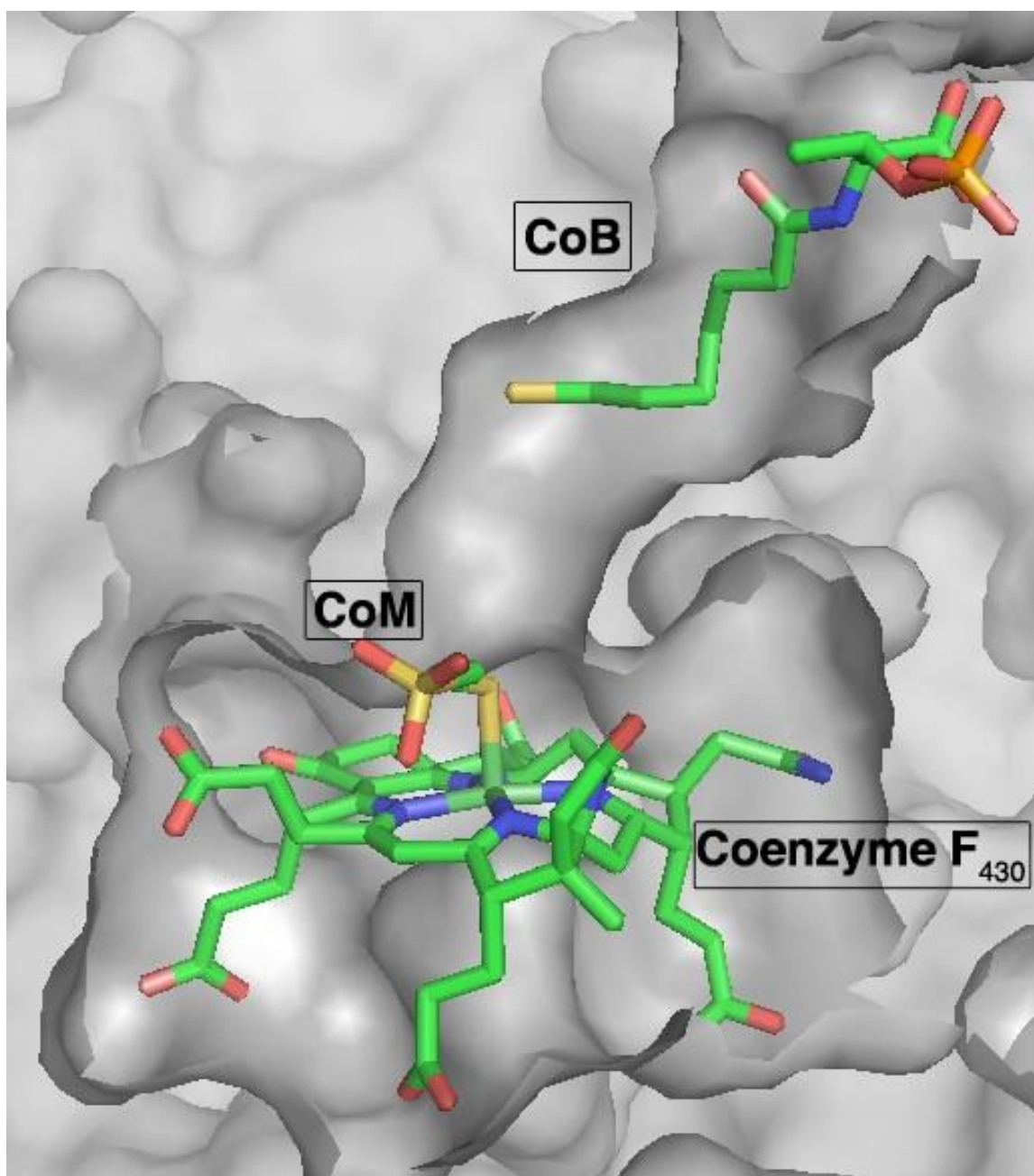


**Figure 1.3. The active site of MCR.** The thiol of coenzyme B extends into the narrow channel leading to the enzyme active site (gray). CoM and coenzyme F<sub>430</sub> are located at the bottom of the channel. The figure was constructed with Pymol and PDB 1MRO.

Two models outlining the roles of CoB, CoM, and  $F_{430}$  in the MCR mechanism have been postulated based on crystallographic, spectroscopic, theoretical, and enzymological studies, although observing reaction intermediates has been problematic [33]. In one model (Figure 1.4A), based on theoretical calculations, a free methyl radical is generated from the attack of the  $F_{430} Ni^I$  on the  $CH_3$ -CoM sulfur, resulting in  $Ni^{II}$ -S-CoM [33,34]. The methyl radical then reacts with the bound CoB, abstracting a proton to form methane and a CoB thiyl radical [34]. Reaction of the CoB radical with  $Ni^{II}$ -S-CoM generates a heterodisulfide radical anion between CoB and CoM, which in turn reduces  $Ni^{II}$  to  $Ni^I$ , releasing the CoB-CoM heterodisulfide [33]. The second proposed mechanism (Figure 1.4B) involves the  $S_N2$  attack of  $F_{430} Ni^I$  on the methyl group of  $CH_3$ -CoM, producing methyl- $F_{430} Ni^{III}$  and free CoM [33,35]. The methyl- $Ni^{III}$  then oxidizes CoM, forming a thiyl radical that can interact with the bound CoB to form the heterodisulfide radical anion [33]. The resulting methyl- $Ni^{II}$  is protonated, releasing methane, and the  $Ni^{II}$  is reduced to  $Ni^I$  by the heterodisulfide radical anion, releasing the CoB-CoM heterodisulfide [33]. Recently, evidence has been observed for the formation of a  $Ni^{III}$ -methyl state of MCR [36].

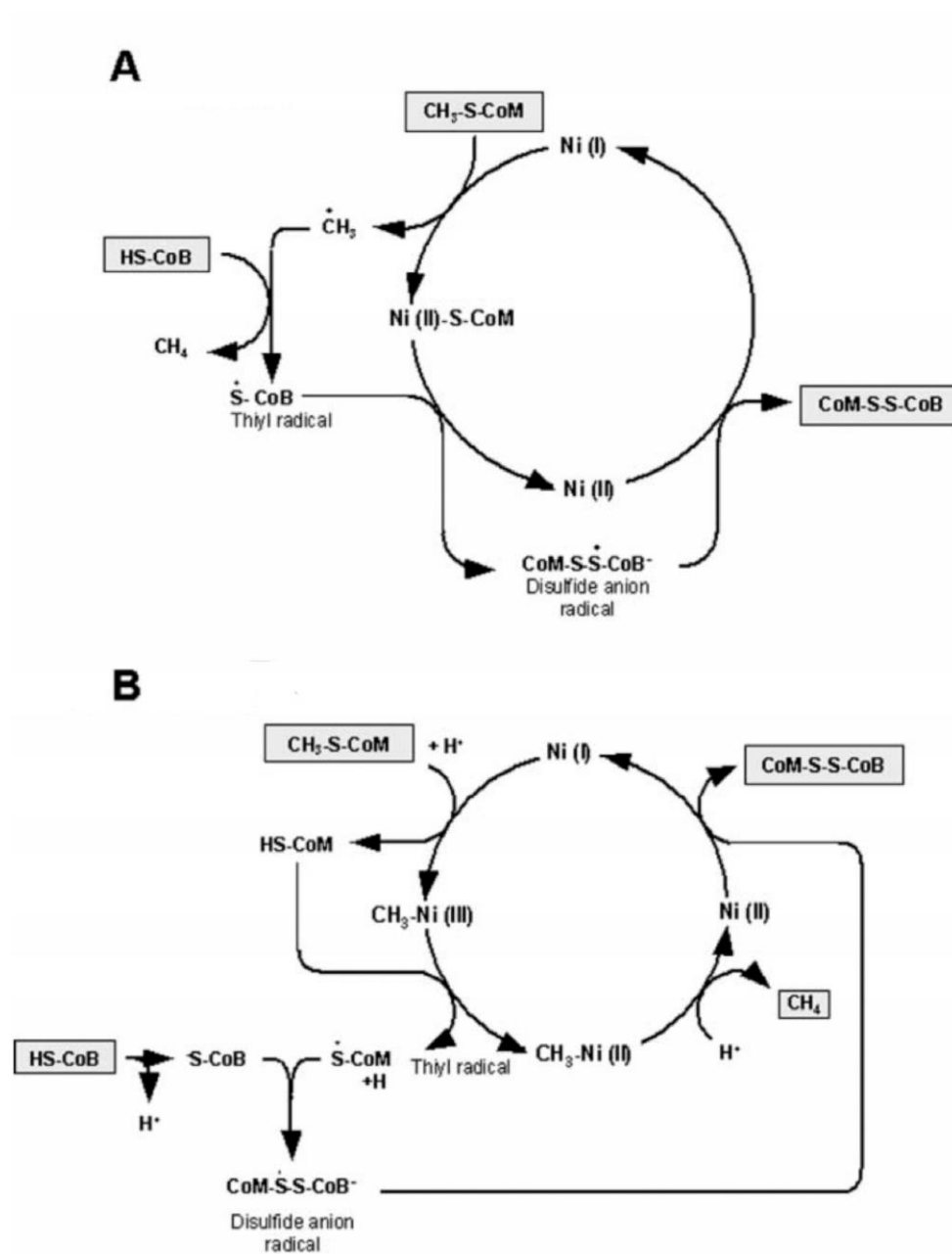


**Figure 1.4. Proposed mechanisms for methyl-coenzyme M reductase.** Adapted from [33].

Aside from the role of CoB in either mechanism, there is evidence that CoB may also play a role in the conformational change observed in MCR. The two active sites of MCR are predicted to be in two different reactive states. These two states are thought to couple the release of the CoB-CoM heterodisulfide out of the hydrophobic channel to the solvent with an exergonic step in the reaction cycle [37]. Therefore, the binding of CoB, which must succeed the binding of CoM, to one active site is proposed to cause a conformation change that results in the release of the heterodisulfide from the second active site in a “two-stroke mechanism” [37].

### **1.3.3. Elucidation of the Biosynthetic Pathway**

The proposed biosynthetic pathway to coenzyme B was almost completely elucidated by the work of Robert H. White through isotope labeling experiments (Figure 1.5). Initial studies involving labeled acetate and succinate fed to *Methanococcus voltae* or rumen isolate 10-16B were crucial in identifying a pathway for the synthesis of 2-oxosuberate, an eight-carbon dicarboxylate that serves as the alkyl portion of CoB [38]. Incorporation of deuterium from [2, 2, 3, 3- $^2\text{H}_4$ ] succinate into carbons 1-4 of 7-mercaptoheptanoic acid identified 2-oxoglutarate, derived from succinate, as a precursor to CoB [38]. Subsequent labeling experiments with [1, 2- $^{13}\text{C}$ ] acetate and [2, 2, 2- $^2\text{H}$ ] acetate indicated a series of carbon chain elongation reactions, extending the carbon chain of the five-carbon 2-oxoglutarate by three methylenes to the eight-carbon 2-oxosuberate [38]. The 2-oxoacid chain elongation pathway was later confirmed from cell free extracts of *Methanosarcina thermophila* [39]. Product analysis from these extracts indicated three consecutive reactions were necessary to extend 2-oxoglutarate by one methylene, producing 2-oxoadipate [39]. These reactions were repeated with 2-

oxoadipate as the starting substrate, producing the seven-carbon 2-oxopimelate and again with 2-oxopimelate, producing the end product 2-oxosuberate (Figure 1.5) [39].

Deuterium labeling studies were also employed to identify the remaining reactions of CoB biosynthesis. These studies indicated the formation of the aldehyde 7-oxoheptanoate from the non-oxidative decarboxylation of 2-oxosuberate, a reaction that is analogous to the production of sulfoacetaldehyde from sulfopyruvate in the CoM biosynthetic pathway [40]. The reduction and thiolation of 7-oxoheptanoate to 7-mercaptoheptanoate has been observed, however the source of sulfur and reducing agent have not been conclusively identified, though there is precedence for coenzyme F<sub>420</sub> to act as the reductant [40]. Studies of cell-free extracts of *M. volta* and *Methanosarcina thermophila* grown in medium containing labeled 7-mercaptoheptanoic acid, 7-mercaptoheptanoyl threonine, or DL-threonine identified the final two steps in the CoB pathway. First, a peptide bond is generated between the carboxyl of 7-mercaptoheptanoate and the amino group of L-threonine in an ATP dependent reaction, producing 7-mercaptoheptanoylthreonine [41]. In a second ATP dependent reaction, the threonine group is phosphorylated, producing 7-mercaptoheptanoylthreonine phosphate (Figure 1.5) [42].

Recently, the work of Namboori and Graham identified the archaeal biosynthetic pathway for the production of UDP-GlcNAc and UDP-ManNAcA from fructose-6-phosphate [43]. The enzymes required for this pathway were cloned from *Methanococcus maripaludis* and *Methanocaldococcus jannaschii* and overexpressed in *E. coli*. Enzyme activity assays and product analysis indicated five enzymes required for acetamido sugar biosynthesis in methanogens: glutamine-fructose-6-phosphate (glutamine-Fru-6-P) transaminase, phosphoglucosamine mutase, glucosamine-6-phosphate (GlcN-6-P) uridylyltransferase/acetyltransferase, UDP-GlcNAc 2-epimerase,

and UDP-ManNAc 6-dehydrogenase [43]. This pathway is the first study to elucidate the reactions required for production of the ManNAcA ( $\beta$ -1 $\rightarrow$ 4) UDP-GlcNAc moiety of UDP-GlcNAc-ManNAcA-CoB.

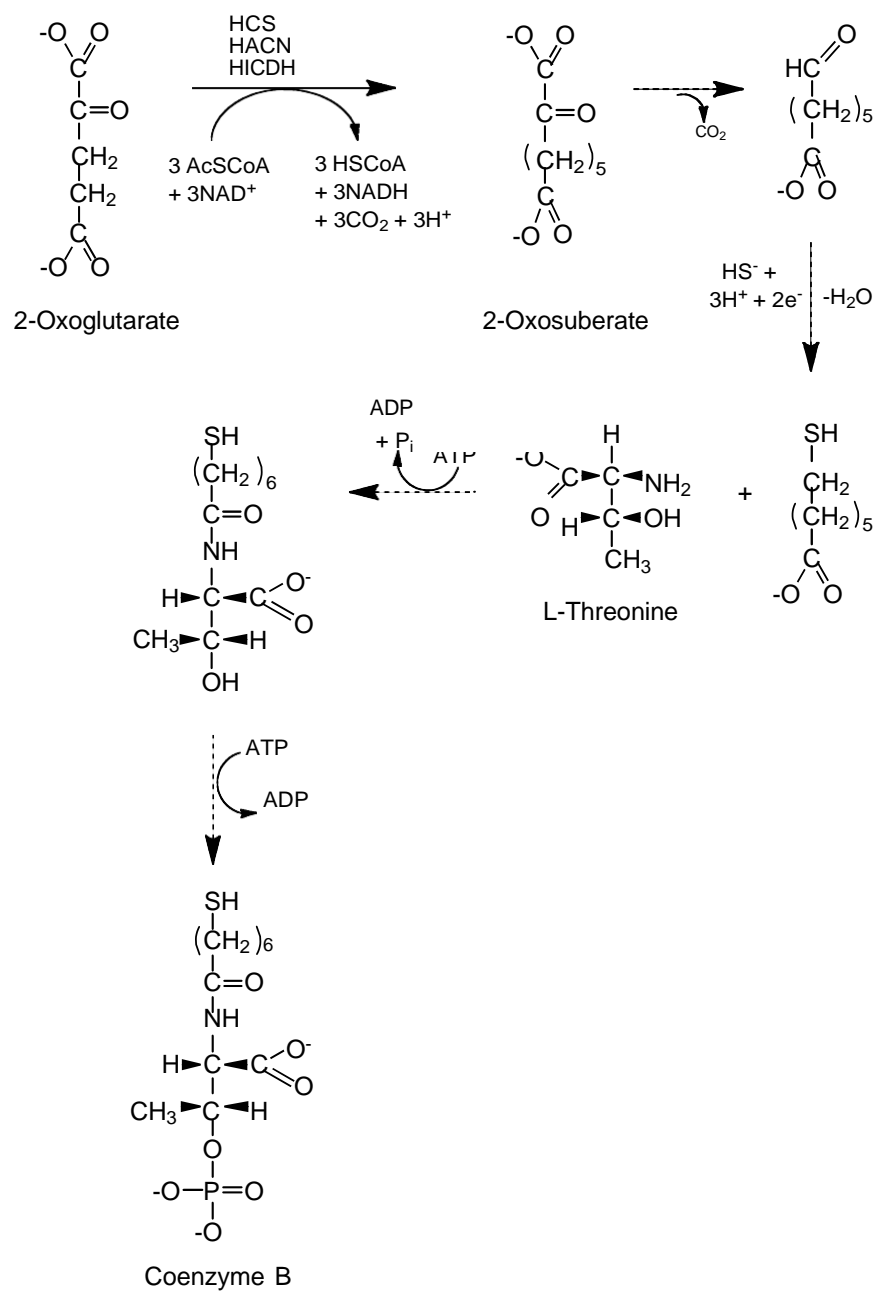


**Figure 1.5. Proposed pathway for coenzyme B biosynthesis.** Dashed arrows indicate a reaction that has not yet been associated with an enzyme.



### 1.3.4. 2-Oxoacid Chain Elongation Pathway

Although a biosynthetic pathway for CoB has been proposed, gene products from *M. jannaschii* have only been assigned for two enzymes, both from the 2-oxoacid chain elongation pathway. Only one has been purified and characterized. The chain elongation pathway is expected to commence with the condensation of acetyl-coenzyme A (acetyl-CoA) with 2-oxoglutarate, producing (*R*)-homocitrate in a reaction catalyzed by the gene product of *MJ0503*, homocitrate synthase (HCS; EC 2.3.3.14) [39]. A second enzyme, predicted to be a homoaconitase (HACN; EC 4.2.1.36) catalyzes the reversible anti-elimination of water from homocitrate, producing the unsaturated intermediate *cis*-homoaconitate. HACN then catalyzes the subsequent rehydration of the intermediate by the anti-addition of water, giving (2*R*,3*S*)-homoisocitrate. Finally, the gene product of *MJ1596*, homoisocitrate dehydrogenase (HICDH; EC 1.1.1.87), catalyzes the NAD<sup>+</sup>-dependent oxidative decarboxylation of (2*R*,3*S*)-homoisocitrate, forming 2-oxoadipate [44]. Remarkably, methanogen HCS, HACN, and HICDH exhibit broad substrate specificity, continuing these 1-carbon elongation reactions by catalyzing the production of 2-oxopimelate and 2-oxosuberate from 2-oxoadipate and 2-oxopimelate, respectively. It is unusual for one enzyme to catalyze more than one reaction in a metabolic pathway. The chain elongation pathway stops at the precursor for 7-oxoheptanoate; 2-oxoazelaic acid, a nine-carbon 2-oxoacid with six methylenes, or higher compounds were not identified in methanogens [45].

While the broad substrate specificity of these enzymes is unusual, analogous chain elongation reactions are ubiquitous in nature. These reactions can essentially be broken down into four steps. First, a 2-oxoacid undergoes an aldol-type condensation with acetyl-CoA, producing an  $\alpha$ -hydroxydicarboxylate. This secondary alcohol is then isomerized, forming a  $\beta$ -hydroxydicarboxylate. Finally, the resulting tertiary alcohol is

dehydrogenated to a  $\beta$ -keto acid, which then undergoes decarboxylation to produce a 2-oxoacid extended by one methylene. The most common and well studied of these elongation reactions is found in the tricarboxylic acid (TCA) cycle where the activities of citrate synthase (CS, EC 2.3.3.1), aconitase (ACN; EC 4.2.1.3), and isocitrate dehydrogenase (ICD; EC 1.1.1.41) function to produce 2-oxoglutarate from oxaloacetate (Figure 1.6). Also, leucine biosynthesis requires isopropylmalate synthase (IPMS; EC 2.3.3.13), isopropylmalate isomerase (IPMI; EC 4.2.1.33), and  $\beta$ -isopropylmalate dehydrogenase (IPMDH; EC 1.1.1.85) to produce 2-oxoisocaproate from 2-oxoisovalerate (Figure 1.6). Euglenoids, higher fungi, some bacteria and archaea use a HCS, HACN, and HICDH to catalyze the production of 2-oxoadipate from 2-oxoglutarate in the  $\alpha$ -aminoadipate pathway for lysine biosynthesis (Figure 1.6). Although these enzymes are homologous to the methanogen HCS and HICDH, 2-oxoadipate is instead converted to L-2-aminoadipate by 2-aminoadipate transaminase (EC 2.6.1.39) and ultimately converted to lysine [46]. These first three enzymes of the  $\alpha$ -aminoadipate pathway are currently being studied as a target for anti-fungal treatment.

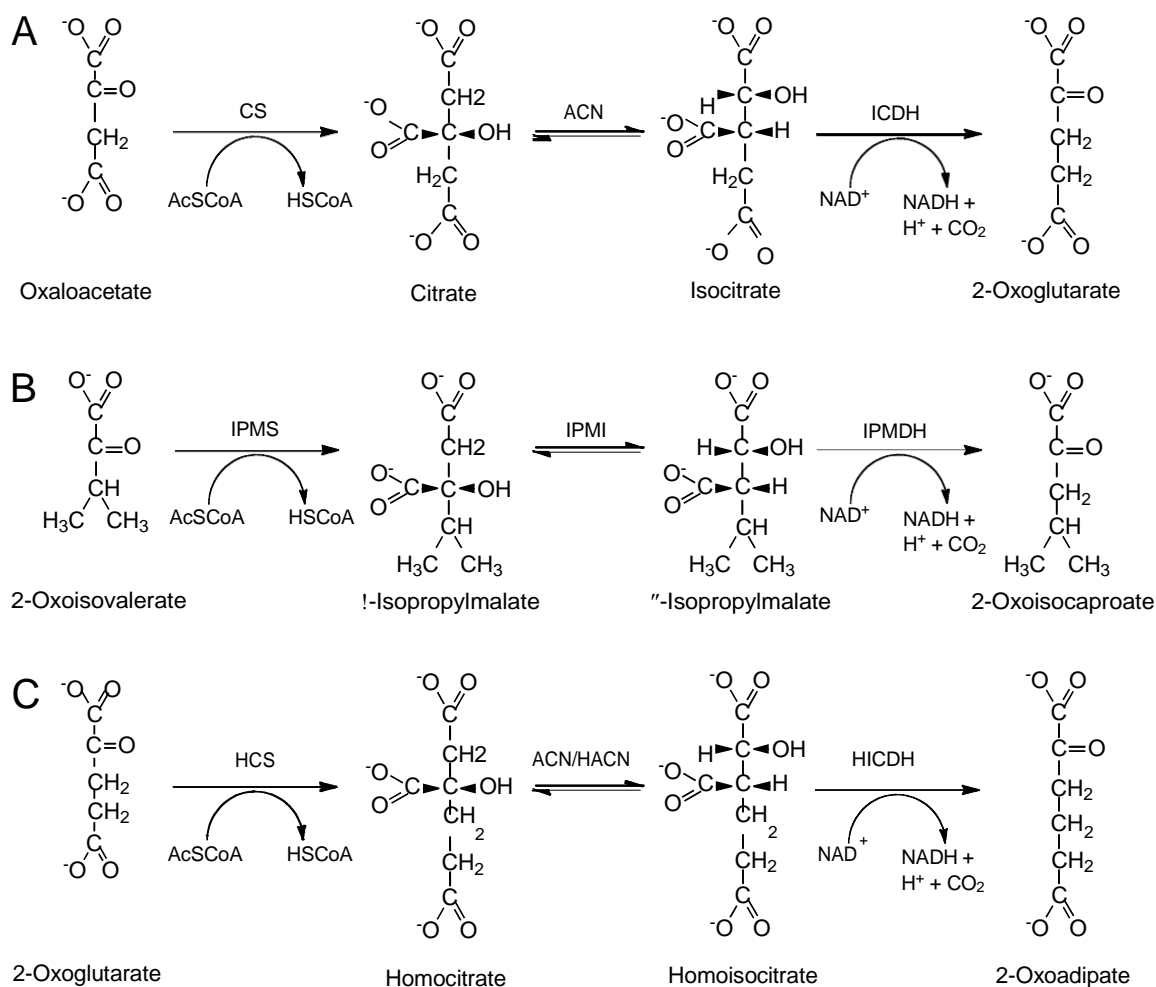


**Figure 1.6. Analogous chain elongation reactions.** A, CS, ACN, and ICDH are used in the TCA cycle to produce 2-oxoglutarate from oxaloacetate. B, IPMS, IPMI, and IPMDH are required for leucine biosynthesis from 2-oxoisovalerate. C, HCS, ACN, HACN, and HICDH convert 2-oxoglutarate to 2-oxoadipate in the  $\alpha$ -aminoadipate pathway for lysine biosynthesis

#### **1.4. IDENTIFICATION OF METHANOGEN HOMOACONITASE, ISOPROPYLMALATE ISOMERASE, AND PROTEINS INVOLVED IN IRON-SULFUR CLUSTER BIOSYNTHESIS**

The broad substrate specificities of the CoB chain elongation reactions may be exploited as a means of controlling methanogenesis, such as inhibitor design. However, despite previous studies, the pathway remains incomplete. The *M. jannaschi* HICDH (HICDH<sub>MJ</sub>) was the only enzyme of the CoB pathway to be overexpressed, purified, and characterized in terms of steady state kinetics with homoisocitrate, homo<sub>2</sub>isocitrate, and homo<sub>3</sub>isocitrate [44]. The previous study involving methanogen HCS analyzed the reaction products from cell free extracts of *M. thermophila* and *E. coli* overexpressing MJ0503 [39]. The results of this study identified *trans*-homoaconitate and (*S*)-homocitrate from the reaction catalyzed by HCS [39]. However, these two compounds have not previously been isolated as natural products and homologs of methanogen HCS in the  $\alpha$ -aminoadipate pathway only produce (*R*)-homocitrate. Also, the subsequent reactions of HCS with 2-oxoadipate and 2-oxopimelate produced only  $\alpha$ -hydroxydicarboxylates of (*R*) stereochemistry and no other *trans*-unsaturated compounds were identified [39]. Because of the nature of that study, the product of the HCS-catalyzed reaction with 2-oxoglutarate remains suspect and requires further study. Finally, the genes responsible for the synthesis of the methanogen homoaconitase remained unknown

##### **1.4.1 The Genome Sequence of *M. jannaschii***

*M. jannaschii*, a thermophilic methanogen isolated from marine hydrothermal vents, was the first member of the domain Archaea to have its genome sequenced. This organism has since served as a model organism for studying methanogenesis. The genome sequence of *M. jannaschii* contains two genes, MJ0499 and MJ1003, that were

annotated as putative IPMI large subunits [47]. Likewise, the genome also contains two genes, *MJ1271* and *MJ1277*, that were annotated as putative IPMI small subunits [47]. These genes share more than 50% sequence identity to each other and are more similar to each other than to any previously characterized IPMIs or HACNs (Figure 1.7). Also, the large and small subunits appear to be randomly placed within the methanogen genomes, further complicating gene assignment by genomic analysis alone. One pair of interacting large and small subunits was predicted to function as HACN<sub>MJ</sub> in CoB biosynthesis and a second pair as IPMI<sub>MJ</sub> in methanogen leucine biosynthesis.



**Figure 1.7. Sequence alignment of the homologous HACN/IPMI large and small subunits from *Methanocaldococcus jannaschii*.** A, *M. jannaschii* MJ1003 (Swiss-Prot accession no. Q58409), *M. jannaschii* MJ0499 (Swiss-Prot accession no. P81291). B, *M. jannaschii* MJ1271 (Swiss-Prot accession no. Q58667), *M. jannaschii* MJ1277 (Swiss-Prot accession no. Q58673). Conserved amino acid residues are shown in white on a black background. Similar residues are shown in black on a gray background. Asterisks indicate cysteine residues conserved in pig heart mACN responsible for binding a [4Fe-4S] cluster

In an effort to identify the genes encoding the HACN<sub>MJ</sub>, the two large and two small subunits were cloned and expressed in *E. coli* and the interacting proteins were purified and characterized based on steady state kinetics and product analysis.

#### **1.4.2. MJ0499-MJ1277 Functions as the *M. jannaschii* IPMI**

The gene products of MJ0499-MJ1277 were identified as the methanogen IPMI, a member of the aconitase superfamily that requires an iron-sulfur cluster for activity [48]. The protein was purified aerobically and the holoenzyme was reconstituted *in vitro*. The steady state kinetics for the substrates involved in leucine biosynthesis were established in both direct and coupled assays with MJ0720 (IPMDH<sub>MJ</sub>). The MJ0499-MJ1277 pair was also identified as the isomerase in the citramalate pathway for isoleucine biosynthesis, as well as exhibiting malease activity. Finally, MJ0720 from *M. jannaschii* was characterized as the IPMDH involved in leucine and isoleucine biosynthesis [48].

#### **1.4.3. MJ1003-MJ1271 Functions as the *M. jannaschii* HACN**

The MJ1003-MJ1271 protein pair was identified as the *M. jannaschii* HACN, an iron-sulfur cluster containing protein homologous to aconitase [49]. The steady state kinetics for the reconstituted holoenzyme were established for *cis*-homoaconitate, *cis*-homo<sub>2</sub>aconitate, and *cis*-homo<sub>3</sub>aconitate in both direct and coupled assays with HICDH<sub>MJ</sub>. Kinetic assays and product analysis provides insight into the intermediates of the chain elongations pathway, and differences with homologous HACNs from the  $\alpha$ -aminoadipate pathway are described.

#### 1.4.4. Structure and Function of MJ1271 and MJ1277

The identified and characterized HACN<sub>MJ</sub> and IPMI<sub>MJ</sub> are highly homologous and are predicted to follow an aconitase-type mechanism in the isomerization of their respective substrates. In an effort to elucidate the active site residues responsible for differences in substrate specificity between the two enzymes, site directed mutagenesis of the HACN<sub>MJ</sub> small subunit, MJ1271, was conducted and the steady state kinetics of the mutant subunits interacting with wild type MJ1003 were established [50]. A crystal structure of MJ1271, solved by Yokoyama and colleagues, as well as a homology model of MJ1277 were used to describe the active sites of *M. jannaschii* HACN and IPMI [50].

#### 1.4.5 Archaeal Iron-Sulfur Cluster Biosynthesis

HACN<sub>MJ</sub> and IPMI<sub>MJ</sub> require an iron-sulfur cluster for activity. However, the archaeal biosynthetic pathway(s) involved in the *in vivo* synthesis of these clusters and the subsequent transfer to their target apoenzymes remains unknown. Although homologs of the SUF pathway for iron-sulfur cluster biosynthesis are present in the genome of *M. jannaschii*, namely SufB and SufC, the function of these proteins has not been identified. Also, many archaea do not possess homologs to any cysteine desulfurase, the sulfur donor for cluster biosynthesis. The *M. jannaschii* MJ0283 and *M. maripaludis* MMP0704 proteins were identified as homologs of the *Salmonella enterica* ApbC protein and *Saccharomyces cerevisiae* Nbp35 protein that function as iron-sulfur cluster carrier proteins [51]. The role of MJ0283 and MMP0704 as archaeal iron-sulfur cluster carrier proteins was elucidated through complementation studies using an established *S. enterica* genetic system possessing an *apbC* mutation. The proteins were also overexpressed and purified from *E. coli* to characterize the iron and sulfur content of the reconstituted proteins [51].



## **Chapter 2: Isoleucine and Leucine Biosynthesis – Isopropylmalate Isomerase**

### **2.1. INTRODUCTION**

Several biosynthetic pathways have been identified for the synthesis of isoleucine, each varying in their production of a 2-oxobutyrate intermediate [52]. Cyanobacteria, fungi, and heterotrophic bacteria synthesize this 2-oxocarboxylic acid using the more widely spread biosynthetic pathway requiring a threonine dehydratase [EC 4.2.1.16] (Figure 2.1). This enzyme catalyzes the PLP-dependent dehydration and deamination of L-threonine, producing 2-oxobutyrate and ammonia [53]. 2-Oxobutyrate is then condensed with hydroxyethyl thiamine pyrophosphate to give  $\alpha$ -aceto- $\alpha$ -hydroxybutyrate in a reaction catalyzed by acetolactate synthase [EC 2.2.1.6]. Three enzymes then work in succession to produce isoleucine from  $\alpha$ -aceto- $\alpha$ -hydroxybutyrate: Acetohydroxy acid isomeroreductase [1.1.1.86], dihydroxy acid dehydratase [4.2.1.9], and valine-3-methyl-2-oxovalerate transaminase [2.6.1.32].

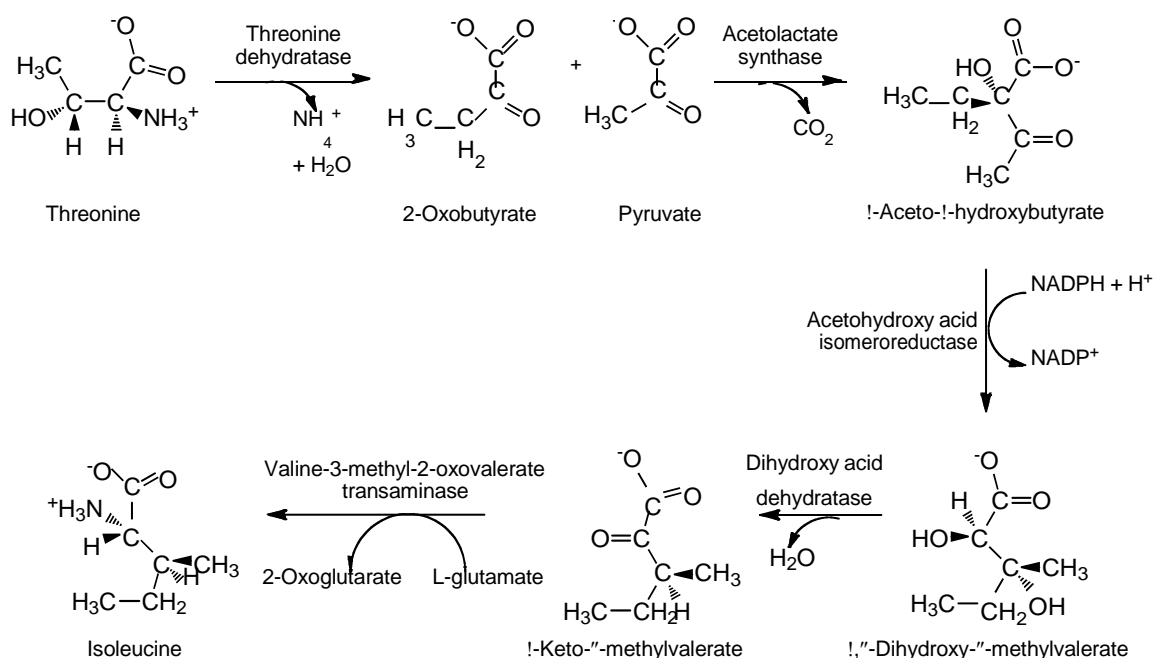


**Figure 2.1. Isoleucine biosynthesis using a threonine dehydratase for the production of 2-oxobutyrate.**

Threonine dehydratase is not present in the genomes of most methanogenic archaea. These organisms still synthesize isoleucine, albeit from a different biosynthetic pathway to 2-oxobutyrate. *Methanobacterium thermoautotrophicum*, *Methanobrevibacter arboriphilus*, and *Methanosarcina barkeri* assimilated exogenous propionate and 2-methylbutyrate into isoleucine [54,55]. However, in the absence of these compounds, labeled acetate was incorporated into isoleucine via citramalate in a chain elongation pathway starting from pyruvate, a pathway that was initially identified in spirochetes [55,56].

The pyruvate pathway to 2-oxobutyrate is analogous to the isopropylmalate pathway for leucine biosynthesis. Citramalate synthase (CMS) [EC 2.3.1.182] catalyzes the production of (*R*)-citramalate from acetyl-CoA and pyruvate. [57]. The product is

then dehydrated to the *cis*-unsaturated intermediate citraconate. The hydration product of citraconate,  $\beta$ -methylmalate, is then oxidatively decarboxylated to 2-oxobutyrate, which is ultimately converted to isoleucine. To produce leucine, 2-oxoisovalerate and acetyl-CoA are first condensed to form  $\alpha$ -isopropylmalate, catalyzed by isopropylmalate synthase (IPMS) [58]. Isopropylmalate isomerase (IPMI), a homolog of aconitase possessing a [4Fe-4S] cluster, then catalyzes the anti-elimination of water from  $\alpha$ -isopropylmalate to form the *cis*-unsaturated intermediate dimethylcitraconate through a mechanism proposed to be similar to mitochondrial aconitase (mACN) [59]. The IPMI-catalyzed hydration of the intermediate produces  $\beta$ -isopropylmalate, which is then oxidatively decarboxylated by the  $\text{NAD}^+$ -dependent isopropylmalate dehydrogenase (IPMDH) to give 2-oxoisocaproate [44].

The CMS from *M. jannaschii*, MJ1392, was previously purified and characterized as specific for pyruvate and acetyl-CoA [57]. The substrate of IPMS, 2-oxoisovalerate, was not detected as a substrate, distinguishing CMS from IPMS. CMS was also identified in *Leptospira interrogans* and a catalytic mechanism was proposed based on crystallographic and site-directed mutagenesis studies [60,61]. The overall mechanism is consistent the mechanism of malate synthase, involving three main steps: (i) enolization; (2) condensation; (3) hydrolysis. A glutamate is proposed to serve as the base for proton abstraction from the acetyl-CoA methyl group, producing an enolate. An arginine residue functions as a general acid, coordinating the acetyl-CoA enolate as well as pyruvate. The divalent metal cation  $\text{Mn}^{2+}$  was required for maximal activity of the *L. interrogans* CMS and is therefore proposed to also coordinate pyruvate via the carbonyl groups. Rotation of the acetyl-CoA puts this substrate in position for a nucleophilic attack on the bound pyruvate, producing the citramalyl-CoA intermediate. An active site

water molecule then hydrolyzes the thioester of citramalyl-CoA, producing the free CoA thiol and citramalate [61].

Although the CMS from *M. jannaschii* and *L. interrogans* have been characterized, the enzymes responsible for the isomerization of (*R*)-citramalate and oxidative decarboxylation of  $\beta$ -methylmalate were not identified. Yeast strains with mutations in the threonine dehydratase gene were able to synthesize isoleucine via the pyruvate pathway and the *S. cerevisiae* IPMI was able to catalyze the hydration of citraconate [52,59]. Therefore, it was proposed that IPMI could function in both leucine and isoleucine biosynthetic pathways (Figure 2.2). Citraconate hydration and  $\beta$ -isopropylmalate dehydrogenase activities were observed in *L. interrogans* extracts supplemented with *E. coli* extracts expressing the *L. interrogans* IPMI and IPMDH. However, these enzymes were not purified and characterized [60].

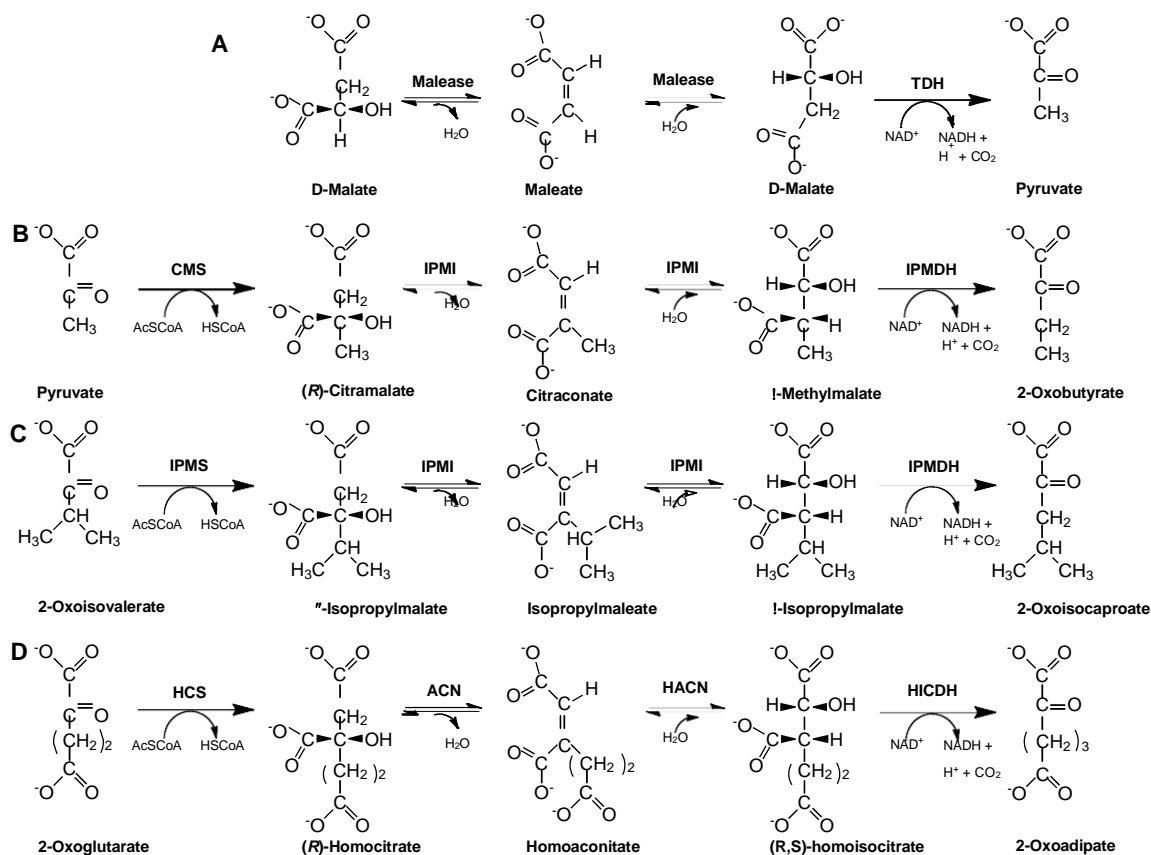


**Figure 2.2. Analogous chain elongation pathways.** (A) Malease catalyzes the hydration of maleate to form D-malate, which can be oxidatively decarboxylated by TDH (or by IPMDH). (B) The pyruvate pathway to 2-oxobutyrate for isoleucine biosynthesis requires CMS, IPMI, and IPMDH enzymes. (C) The isopropylmalate pathway for leucine biosynthesis uses IPMS and shares the IPMI and IPMDH enzymes with the pyruvate pathway. (D) the homocitrate pathway for lysine production in some organisms requires a homocitrate synthase (HCS), aconitase (ACN), homoaconitase (HACN), and homoisocitrate dehydrogenase (HICDH).

The *M. jannaschii* genome contains two genes encoding putative IPMI large subunits (MJ0499 and MJ1003) and two genes encoding putative IPMI small subunits (MJ1271 and MJ1277) (Figures 1.6 and 2.3). One pair of large and small subunits was predicted to function as the homoaconitase in CoB biosynthesis. A second pair of subunits was predicted to function as the IPMI in methanogen leucine biosynthesis. The *M. jannaschii* IPMI was also proposed to function as the citramalate isomerase required for the pyruvate pathway.

MJ1271	.....MIIKGRAHKFG.DDVD	TD	II	PGPYL.RTTDPYELASHCMAGIDE
MJ1277	...MRSIIKGRVWKFG.NNVD	TD	II	LPARYL.VYTKPEELAQFVMTGADP
Tth LeuD	MLEKFTVIRGKAVPLRGEDID	TD	RI	LPARFMKVLTTFEG.LGQYLFYDERF
PhHACN-s	.....MITTGKVWKFG.DDIST	DE	IT	PGRYN.LTKDPKELAKIAFIEVRP
Tth LysU	.....MPRVWKFG.DQINTD	DI	LP	PGKYAPFMVGEDRFHLYAFAHLRP
Ec LeuD	MAEKFIKHTGLVVPLDAANVD	D	P	QFLQKVTRTG.FGAHLFNDWRF
MJ1271	NFPKKVKEGD.....	VIV	AGENFGCGSSREQ	AVIAIKYCGIK
MJ1277	DFPKVKPGD.....	II	VGGKNFGCGSSREH	APLGLKGAGIS
Tth LeuD	DEKGNPKPHP...LNDPRYRGAT	ILL	VESGFGSGSSREH	APQAIKRAGFK
PhHACN-s	DFARNVRPGD.....	VVV	AGKNFGIGSSRES	AALALKALGIA
TthLysU	EFAKEVRPGD.....	ILV	FGRNAGLGSSREY	APALKRLGVR
Ec LeuD	LDEKGQQPNPDFVLNFPQYQGAS	ILL	ARENFG	SSRE
				WALTDY
MJ1271	AVI	K	AR	F
MJ1277	CVIAESFARIF	YRN	AINVGLPLIECKG.....	ISEKVN
Tth LeuD	AIIGESFAEIFFGN	ATAIGLPCVSLSPEDLG	VLF	RSVEENPELEVEIDL
PhHACN-s	GVIAESFGRIF	YRN	AINIGIPLLLGK.....	TEGLKDGDLVTN
TthLysU	AIIA	SYARIFFRNLVNLGIVPF	ESEE.....	VVDALEDGDEVELDLESG
Ec LeuD	VVI	P	AD	F
				G
				FNNQLLPVKLSDAEVD
				ELFALVKANPGIHFDVDLE
MJ1271	EIVITNKNKTIKC.....	ETPKGLEREILAAGGLV	NYLK	KKRKLI
MJ1277	EIKNLTTEVLKG.....	QKLPEFMMEILEAGGLMP	YLK	KMA
Tth LeuD	NQEVRF	GDRTAPLSIREEAREALVEGLWDPIGELLEAGELLDQ	F	DQKLPY
PhHACN-s	..EVRKGDEILMF.....	EPLED	F	LLEIVREGGILEYIRRRGDL
Tth LysU	..VLTRGEERFAL.....	RPPPP	F	LLEALKEGSLLDYYKKHGRF
Ec LeuD	AQEVKAGEKTYRFTIDAFRRHCMMNGL	DSIGLTLQHDDAIAAYEAKQPA		
MJ1271	QSKKGVKT			
MJ1277	ESQ.....			
Tth LeuD	PRRTE...			
PhHACN-s	CIR.....			
Tth LysU	PGE.....			
Ec LeuD	FMN.....			

**Figure 2.3. Sequence alignment of hydrolyase small subunits.** The sequences are *Methanocaldococcus jannaschii* MJ1271 (Swiss-Prot accession no. Q58667), *M. jannaschii* MJ1277 (Swiss-Prot accession no. Q58673), *Thermus thermophilus* isopropylmalate dehydratase (Tth LeuD; RefSeq accession no. YP\_004837.1), *Pyrococcus horikoshii* HACN (PhHACN-s; Swiss-Prot 059393), *T. thermophilus* HACN (Tth LysU; RefSeq accession no. YP\_005515.1), *Escherichia coli* isopropylmalate dehydratase (Ec LeuD; Swiss-Prot accession no. P30126). Conserved amino acid residues are shown in white on a black background. Similar residues are shown in black on a gray background.

In this study, the MJ0499/MJ1277 pair of proteins was identified as the IPMI involved in leucine and isoleucine biosynthesis [48]. After reconstitution of the [4Fe-4S] center, the holoenzyme catalyzed the reversible hydration of citraconate and dehydration of (*R*)-citramalate,  $\alpha$ -isopropylmalate, and  $\beta$ -isopropylmalate. The broad substrate specificity of MJ0499/MJ1277 was also extended to the hydration of the minimal substrate, maleic acid, to D-malate. The *M. jannaschii* IPMDH catalyzed the oxidative decarboxylation of  $\beta$ -methylmalate, as well as  $\beta$ -isopropylmalate and D-malate. Therefore the *M. jannaschii* IPMI and IPMDH proteins function in both the isopropylmalate pathway and the pyruvate pathway to 2-oxobutyrate.

## **2.2. MATERIALS AND METHODS**

### **2.2.1. Chemicals**

$\alpha$ -Isopropylmalic acid was purchased from Aldrich. Other commercially available reagent grade chemicals were used without further purification. (2*R*,3*S*)-3-isopropylmalate was chemically synthesized (Abdul Waheed). DL-*threo*-3-isopropylmalic acid was purchased from Wako Chemicals for analytical comparison.

### **2.2.2. Cloning of MJ0499-MJ1277, MJ1003-MJ1277, and MJ0720**

Genes were amplified from chromosomal DNA of *Methanocaldococcus jannaschii* JAL-1 using PCR. The large subunit genes at loci MJ0499 (RefSeq accession no. NP\_247475) and MJ1003 (NP\_247997) were cloned between NdeI and KpnI sites of plasmid pCDF-Duet1 (Novagen) to create vectors pDG142 and pDG141, respectively. The MJ1271 small-subunit gene (NP\_248267) was cloned between NcoI and BamHI sites of plasmid pDG142 to create vector pDG159 and between the same sites in the



plasmid pDG141 to create pDG152. The *MJ1277* small-subunit gene (NP\_248273) was cloned between NcoI and BamHI sites of plasmid pDG141 to create pDG157. The IPMDH gene at locus *MJ0720* (NP\_247705) was amplified using PCR and cloned between the NdeI and BamHI sites of plasmid pET-19b (Novagen) to create vector pMYL1. The translational start site for that protein was originally predicted to be encoded by a GTG codon, which can be recognized as an initiator codon in some archaea [44]. However, there is an ATG codon downstream from the GTG codon that is closer to the predicted start site of conserved, orthologous archaeal genes. Because the GTG codon appears to be part of a ribosome binding site “GGTGAT,” we believe the ATG codon is probably the relevant initiator codon. The *MJ0720* protein was expressed from this downstream start site fused to an amino-terminal polyhistidine tag in *E. coli*.

Plasmids were propagated in *E. coli* DH5 $\alpha$  (Invitrogen). Dideoxyribonucleotide sequencing confirmed the sequences of inserts in recombinant plasmids.

**Table 2.1. Oligodeoxyribonucleotide primers used for PCR.** Restriction enzyme recognition sites used for cloning are underlined, and initiator codons are italicized.

<b>Primer</b>	<b>Oligodeoxribonucleotide sequence</b>
MJ1003Fwd	(5'-GGT <u>CATATG</u> ACATTGGTAGAGAAGATAC-3')
MJ1003Rev	(5'-GCGGGTACCTTAATCCAATTTGTTGGT-3')
MJ0499Fwd	(5'-GGT <u>CATATG</u> GGAATGACAATTGTAGAG-3')
MJ0499Rev	(5'-GCGGGTACCTTATAAATCCCTTGGGTC-3')
MJ1271Fwd	(5'-CATGCCATGGTTATTAAGGGAAGAGC-3')
MJ1271Rev	(5'-CGGGATCCTTATGTTTTTACACCTTTTTTTGATTG-3')
MJ1277Fwd	(5'-CATGCCATGGGAAGTATAATAAAGGGAAGAG-3')
MJ1277Rev	(5'-CGGGATCCTTATTGGCTTTCAGCCATCTTTTCTTTAAG-3')
MJ0720Fwd	(5'-GCGC <u>ATATG</u> CATAAAATATGTGTTATAG-3')
MJ0720Rev	(5'-GCGGATCCTTATTCTTCTCTTACTC-3')

**Table 2.2. List of plasmids and microorganisms.**

Strain or plasmid	Description	Source and/or reference
<i>Methanocaldococcus jannaschii</i>		
JAL-1	Wild type	DSM 2661
<i>Escherichia coli</i>		
DH5a	General cloning host	Invitrogen
BL21(DE3)	Protein expression host	Novagen
Plasmids pCDF-Duet1	Protein coexpression vector	Novagen
pET-19b	Expression vector for proteins with an N-terminal decahistidine tag	Novagen
pDG141	MJ1003 PCR product obtained using primers MJ1003Fwd and MJ1003Rev cloned into NdeI/KpnI sites of pCDF-Duet1	This study
pDG142	MJ0499 PCR product obtained using primers MJ0499Fwd and MJ0499Rev cloned into NdeI/KpnI sites of pCDF-Duet1	This study
pDG152	MJ1271 PCR product obtained using primers MJ1271Fwd and MJ1271Rev cloned into NcoI/BamHI sites of pDG141	This study
pDG157	MJ1277 PCR product obtained using primers MJ1277Fwd and MJ1277Rev cloned into NcoI/BamHI sites of pDG141	This study
pDG159	MJ1271 NcoI/BamHI fragment from pDG152 cloned into same sites of pDG142	This study
pDG160	MJ1271 PCR product cloned into NcoI/BamHI sites of pET-19b	This study
pDG163	MJ1277 PCR product cloned into NcoI/BamHI sites of pET-19b	This study
pDG164	MJ1277 NcoI/BamHI fragment from pDG157 cloned into same sites of pDG142	This study
pDG329	TDH NdeI/BamHI fragment from pTDH1 cloned into same site of pET-19b	This study
pMYL1	MJ0720 PCR product obtained using primers MJ0720Fwd and MJ0720Rev cloned into NdeI/BamHI sites of pET-19b	This study
pTDH1	<i>Pseudomonas putida</i> R-TDH in pET-3a	67

### 2.2.3. Protein expression and purification

*E. coli* BL21(DE3) strains transformed with expression vectors were grown in Luria broth containing appropriate antibiotics at 37°C with shaking at 250 rpm. Cells containing pCDF-Duet1 derivatives were grown in the presence of streptomycin (50 µg ml<sup>-1</sup>). Cells containing pET-19b derivatives were grown in the presence of ampicillin (100 µg ml<sup>-1</sup>). When cultures reached an optical density at 600 nm of 0.6 to 0.8 protein expression was induced by the addition of α-D-lactose (1%, wt/vol) and shaking was continued at 20°C for 15 h. Cells were harvested by centrifugation and stored at -20°C.

### 2.2.4. Protein purification

The MJ0499 and MJ1277 proteins were copurified from cells containing pDG164 by heat treatment, followed by anion-exchange chromatography. *E. coli* cells containing heterologously expressed protein were suspended in 20 mM Tris-HCl (pH 8.0), lysed by passing through a French pressure minicell at 8,000 lb/in<sup>2</sup> (Thermo Electron), and sonicated on ice for 2 min using a Sonifier 450 with a microtip (15 W, 30% duty; Branson) to reduce viscosity. Lysates were clarified by centrifugation (14,000 X g for 10 min at 4°C), and the supernatant was stored on ice. This heat-stable protein was applied to a 5-ml HiTrap desalting column (GE Healthcare) equilibrated with 20 mM Tris-HCl (pH 8.0). Fractions containing desalted protein were pooled and applied to a 5-ml HiTrap DEAE FF column (GE Healthcare) equilibrated in 20 mM Tris-HCl (pH 8.0). Chromatography was performed using an ÄKTApriime system (GE Healthcare) at a flow rate of 5 ml min<sup>-1</sup>. Protein was eluted from the column with a linear gradient to 0.5 M NaCl-20mM Tris-HCl (pH 8.0) over 20 min. Fractions containing the target protein were identified by absorbance at 280 nm and sodium dodecyl sulfate polyacrylamide gel electrophoresis (SDS-PAGE). Fractions containing the proteins of interest were

combined, loaded into SpectraPor4 dialysis tubing (molecular mass cutoff = 14,000), and dialyzed overnight in 2 liters of buffer containing 20 mM Tris-HCl (pH 8.0 at 4°C). The protein was transferred to fresh buffer and dialyzed for 5 h. Protein was concentrated inside the dialysis tubing using polyethylene glycol (20,000 Da). The MJ1003-MJ1277 and MJ1003-MJ1271 proteins were copurified from cells containing pDG141 and pDG163 and pDG160 and pDG152, respectively, as described above. Total protein concentration was determined using the Bio-Rad protein assay with bovine serum albumin as a standard.

The polyhistidine-tagged *M. jannaschii* IPMDH protein was purified by heat treatment followed by nickel affinity chromatography. *E. coli* (pMYL1) cells containing heterologously expressed protein were suspended in His-tag binding buffer containing 5 mM imidazole, 500 mM sodium chloride, and 20 mM Tris-HCl (pH 7.6), and cell extracts were prepared as described above. Extracts were heated at 60°C for 10 min, and the denatured protein was removed by centrifugation. The soluble protein was applied to a 5-ml HisTrap FF column (GE Healthcare) charged with NiCl<sub>2</sub> and equilibrated in His tag binding buffer at a flow rate of 5 ml min<sup>-1</sup>. Protein was eluted from the column with a linear gradient to 0.5 M imidazole, 0.5 M sodium chloride, and 20 mM Tris-HCl (pH 7.6) over 20 min. Fractions containing the target protein were combined and concentrated in a stirred ultrafiltration cell (Amicon) with a filter having a 10-kDa molecular mass cutoff (Pall) under nitrogen gas 4°C.

After concentration, the buffer was exchanged with 20 mM Tris-HCl (pH 7.6) in an ultrafiltration cell. The purified protein precipitated and lost activity during storage at 4°C. However, it could be stored in aliquots containing 20% glycerol, frozen at -40°C or -80°C, and thawed without significant loss of activity. Protein stored in this manner remained active for at least 2 weeks.

### **2.2.5. Analytical size exclusion chromatography**

Interactions between large and small subunits were tested by measuring apparent masses of protein pairs using size exclusion chromatography, as described previously [62]. The compositions of protein fractions were determined by SDS-PAGE with silver staining (Bio-Rad). Separations were performed aerobically on purified, unreconstituted apoenzymes.

### **2.2.6. Reconstitution of Fe-S centers**

Purified hydrolyase holoenzymes were reconstituted in 2-ml glass serum vial (Wheaton) containing a magnetic stir bar and sealed with a 13-mm butyl rubber stopper. All buffers and reagents were degassed under a continuous flow of argon for at least 10 min. Anaerobic transfers were performed using gastight syringes (Hamilton). For reconstitution, purified apoprotein (0.5 to 1.0 mg ml<sup>-1</sup>) was mixed with 50 mM Tris-HCl (pH 8.0) and 3 mM dithiothreitol [63]. The sealed solutions were placed in an ice-water bath at 0 to 4°C, and the solution was degassed with argon for 10 min while being stirred. To the reconstitution mixture, Fe(NH<sub>4</sub>)<sub>2</sub>(SO<sub>4</sub>)<sub>2</sub> · 6H<sub>2</sub>O was added to a final concentration of 0.5 mM. After 10 min, Na<sub>2</sub>S · 9H<sub>2</sub>O was added dropwise to a final concentration of 0.5 mM, and the reconstitution mixture was stirred under argon until maximum activity was observed (typically 2 h). The final reconstitution volume was 1 ml. Hydrolyase activity was monitored in a standard assay with 0.4 mM citraconate as described below.

### **2.2.7. Measurement of hydrolyase activities**

All continuous assays used a DU-800 spectrophotometer with a Peltier temperature-controlled sampler (Beckman). Reactions (1 ml) were conducted in quartz

semimicrocells with screw-cap septa (Starna), including 300 mM KCl, 10 mM MgCl<sub>2</sub>, 50 mM TES [N-tris(hydroxymethyl)methyl-2-aminoethanesulfonic acid]-KOH (pH 7.5), 2.5 or 10 µg ml<sup>-1</sup> reconstituted protein, and various substrate concentrations. The sealed quartz cell containing buffer and substrate was degassed under argon for 10 min and equilibrated at 60°C for 10 min. Reactions were initiated by the addition of reconstituted enzyme, and the change in UV absorbance was monitored at 60°C. Initial rates were measured from the linear portion of the reaction progress curve between 5 and 60 s. For α-isopropylmalate, β-isopropylmalate, and (*R*)-citramalate, the formation of the reaction intermediate was observed by measuring the increase in absorbance at 235 nm, as measured in the reaction buffer at 60°C with µg ml<sup>-1</sup> of reconstituted protein. The molar absorption coefficient at 235 nm ( $\epsilon_{235}$ ) for both citraconate and isopropylmaleate was 4,668 M<sup>-1</sup> cm<sup>-1</sup>. The hydration of citraconate and maleate was observed as a decrease in absorbance with 2.5 µg ml<sup>-1</sup> of reconstituted enzyme. Maleate hydration to produce malate was monitored at 235, 245, and 255 nm using molar absorption coefficients of 2,318, 1,297, and 582 M<sup>-1</sup> cm<sup>-1</sup>, respectively, measured in the reaction buffer at 60°C. Citraconate hydration was monitored at 235 nm, with a molar absorption coefficient of 4,530 M<sup>-1</sup> cm<sup>-1</sup>. Reaction progress curves were linear from 5 to 60 s. One unit of hydrolyase activity catalyzed the conversion of 1 µmol substrate to product per minute. Steady-state kinetic constants were estimated by nonlinear regression of initial rate data fit to the Michaelis-Menten-Henri equation using the KaleidaGraph program (Synergy Software).

### **2.2.8. Measurement of oxidative decarboxylation activities.**

The rate of oxidative decarboxylation catalyzed by IPMDH<sub>MJ</sub> was measured by monitoring the reduction of NAD<sup>+</sup> to NADH at 340 nm, assuming a molar absorption

coefficient for NADH of  $6,220 \text{ M}^{-1} \text{ cm}^{-1}$ . Assays were conducted aerobically in optical glass cuvettes (Starna) with 200 mM KCl, 10 mM  $\text{MgCl}_2$ , 50 mM TAPS [Tris(hydroxymethyl)methyl-3-aminopropanesulfonic acid]-KOH (pH 8.5), 5 mM  $\text{NAD}^+$ ,  $2.5 \text{ } \mu\text{g ml}^{-1}$  IPMDH<sub>MJ</sub>, and various substrate concentrations. Reaction mixtures were equilibrated at 60°C for 10 min, and reactions were initiated with  $\text{NAD}^+$ . Initial rates were measured using a linear portion of the reaction progress curve, from 5 to 60 seconds for  $\beta$ -isopropylmalate and 120 to 180 seconds for D-malate. One unit of enzymatic activity catalyzed the reduction of 1  $\mu\text{mol NAD}^+$  per min in a 1 ml reaction mixture. Apparent kinetic constants were estimated as described above.

#### **2.2.9. Coupled assay of dehydratase activity**

The  $\beta$ -hydrating activity of enzymes incubated with unsaturated intermediates was measured in reaction mixtures containing IPMDH<sub>MJ</sub> and  $\text{NAD}^+$  as described above. Reaction mixtures contained 300 mM KCl, 10 mM  $\text{MgCl}_2$ , 50 mM TES-KOH (pH 7.5),  $30 \text{ } \mu\text{g ml}^{-1}$  IPMDH<sub>MJ</sub>, 5 mM  $\text{NAD}^+$ , and various substrate concentrations. Reaction mixtures were made anaerobic and preincubated at 60°C as described above, before the addition of  $2.5 \text{ } \mu\text{g ml}^{-1}$  MJ0499/MJ1277 to initiate the reaction. Initial rates were measured between 5 and 60 seconds for citraconate and between 120 and 180 seconds for maleate.

#### **2.2.10. Identification of dehydratase reaction products**

Hydroxyacids and unsaturated carboxylic acids were derivatized with ethylchloroformate and analyzed by gas chromatography-mass spectrometry (GC-MS) [64]. Reaction products were mixed with ethylchloroformate in a solution of water-

trifluoroethanol-pyridine (60:32:8, vol/vol/vol) [65]. Derivatives were analyzed on a Finnigan MAT GCQ GC-MS with a DB-5MS capillary column (0.32 mm by 29 m, 0.5-mm film; J&W Scientific) and analyzed by chemical ionization MS in the positive mode, as described previously [62]. Using this method, the trifluoroethyl ester derivatives had the following retention times and mass spectral data. The molecular ion ( $MH^+$ ) is shown first, if observed (a minus sign indicates that  $MH^+$  was not found), followed by the base peak (*italics*), and characteristic fragment ions are listed in decreasing order of intensity. The derivatives were as follows: citraconate diester, 3.73 min (295, *195*, 275); (*R*)-citramalate, 3.87 min (-, *185*, 195, 275, 213); D-malate diester, 4.06 min (299, *171*, 261, 278, 199);  $\beta$ -isopropylmalate diester, 4.61 min (-, *199*, 213, 241);  $\alpha$ -isopropylmalate diester, 4.65 min (341, *213*, 195, 241, 321). In most spectra the base peak was assigned as the fragment ion following the neutral loss of  $CF_3CH_2OH$  or  $CH_3CH_2COOH$  from the molecular ion.

Alternatively, trimethylsilyl (TMS) derivatives of the hydroxycarboxylic acids were prepared by reacting dried sample with 50  $\mu$ l *N*-methyl-*N*-(TMS)-trifluoroacetamide and 50  $\mu$ l pyridine in a sealed vial at 60°C for 20 min. Derivatives were analyzed by GC-MS as described above. The mass range scanned was 70-700 atomic mass units. The derivatives were as follows: citraconate-(TMS)<sub>2</sub>, 5.54 min (275, *185*, 149, 73, 259, 277, 73); citramalate-(TMS)<sub>3</sub>, 6.03 min (365, 247, 349, 321, 277, 73);  $\beta$ -isopropylmalate-(TMS)<sub>3</sub>, 6.30 (-, 275, 191, 377, 73);  $\alpha$ -isopropylmalate-(TMS)<sub>3</sub>, 6.35 (393, *213*, 275, 377, 73).

For quantitative analysis of reaction mixtures, carboxylic acids were separated by reversed-phase high-pressure liquid chromatography (HPLC). Reaction mixtures or standard compounds were applied to a Luna C<sub>18</sub>(2) column (4.6 by 150 mm, 5  $\mu$ M; Phenomenex) with a Security Guard ODS cartridge (4 by 3 mm; Phenomenex) that was



equilibrated in mobile phase containing 25 mM phosphoric acid and 2% (vol/vol) methanol (pH 2.5). Isocratic elution with this mobile phase was used at a flow rate of 1 ml min<sup>-1</sup> at 35°C. Samples (25 µl) were injected using a Beckman 508 autosampler. Organic acids were detected using a Beckman 168 photodiode array detector. Data were collected and chromatograms were integrated using the 32 Karat software (Beckman). Under these conditions, retention factors for standard compounds were 0.63 (D-malate), 0.97 (2-oxoglutarate), 1.4 (maleate), 2.1 (homoisocitrate), 2.0 (fumarate), 2.3 (*cis*-aconitate), 2.7 (*R*-citramalate), 2.7 (*trans*-aconitate), and 4.7 (citraconate), with a holdup time of 1.47 min. Less-polar compounds were resolved using a mobile phase containing 25 mM phosphoric acid and 30% (vol/vol) methanol (pH 2.5). Under these conditions, retention factors for standard compounds were 0.4 (*R*-citramalate), 0.7 (citraconate), 2.5 (β-isopropylmalate), 2.9 (α-isopropylmalate), and 4.2 (isopropylmaleate), with a holdup time of 1.55 min. Analyte concentrations were calculated from the integrated peak areas of the chromatogram at 220 nm absorbance using the method of standard additions.

#### **2.2.11. Stereochemical analysis of malate product.**

Tartrate dehydrogenase (TDH) [EC 1.1.1.93] was used to confirm the stereochemistry of IPMI hydration products. Plasmid pTDH1, which encodes the TDH enzymes from *Pseudomonas putida* ATCC 17642, was a gift from Paul Cook (University of Oklahoma) [66]. Dideoxynucleotide sequencing using T7 promoter and T7 terminator oligonucleotide primers identified several discrepancies with the originally published TDH sequence [67]. The NdeI/BamHI fragment of plasmid pTDH1 was subcloned into pET-19b to produce plasmid pDG329, which encodes TDH fused to an amino-terminal decahistidine tag. The His<sub>10</sub>TDH protein was expressed from pDG329 in *E. coli* BL21(DE3). Protein was purified by heating the extract at 50°C for 10 min, precipitating

the denatured protein, and isolating the His<sub>10</sub>TDH by nickel affinity chromatography as described above.

Reaction mixtures to determine the stereochemistry of malate produced by the malease activity of the MJ0499/MJ1277 combination contained 5 mM maleate, reconstituted MJ0499/MJ1277 protein (5 µg ml<sup>-1</sup>), and reaction buffer incubated at 60°C for 24 h. Portions of reaction product were added to an aerobic solution containing IPMI buffer salts, TDH (His<sub>10</sub>TDH; 20 µg ml<sup>-1</sup>), and 1 mM NAD<sup>+</sup> in a volume of 1 ml. After incubation at 37°C for 1 h, the absorbance of the solution at 340 nm was measured and D-malate product concentrations were calculated according to a linear standard curve from 5 to 200 µM D-malate. Another portion of the malease reaction product was analyzed using L-malate dehydrogenase (U.S. Biochemicals) in a 1-ml reaction mixture containing 20 µg ml<sup>-1</sup> enzyme, 100 µM phenazine methosulfate, 150 µM thiazolyl blue, and 1 mM NAD<sup>+</sup>. Reaction mixtures were incubated at room temperature for 30 min, the absorbance of the solution at 570 nm was measured, and L-malate concentrations were estimated according to a linear standard curve from 5 to 200 µM L-malate [68]. The limit of detection for this method was approximately 1.5 µM L-malate.

## **2.3. RESULTS**

### **2.3.1. Protein expression, purification, and subunit interaction.**

The MJ0499 and MJ1277 pair of proteins were heterologously expressed in *E. coli* and purified from the soluble cell lysate by heat treatment at 60°C followed by anion-exchange chromatography. MJ0499 and MJ1277 comprised approximately 90% of the resulting total protein, as estimated by SDS-PAGE and densitometry (Figure 2.4). The apparent mass of MJ0499 was 44 kDa, matching the theoretical mass of 46.1 kDa.

Likewise, the apparent mass of MJ1277 correlated well with its theoretical mass (16 kDa and 18.4 kDa, respectively). The large and small subunits coeluted during analytical size exclusion chromatography with a Stokes radius of 42 Å, corresponding to a 143 kDa protein (Figure 2.5). Therefore, the MJ0499/MJ1277 pair probably associates as a heterotetramer of two large and two small subunits. The purified MJ1003/MJ1277 pair of proteins coeluted with a Stokes radius of 43 Å, corresponding to a heterotetrameric complex with a molecular mass of 153-kDa (Figure 2.5). The MJ0499 and MJ1271 subunits did not copurify during anion-exchange chromatography and eluted as monomers during size exclusion chromatography.

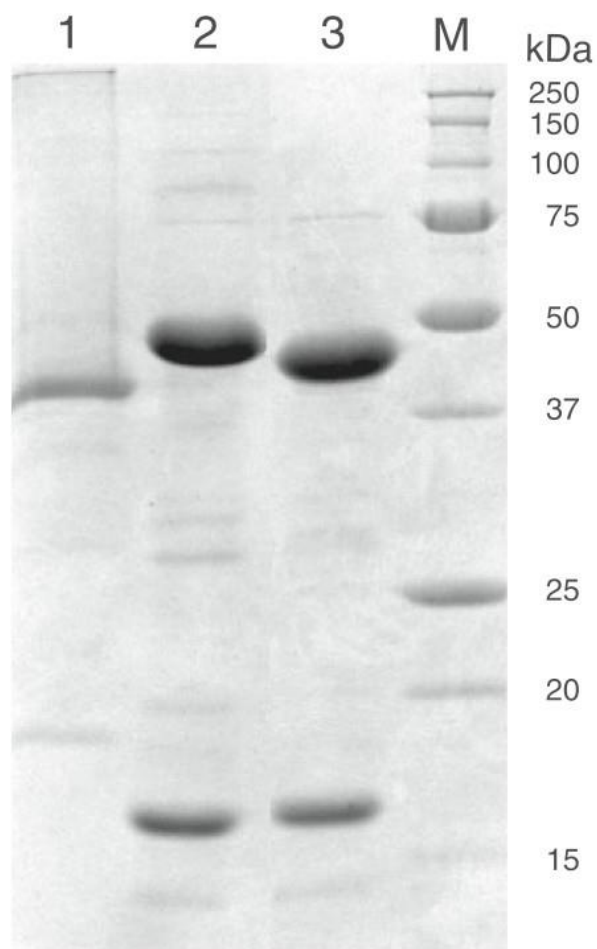


**Figure 2.4. Purified IPMDH<sub>MJ</sub> and combinations of large and small subunits of the hydrolyase apoenzymes.** Lane 1, 8 µg His<sub>10</sub>MJ0720 (IPMDH<sub>MJ</sub>); lane 2, 10 µg MJ1003-MJ1277; lane 3, 10 µg MJ0499-MJ1277; lane M, protein size markers (Bio-Rad). Proteins were separated by SDS-PAGE on a 15% acrylamide gel and stained with Coomassie blue.

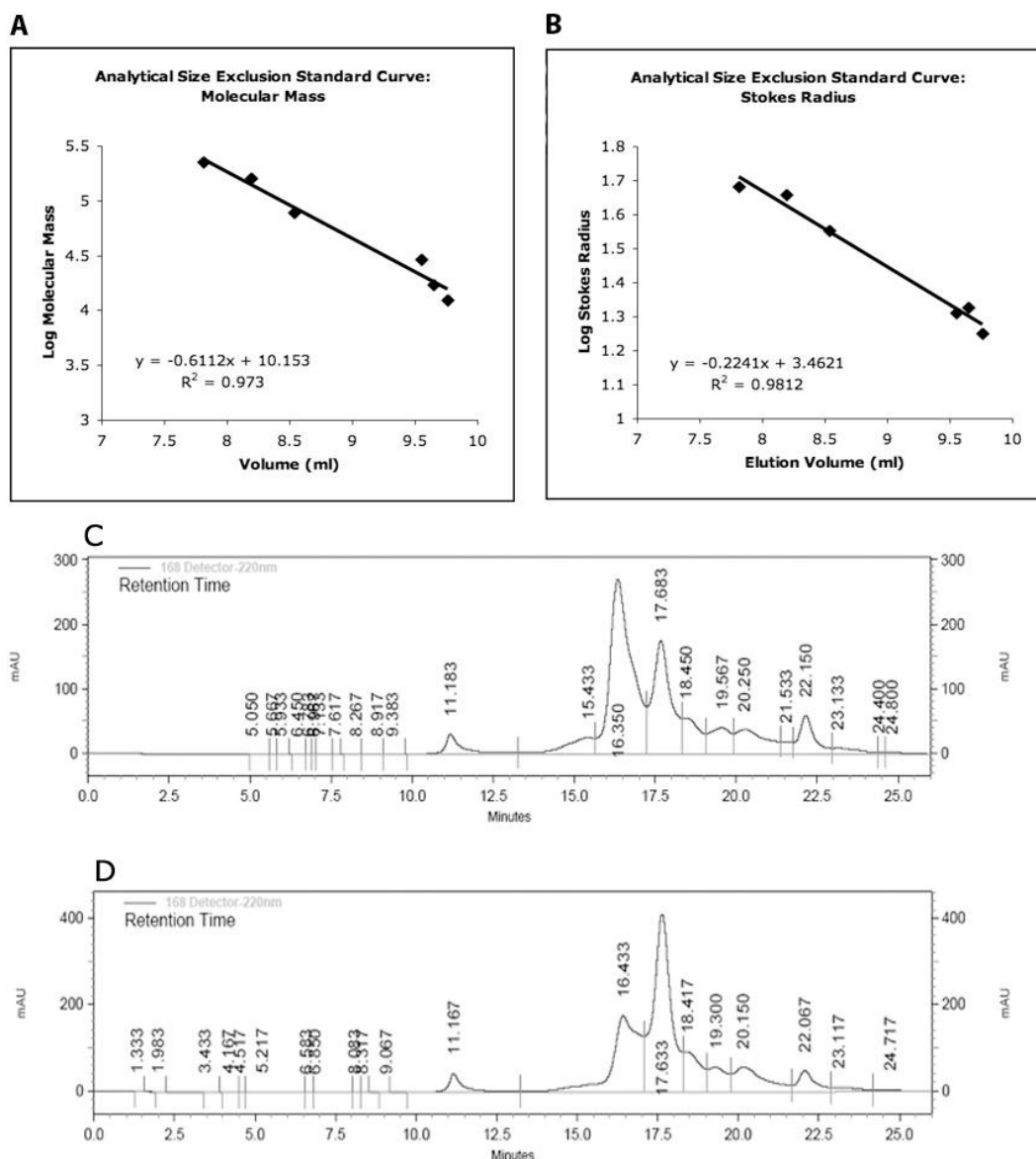


**Figure 2.5 MJ0499-MJ1277 and MJ1003-MJ1277 Subunit Interaction.** Proteins were separated by analytical size exclusion chromatography HPLC with UV absorbance detection at 220nm in milli-absorbance units (mAU). Standard curves based on elution volume with respect to (A) molecular mass and (B) Stokes radius of the following standards: cytochrome c, myoglobin, carbonic anhydrase, conalbumin, alcohol dehydrogenase, aldolase, and  $\beta$ -amylase. (C) Chromatogram of 1  $\mu\text{g ml}^{-1}$  purified MJ1003-MJ1277. The peak at 16.350 min corresponds to MJ1003-MJ1277, as confirmed by SDS-PAGE. (D) Chromatogram of 1  $\mu\text{g ml}^{-1}$  purified MJ0499-MJ1277. The peak at 16.433 min corresponds to MJ0499-MJ1277, as confirmed by SDS-PAGE.

### 2.3.2. Reconstitution of iron-sulfur clusters

Members of the aconitase family of proteins require an active site iron-sulfur cluster. These clusters are sensitive to oxidants, such as hydrogen peroxide, oxygen, and superoxide [69]. Therefore, the aerobic purification of MJ0499/MJ1277 resulted in an inactive enzyme (apoenzyme), i.e. the hydration of citraconate was not observed. The cluster was chemically reconstituted by incubating the apoenzyme with iron and sulfide under anaerobic reducing conditions. The reconstituted enzyme possessed a broad peak between 400 to 450 nm, indicative of an iron-sulfur cluster [70,71].

### 2.3.3. Identification of the citramalate/isopropylmalate isomerase

The reconstituted MJ0499/MJ1277 was identified as the hydrolyase responsible for hydration of citraconate in the pyruvate pathway to 2-oxobutyrates. This enzyme catalyzed the hydration of 300  $\mu$ M citraconate with a specific activity of 15 units  $\text{min}^{-1} \text{mg}^{-1}$ , and the reaction products, citramalate and  $\beta$ -methylmalate, were identified by reversed-phase HPLC. MJ0499/MJ1277 also catalyzed the dehydration of (*R*)-citramalate,  $\alpha$ -isopropylmalate, and the hydration of  $\beta$ -isopropylmalate, thus establishing this protein pair as the citramalate/isopropylmalate isomerase involved in both isoleucine and leucine biosynthesis. The hydration of the minimal substrate maleic acid was also observed in a direct assay. No activity was observed in direct assays consisting the holoenzyme and the following compounds: fumarate, mesaconate, *cis*-aconitate, *trans*-aconitate, D-tartrate, L-tartrate, L-malate, DL-isocitrate, citrate, (*R*)-homocitrate, and (*S*)-citramalate. Therefore, the MJ0499/MJ1277 requirements for substrate specificity consist of cis-unsaturated intermediates with  $\gamma$ -chain consisting of a methyl group, an isopropyl group, or the replacement of the  $\gamma$ -chain with hydrogen, as well as their D- $\alpha$ -hydroxy or  $\beta$ -hydroxy analogs. No activity was observed with the reconstituted

MJ1003/MJ1277 protein pair or a control reconstitution mixture containing no protein for any of the tested compounds.

The steady state kinetic parameters for the direct hydration and dehydration reactions catalyzed by MJ0499/MJ1277 were established from the initial rate data fit with the Michaelis-Menten-Henri equation (Figure 2.6 and Table 2.3). MJ0499/MJ1277 catalyzed the hydration of maleic acid with a five-fold increase in  $K_m$  over the hydration of citraconate and a two-fold increase in  $k_{cat}$ . However, the resulting specificity constants with these substrates were similar. The hydration of (*R*)-citramalate,  $\alpha$ -isopropylmalate, and the dehydration  $\beta$ -isopropylmalate were catalyzed at a rate 10 to 25% lower than for citraconate hydrolysis. The specificity constants were also considerably lower for these compounds. MJ0499/MJ1277 recognizes the  $\alpha$ -hydroxyacids with specificity constants two orders of magnitude lower than that of citraconate and one order of magnitude for  $\beta$ -isopropylmalate.

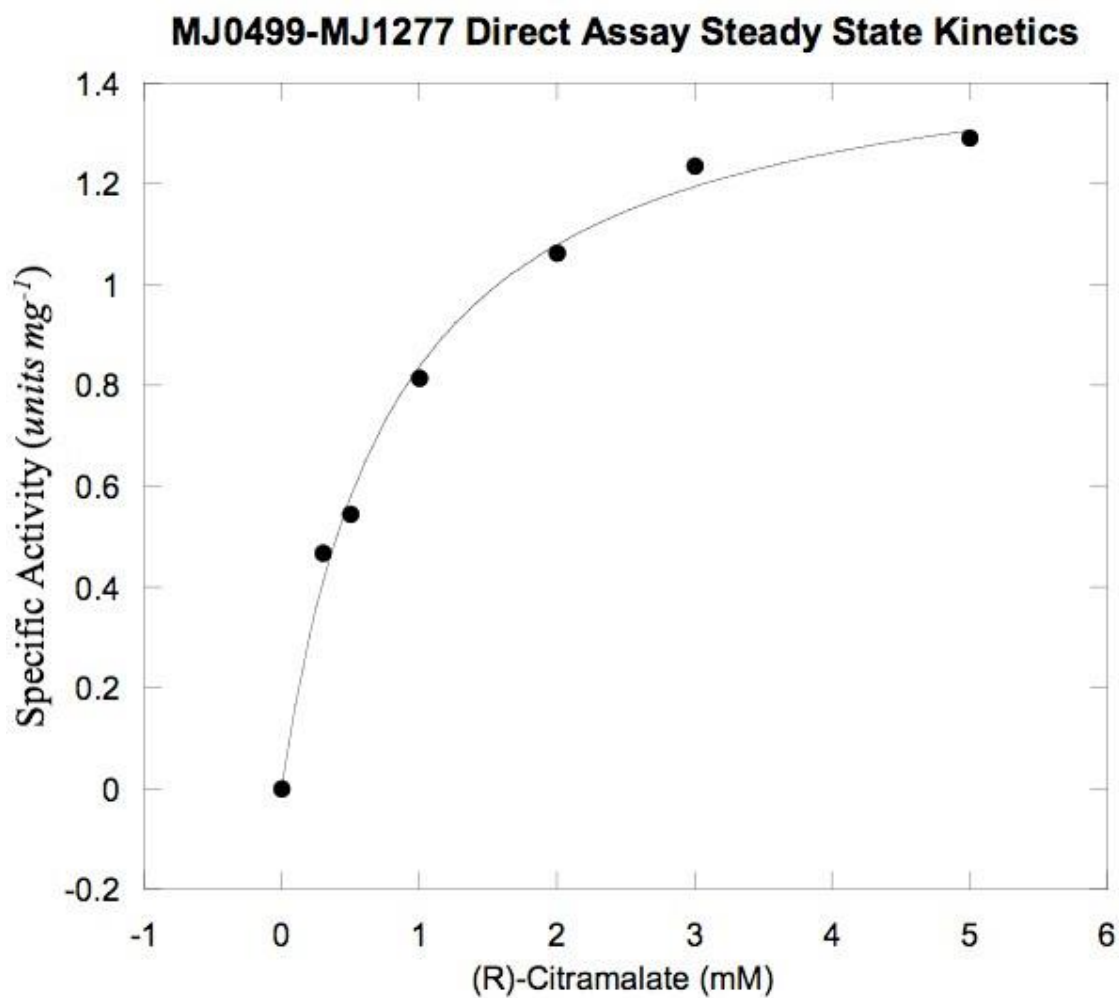


**Figure 2.6. Representative of the steady-state kinetics of MJ0499-MJ1277.** Steady-state kinetic constants for MJ0499-MJ1277 were estimated by nonlinear regression of initial rate data fit to the Michaelis-Menten-Henri equation, as described in the text.



Equilibrium constants were established for the citraconate hydration and  $\beta$ -isopropylmalate dehydration reactions from the anaerobic incubation of 5  $\mu\text{g ml}^{-1}$  reconstituted MJ0499/MJ1277 with 2 mM of either substrate at 60°C for 24 h. Citramalate could not be separated from  $\beta$ -methylmalate under the HPLC conditions used. Therefore, the equilibrium ratio of citramalate (with  $\beta$ -methylmalate) to citraconate was measured as 50:1. The three substrates of MJ0499/MJ1277 in the isopropylmalate pathway,  $\alpha$ -isopropylmalate,  $\beta$ -isopropylmalate, and dimethylcitraconate, were identified as separate peaks with an equilibrium ratio of 9:30:1, averaged from two analyses. The products of this reaction were confirmed as their TMS derivative by GC-MS.

The equilibrium ratio of malate to maleic acid was estimated to be 146:1 in a reaction mixture consisting of 2 mM maleic acid and 5  $\mu\text{g ml}^{-1}$  reconstituted MJ0499/MJ1277. No malease activity was observed in a similar reaction with the addition of 5 mM D-malate and maleic acid was not measured after incubating 2 mM D-malate with reconstituted MJ0499/MJ1277. In a direct assay containing 200  $\mu\text{M}$  maleic acid and 2.5  $\mu\text{g ml}^{-1}$  reconstituted enzyme, the addition of 500  $\mu\text{M}$  D-malate resulted in 50% inhibition of malease activity. The same level of inhibition was reached in the presence of 5 mM L-malate. Therefore, the greater product inhibition of D-malate suggests that this is the correct enantiomer of the MJ0499/MJ1277 catalyzed hydration of maleic acid.

To identify the stereochemistry of the MJ0499/MJ1277 catalyzed hydration of maleic acid, L-malate dehydrogenase [EC 1.1.1.37] and TDH were used in discontinuous assays. L-Malate dehydrogenase catalyzes the stereospecific dehydrogenation of L-malate to oxaloacetate and TDH catalyzes the oxidative decarboxylation of D-malate, producing pyruvate [67]. Reaction mixtures consisting of 5  $\mu\text{g ml}^{-1}$  reconstituted MJ0499/MJ1277 were incubated under anaerobic conditions for 24 h at 60°C. Based on

standard curves generated from L-malate with L-malate dehydrogenase and D-malate with TDH, only D-malate was identified from the reaction mixture ( $5.07 \pm 0.05$  mM). No L-malate was identified above background ( $<8$   $\mu$ M). Therefore, D-malate is the sole product of maleic acid hydration by MJ0499/MJ1277.

**Table 2.3. Steady – state kinetic parameters for MJ0499 – MJ1277<sup>a</sup>.**

<b>Substrate</b>	<b><math>K_m</math> (<math>\mu</math>M)</b>	<b><math>V_{max}</math> (U mg<sup>-1</sup>)</b>	<b><math>k_{cat}</math> (s<sup>-1</sup>)</b>	<b><math>k_{cat}/K_m</math> (M<sup>-1</sup> s<sup>-1</sup>)</b>
<b>Citraconate<sup>b</sup></b>	80 $\pm$ 20	15 $\pm$ 0.9	16	2.0 X 10 <sup>5</sup>
<b>Citraconate<sup>c</sup></b>	20 $\pm$ 10	13 $\pm$ 0.7	14	3.5 X 10 <sup>5</sup>
<b>(R)-Citramalate<sup>b</sup></b>	810 $\pm$ 80	1.5 $\pm$ 0.05	1.6	2.0 X 10 <sup>3</sup>
<b><math>\alpha</math>-Isopropylmalate<sup>b</sup></b>	1900 $\pm$ 400	4.2 $\pm$ 0.3	4.5	2.4 X 10 <sup>3</sup>
<b><math>\beta</math> -Isopropylmalate<sup>b</sup></b>	39 $\pm$ 7	1.8 $\pm$ 0.1	1.9	5.0 X 10 <sup>4</sup>
<b>Maleate<sup>b</sup></b>	400 $\pm$ 50	34 $\pm$ 2	36	9.0 X 10 <sup>4</sup>
<b>Maleate<sup>b</sup></b>	180 $\pm$ 30	19 $\pm$ 0.9	20	1.1 X 10 <sup>5</sup>

<sup>a</sup>Kinetic parameters were estimated by nonlinear regression, and the standard errors of those parameters are shown. Turnover numbers were calculated assuming one active site per MJ0499/MJ1277 pair.

<sup>b</sup>Initial rates of hydrolyase activity were determined by measuring UV absorbance.

<sup>c</sup>Initial rates of hydratase activity were measured in a coupled assay for NADH production using excess IPMDH<sub>MJ</sub>.

#### **2.3.4. Characterizing isopropylmalate/ $\beta$ -methylmalate dehydrogenase.**

The IPMDH<sub>MJ</sub> was previously expressed and partially purified from *E. coli* cell extracts [44]. However, only  $\beta$ -isopropylmalate was tested as a substrate. To further characterize the IPMDH<sub>MJ</sub>, MJ0720 was heterologously expressed with an amino-terminal polyhistidine tag. The protein was purified to homogeneity by heat treatment followed by nickel affinity chromatography. The purified protein had a Stokes radius of 51 Å, as measured by analytical size exclusion chromatography, which corresponds to a molecular mass of 183 kDa. The denatured IPMDH<sub>MJ</sub> had an apparent mass of 40 kDa

(expected 39.1 kDa) according to SDS-PAGE analysis. Therefore, the native protein is probably a homotetramer. A mixture of MJ0499/MJ1277 and IPMDH<sub>MJ</sub> eluted separately from the size exclusion column, indicating no complex formation between the isomerase and the dehydrogenase.

The IPMDH kinetic parameters were measured in the previously described reaction conditions [44] (Figure 2.7 and Table 2.4) . Reactions were initiated upon addition of NAD<sup>+</sup> and the reaction progress curve was monitored as a change in absorbance at 60°C, corresponding to the production of NADH. IPMDH<sub>MJ</sub> catalyzed the oxidative decarboxylation of  $\beta$ -isopropylmalate and D-malate in the presence of NAD<sup>+</sup> but not NADP<sup>+</sup>, as previously observed. No activity above background was observed with the following compounds: L-malate, L-tartrate, D-tartrate, DL-isocitrate, or DL-lactate.

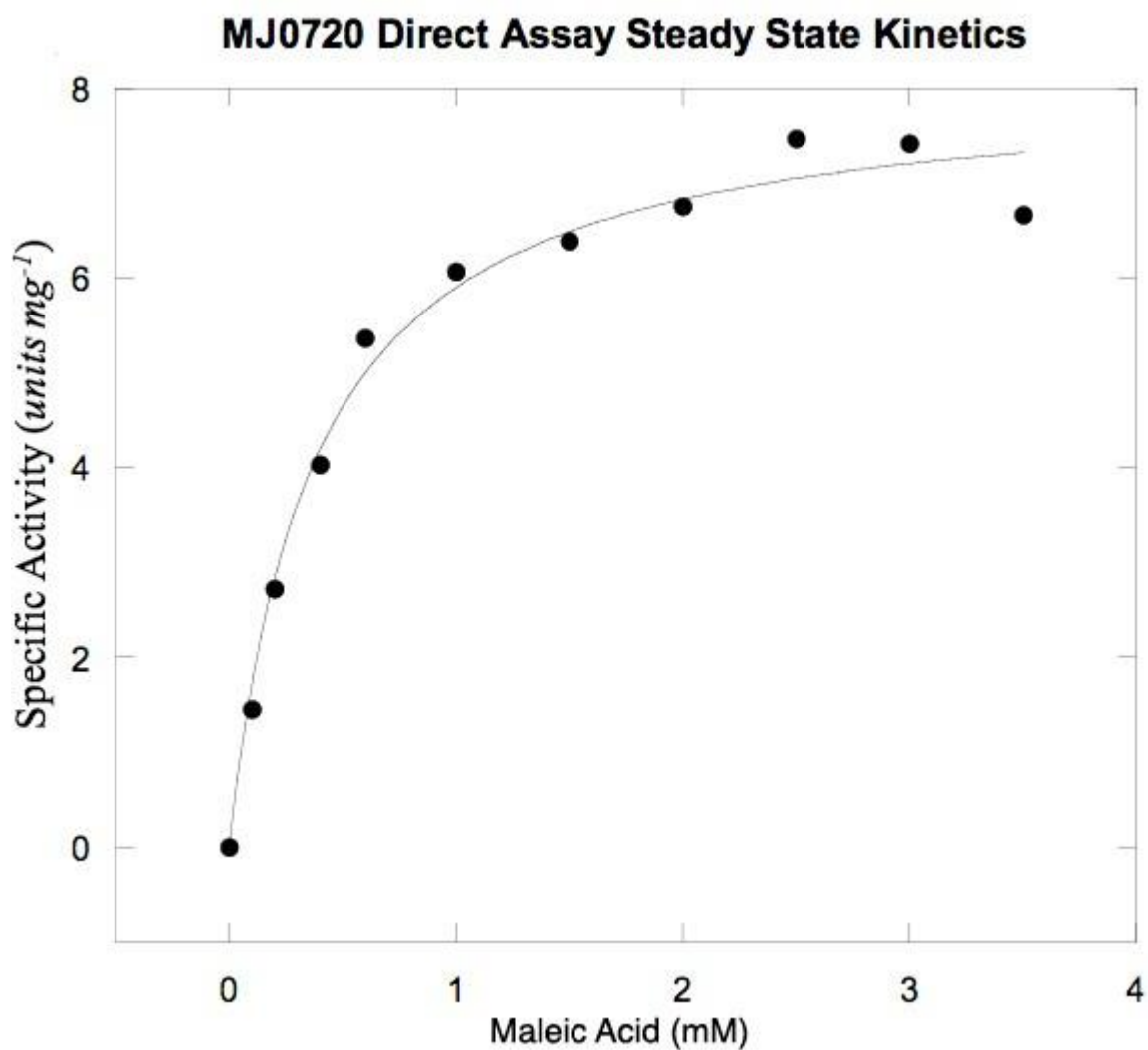


**Figure 2.7. Representative of the steady-state kinetics of MJ0720.** Steady-state kinetic constants for MJ0720 were estimated by nonlinear regression of initial rate data fit to the Michaelis-Menten-Henri equation, as described in the text.

**Table 2.4. Kinetic parameters for IPMDH homologs.**

Enzyme (reference)	$\beta$ -Isopropylmalate		D-Malate	
	$K_m$ ( $\mu$ M)	$k_{cat}/K_m$ ( $M^{-1} s^{-1}$ )	$K_m$ ( $\mu$ M)	$k_{cat}/K_m$ ( $M^{-1} s^{-1}$ )
IPMDH <sub>MJ</sub> <sup>a</sup>	24 $\pm$ 3	$8.8 \times 10^4$	410 $\pm$ 40	$1.4 \times 10^4$
<i>Sulfolobus sp.</i> IPMDH (72)	1.2	$3.0 \times 10^6$	390	$1.0 \times 10^4$
<i>P. putida</i> TDH (67)	14	$1.1 \times 10^4$	60	$2.2 \times 10^5$
<i>T. thermophilus</i> IPMDH (73)	17	$1.4 \times 10^4$	1,510	$7.3 \times 10^3$

<sup>a</sup> Data from this work. Initial rates were determined by measuring an increase in absorbance at 340 nm due to NADH in reaction mixtures incubated at 60°C.

### 2.3.5. Coupled assay for $\beta$ -methylmalate oxidative decarboxylation

The IPMDH<sub>MJ</sub> required for methanogen leucine biosynthesis was proposed to also function as the  $\beta$ -methylmalate dehydrogenase in pyruvate pathway. However,  $\beta$ -methylmalate is not a commercially available substrate. Therefore, a coupled assay was established with MJ0499/MJ1277 and IPMDH<sub>MJ</sub>, producing the required  $\beta$ -hydroxyacid from the MJ0499/MJ1277 catalyzed hydration of citraconate. To test the IPMDH catalyzed oxidative decarboxylation of  $\beta$ -methylmalate, anaerobic reactions containing citraconate, NAD<sup>+</sup>, and IPMDH<sub>MJ</sub> were equilibrated to 60°C followed by the addition of reconstituted MJ0499/MJ1277. The rate of  $\beta$ -methylmalate oxidative decarboxylation was measured as the oxidation of NAD<sup>+</sup> at 60°C.

The MJ0499/MJ1277 coupled assay conditions were optimized from standard reactions of 2.5  $\mu$ g ml<sup>-1</sup> MJ0499/MJ1277, 30  $\mu$ g ml<sup>-1</sup> IPMDH<sub>MJ</sub>, 1 mM NAD<sup>+</sup>, and 300  $\mu$ M citraconate (Figures 2.8 and 2.9). The requirement for the divalent metal cation Mg<sup>2+</sup> was observed up to 10 mM MgCl<sub>2</sub>; only 5% of the maximal activity was observed in the absence of MgCl<sub>2</sub>. Activity also increased with increasing concentrations of KCl, with a maximal activity at 300 mM. Citraconate was efficiently converted to 2-oxobutyrates over a broad pH range, from pH 6.0 to 8.0, with maximal activity at pH 7.5. The activity

of the two enzymes increased from 50°C to a maximum at 70°C. However, 60°C was used for kinetic assays for technical reasons.

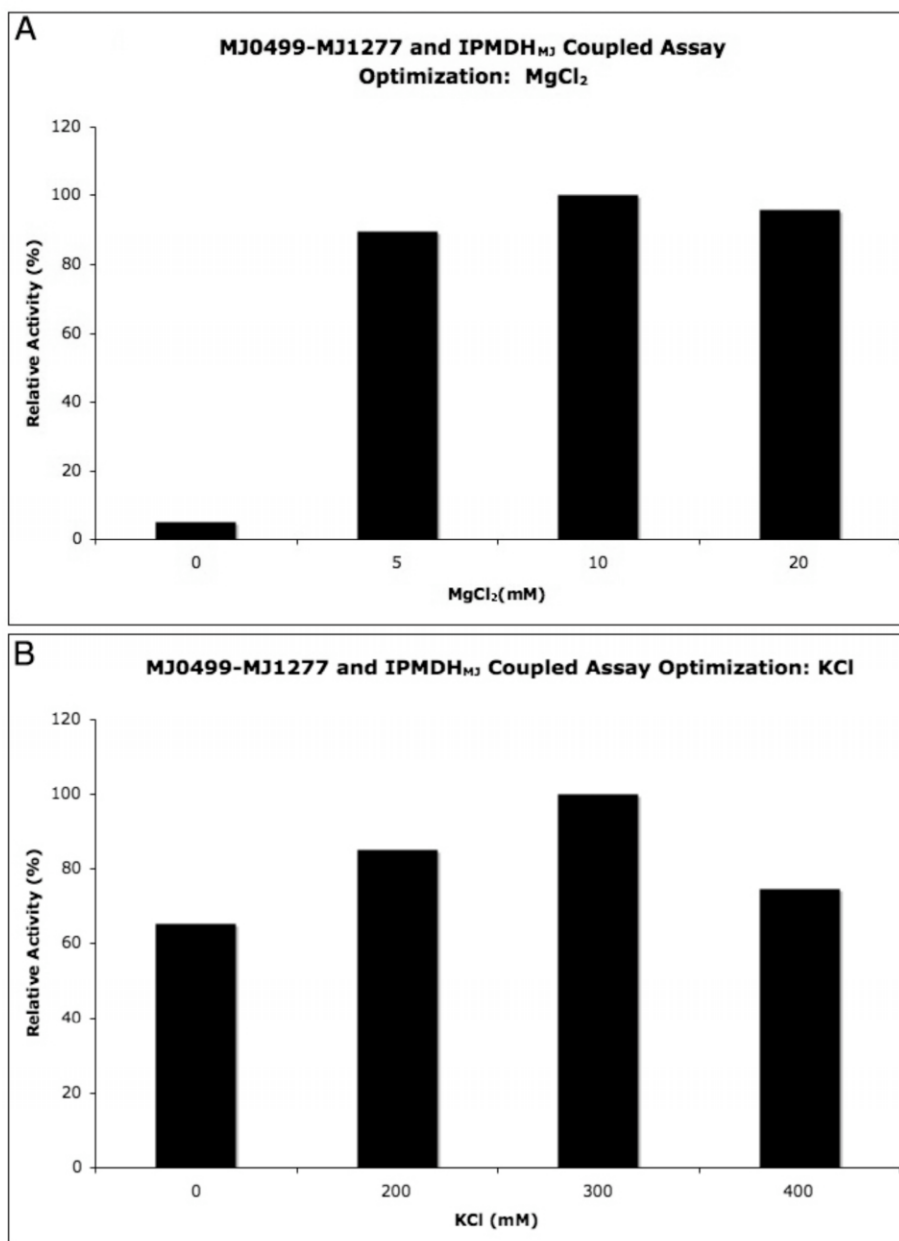


**Figure 2.8. MJ0499-MJ1277 and IPMDH<sub>MJ</sub> Coupled Assay Optimization: MgCl<sub>2</sub> and KCl.** The coupled assay was optimized based on the specific activity of 2.5 µg ml<sup>-1</sup> reconstituted MJ0499-MJ1277 with 30 µg ml<sup>-1</sup> IPMDH<sub>MJ</sub> and 200 µM citraconate. *A*, optimization of Mg<sup>2+</sup> concentration. *B*, optimization of KCl concentration.

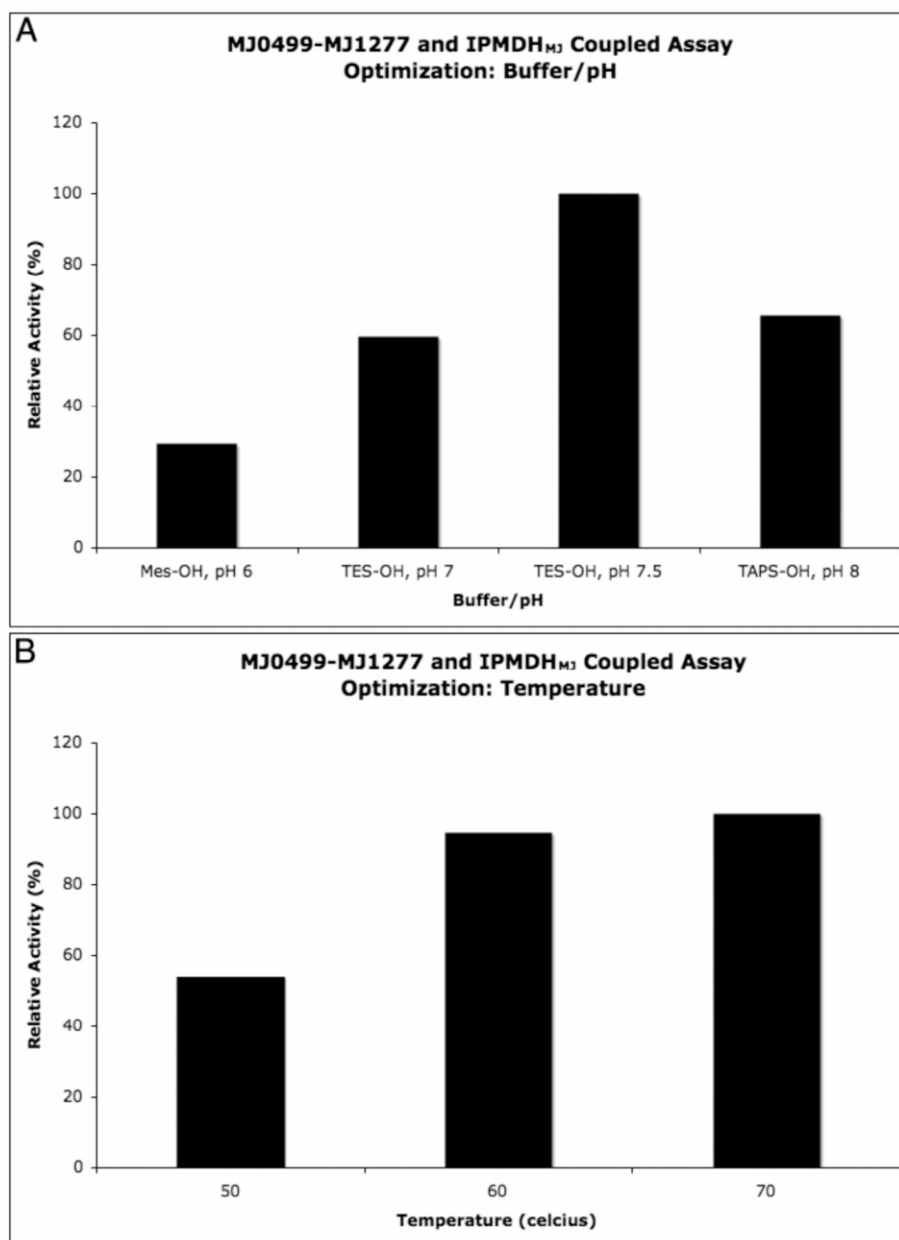


**Figure 2.9. MJ0499-MJ1277 and IPMDH<sub>MJ</sub> Coupled Assay Optimization: buffer, pH, and temperature.** The coupled assay was optimized based on the specific activity of 2.5 $\mu\text{g ml}^{-1}$  reconstituted MJ0499-MJ1277 with 30  $\mu\text{g ml}^{-1}$  IPMDH<sub>MJ</sub> and 200  $\mu\text{M}$  citraconate. A, optimization Buffer and pH. B, optimization reaction temperature.



The optimized coupled assay was used to estimate the apparent kinetic parameters for the hydration of unsaturated intermediates in the  $\beta$ -hydroxyacid direction (Table 2.3 and Figure 2.10). The rate of citraconate hydration to  $\beta$ -methylmalate was measured with similar Michaelis constants and rates in the direct assay. The hydration of maleic acid to D-malate was also measured with a similar specificity constant compared to the hydration of maleic acid by MJ0499/MJ1277 alone.

### MJ0499-MJ1277 and IPMDH<sub>MJ</sub> Coupled Assay Steady State Kinetics

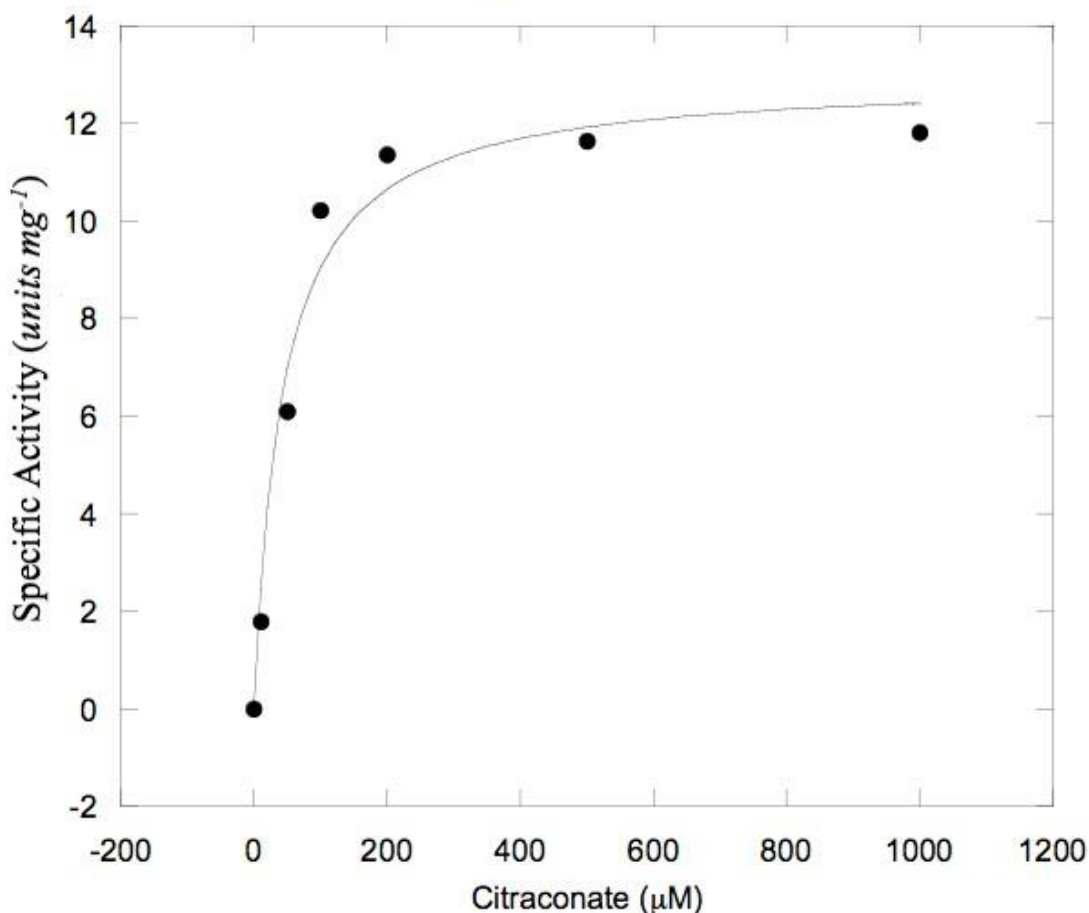


**Figure 2.10. Representative of the steady-state kinetics of MJ0499-MJ1277 and IPMDH<sub>MJ</sub> coupled assay.** Steady-state kinetic constants for MJ0499-MJ1277 with IPMDH<sub>MJ</sub> were estimated by nonlinear regression of initial rate data fit to the Michaelis-Menten-Henri equation, as described in the text.

## 2.4. DISCUSSION

The MJ0499/MJ1277 pair of proteins functions as the isopropylmalate/citramalate isomerase in methanogen leucine and isoleucine biosynthesis. The thermostable enzyme exhibits optimal activity at higher temperatures over a broad pH range. No activity above background was observed for the aerobically purified IPMI. Activity was measured after incubating the apoprotein with iron and sulfide under anoxic conditions, consistent with [Fe-S] cluster containing proteins. IPMI<sub>MJ</sub> catalyzes similar chemistry to mACN and sequence alignments indicate similar structural organization between the two enzymes. The large subunit, MJ0499, is homologous to domains 1, 2, and 3 of mACN containing most of the active site residues, including the three cysteine residues required for binding the [4Fe-4S] cluster [74]. The small subunit, MJ1277, is homologous to domain 4 of mACN. Gel filtration analysis of the interacting pair suggests a heterotetramer of two large and two small subunits. The *S. cerevisiae* IPMI is a monomer while the *Neurospora sp.* IPMI functions as a trimer or tetramer. The two *P. pseudoalcaligenes* malease subunits interact as a dimer [75]. Further studies of the IPMI<sub>MJ</sub> will be required to determine the actual shape and subunit interaction of the apoprotein as well as the holoenzyme.

MJ0499/MJ1277 catalyzes the dehydration of (*R*)-citramalate and  $\alpha$ -isopropylmalate with similar specificity constants, as measured in direct assays. The specific activity of  $\alpha$ -isopropylmalate dehydration (4.2 U mg<sup>-1</sup>) is similar to the reported *S. cerevisiae* IPMI activity (6 U mg<sup>-1</sup>) [59]. However, the  $k_{cat}/K_m$  values are approximately two orders of magnitude lower than the hydration of citraconate and maleic acid. The hydrolysis of these *cis*-unsaturated intermediates is favorable, as observed from equilibrium studies. The calculated  $\Delta G'^{\circ}$  for the hydration of maleic acid by IPMI<sub>MJ</sub> was -14 kJ mol<sup>-1</sup> (at 60°C), which is consistent with the *P. pseudoalcaligenes*

malease ( $-19 \text{ kJ mol}^{-1}$  at  $23^{\circ}\text{C}$ ) [76]. The direct assay for citraconate hydration measures formation of (*R*)-citramalate and  $\beta$ -methylmalate. A coupled assay with IPMI<sub>MJ</sub> and IPMDH<sub>MJ</sub> was developed to measure only hydration of citraconate to  $\beta$ -methylmalate, allowing for the comparison of kinetic parameters with the direct assay. The Michaelis constant and turnover were similar between the two assays with citraconate as the substrate, suggesting that  $\beta$ -methylmalate is the dominant product in the direct assay.

Maleate hydratases [EC 4.2.1.31] catalyze the stereospecific *trans*-addition of water to maleic acid, producing D-malate [70]. These enzymes have been isolated as either a monomer or a dimer consisting of a large and small subunit [75]. The hydratase activity of most maleases requires the addition of iron and sulfide under reducing conditions, consistent with enzymes that require an iron-sulfur cluster for catalysis, such as mACN or IPMI. However, the isolated *P. pseudoalcaligenes* maleate hydratase was colorless and resistant to oxidation and metal chelators [75]. Also, the presence of iron inhibited the activity of the enzyme. Therefore, the *P. pseudoalcaligenes* malease may not require an iron-sulfur cluster for activity. In addition to functioning as the citramalate/isopropylmalate isomerase, the IPMI<sub>MJ</sub> also catalyzed the hydration of maleic acid to D-malate. The  $K_m$  value for maleic acid hydration was similar to previously reported value for the *P. pseudoalcaligenes* maleate hydratase (400 and 350  $\mu\text{M}$ , respectively). The *P. pseudoalcaligenes* enzyme also catalyzed the hydration of citraconate, though with a  $K_m$  approximately twice that of IPMI<sub>MJ</sub> (200  $\mu\text{M}$  and 80  $\mu\text{M}$ , respectively) [75].

The IPMI<sub>MJ</sub> is involved in both the isomerization of  $\alpha$ -isopropylmalate as well as (*R*)-citramalate for the production of leucine and isoleucine, respectively. IPMDH<sub>MJ</sub> also functions in leucine and isoleucine biosynthesis, catalyzing the oxidative decarboxylation of  $\beta$ -isopropylmalate with similar specificity constants to the *T. thermophilus* IPMDH

and *P. putida* TDH [67,73]. The *Sulfolobus sp* IPMDH had a 20-fold lower  $K_m$  for  $\beta$ -isopropylmalate and a specificity constant two orders of magnitude greater than IPMDH<sub>MJ</sub> [72]. However, the  $K_m$  and specificity constants for D-malate were almost identical for IPMDH<sub>MJ</sub> and IPMDH from *Sulfolobus sp*. The *T. thermophilus* IPMDH was less proficient with D-malate as a substrate, having a  $K_m$  four times greater than *M. jannaschii* and *Sulfolobus sp*. The *M. jannaschii* IPMDH was also observed to oxidatively decarboxylate  $\beta$ -methylmalate to produce 2-oxobutyrates, as observed in the coupled assay with IPMI<sub>MJ</sub> and citraconate as the substrate. Thus, IPMI<sub>MJ</sub> and IPMDH<sub>MJ</sub> are broad specificity enzymes, recognizing substrates with small hydrophobic  $\gamma$ -chains. The involvement of these two enzymes in leucine and isoleucine biosynthesis is consistent with yeast strains with mutations in threonine dehydratase and *Serratia marcescens* isoleucine auxotrophs, both of which produced isoleucine via the pyruvate pathway [77]. Therefore, the IPMS and CMS are the only enzymes specific for their respective pathways.

## Chapter 3: Enzymology of the *M. jannaschii* Homoaconitase Involved in Coenzyme B Biosynthesis

### 3.1. INTRODUCTION

Two pathways for lysine biosynthesis have evolved: the diaminopimelate pathway of lower fungi, plants, most bacteria and some archaea, and the  $\alpha$ -aminoadipate pathway in higher fungi, euglenoids, some bacteria and archaea. No organism has been identified utilizing both pathways. Despite possessing homologs of the first three enzymes in the  $\alpha$ -aminoadipate pathway, methanogens generate lysine via the diaminopimelate intermediate [78]. Methanogen homocitrate synthase (HCS), homoaconitase (HACN), homoisocitrate dehydrogenase (HICDH) are instead proposed for the synthesis of 2-oxosuberate required for the heptanoyl group of CoB [11,39]. The gene products of *Methanocaldococcus jannaschii* MJ0503 and MJ1596 were previously identified as the HCS and HICDH, respectively [11].

HCS<sub>MJ</sub> belongs to the acetyltransferase family of proteins that includes isopropylmalate synthase (IPMS), citrate synthase (CS), citramalate synthase (CMS), malate synthase (MS), and HCS from the  $\alpha$ -aminoadipate pathway. These enzymes catalyze the condensation of acetyl-CoA with their respective 2-oxoacid substrates to produce an  $\alpha$ -hydroxyacid. Members of the acyltransferase family have only been observed to catalyze the formation of one product, although their respective products differ in stereochemistry [57,58,80,81].

HCS<sub>MJ</sub> is a homolog of the  $\alpha$ -aminoadipate HCS, sharing more than 30% identity and 50% similarity to the *Saccharomyces cerevisiae* and *Thermus thermophilus* HCS.

Only (*R*)-homocitrate was produced from the *S. cerevisiae* HCS [80]. However, a study using *Methanosarcina thermophila* cell extracts identified *trans*-homoaconitate and (*S*)-homocitrate as the products of the HCS<sub>MJ</sub> catalyzed reaction of 2-oxoglutarate with acetyl-CoA (Figure 3.1) [39]. The *MJ0503* gene has since been annotated as a *trans*-homoaconitate synthase. In subsequent reactions, HCS<sub>MJ</sub> only catalyzed the production of (*R*)-homo<sub>2</sub>citrate and (*R*)-homo<sub>3</sub>citrate and no other *trans* isomers were identified (Figure 3.1) [39]. (*R*)-Homocitrate is also a component of the iron-molybdenum cofactor of nitrogenase in some bacteria and methanogens, further implying that (*S*)-homocitrate is not the correct enantiomer of the first HCS<sub>MJ</sub> product [81]. Previous attempts to heterologously express HCS<sub>MJ</sub> from *E. coli* resulted in mostly insoluble protein (Drevland and Graham, unpublished results). Therefore, the intermediates from the first committed step of CoB biosynthesis are currently unknown.

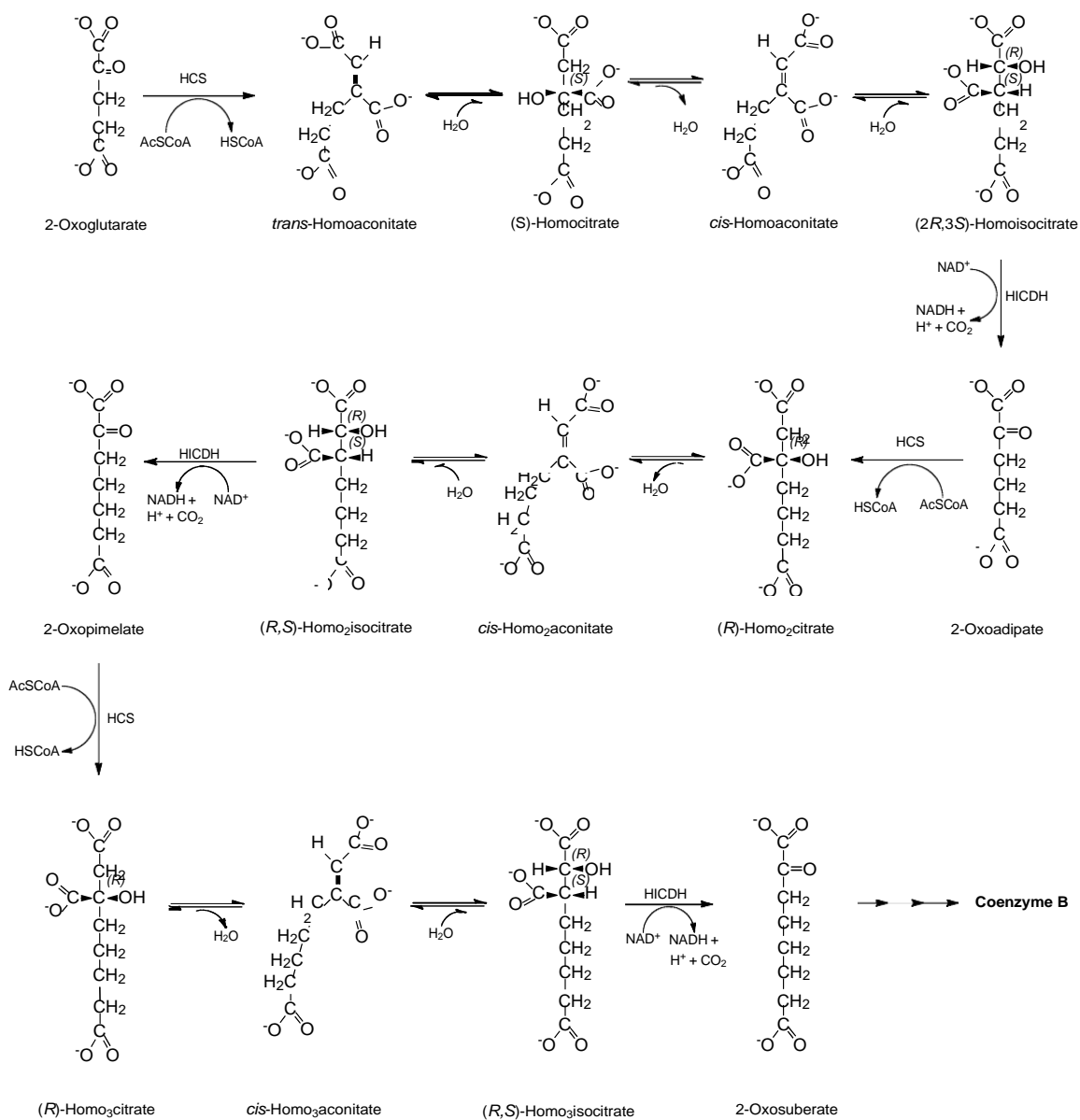


**Figure 3.1. Initially proposed 2-oxoacid chain elongation pathway for coenzyme B biosynthesis.**

HICDH is a member of the NAD(P)-dependent  $\beta$ -hydroxyacid oxidative decarboxylase family, including isocitrate dehydrogenase (ICDH), isopropylmalate dehydrogenase (IPMDH), tartrate dehydrogenase (TDH), and 6-phosphogluconate dehydrogenase (6-PGDH) [EC1.1.1.43]. HICDH catalyzes the oxidation and decarboxylation of (2*R*, 3*S*)-homoisocitrate, forming 2-oxoadipate in a random steady state kinetic mechanism that is consistent among members of this family [82]. The *M. jannashii* HICDH was previously reported to oxidatively decarboxylate (2*R*,3*S*)-homoisocitrate, (2*R*,3*S*)-homo<sub>2</sub>isocitrate, and (2*R*,3*S*)-homo<sub>3</sub>isocitrate with similar  $K_m$  and turnover numbers, although isocitrate was not a substrate [44]. Though broad substrate specificity of HICDH<sub>MJ</sub> is required for the CoB chain elongation pathway, such specificity is not unique to methanogens. *S. cerevisiae* and *Deinococcus radiodurans* HICDHs recognized a number of substrate analogs, including homo<sub>2</sub>isocitrate and homo<sub>3</sub>isocitrate, although with Michaelis constants approximately ten-fold higher than HICDH<sub>MJ</sub> [83].

HACNs are members of the aconitase family of hydrolyases possessing an oxygen sensitive iron-sulfur cluster required for catalysis [69]. Homoaconitase activity was initially observed during early studies of yeast lysine biosynthesis [84,85]. Homocitrate and *cis*-homoaconitate were identified from *S. cerevisiae* lysine auxotrophs grown in the presence of labeled <sup>14</sup>C-acetyl-CoA or <sup>14</sup>C-glucose [85,86]. The enzymatic oxidative decarboxylation of homoisocitrate to 2-oxoadipate was also observed from *S. cerevisiae* cell extracts [87,88]. The similarity of these intermediates and enzymatic activities to reactions of the TCA cycle suggested an aconitase-type enzyme was responsible for the isomerization of homocitrate to homoisocitrate. Indeed, the hydration of *cis*-homoaconitate to isohomocitrate was observed from *S. cerevisiae* cell extracts as well as the enzymatic dehydration of isohomocitrate to the unsaturated intermediate. The



hydration of *cis*-homoaconitate was separated from the activity of aconitase, indicating the presence of a separate enzyme, homoaconitase [84].

After the initial identification of HACN from *S. cerevisiae*, homologs were identified from *Aspergillus sp.*, *Pyrococcus horikoshii*, and *T. thermophilus* [89,90,91]. HACNs are either monomeric (fungal) or heterodimeric (bacteria and archaea) proteins with a molecular mass of approximately 60-80 kDa. Despite the homology to ACN and IPMI, genetic and biochemical studies of the *S. cerevisiae* and *A. nidulans* HACNs (Lys4 and LysF, respectively) have only identified the hydration of *cis*-homoaconitate to homoisocitrate (or the reverse dehydration reaction) from cell extracts; the initial dehydration of homocitrate has gone undetected [92]. The lack of homocitrate dehydratase activity was also confirmed from the purified *T. thermophilus* HACN [93]. Only homoisocitrate was observed as a product from the incubation of *cis*-homoaconitate with the thermophilic HACN and no activity was observed in a coupled assay with the *T. thermophilus* HICDH in the presence of (*R*)- or (*S*)-homocitrate. An aconitase was proposed to catalyze the initial dehydration reaction (Figure 3.2) [93].

The requirement of two aconitase-like enzymes for an isomerization reaction is not unprecedented. 2-Methylcitrate dehydratase [EC 4.2.1.79] only catalyzes the initial dehydration of (2*S*,3*S*)-methylcitrate to 2-methyl-*cis*-aconitate in fungal and bacterial propionate metabolism (Figure 3.2) [94]. Aconitase was proposed to complete the isomerization, catalyzing the hydration of 2-methyl-*cis*-aconitate to (2*R*,3*S*)-methylisocitrate. However, unlike the isomerization of (*R*)-homocitrate to (2*R*,3*S*)-homoisocitrate, the isomerization of (2*S*,3*S*)-2-methylcitrate results in reverse stereochemistry.

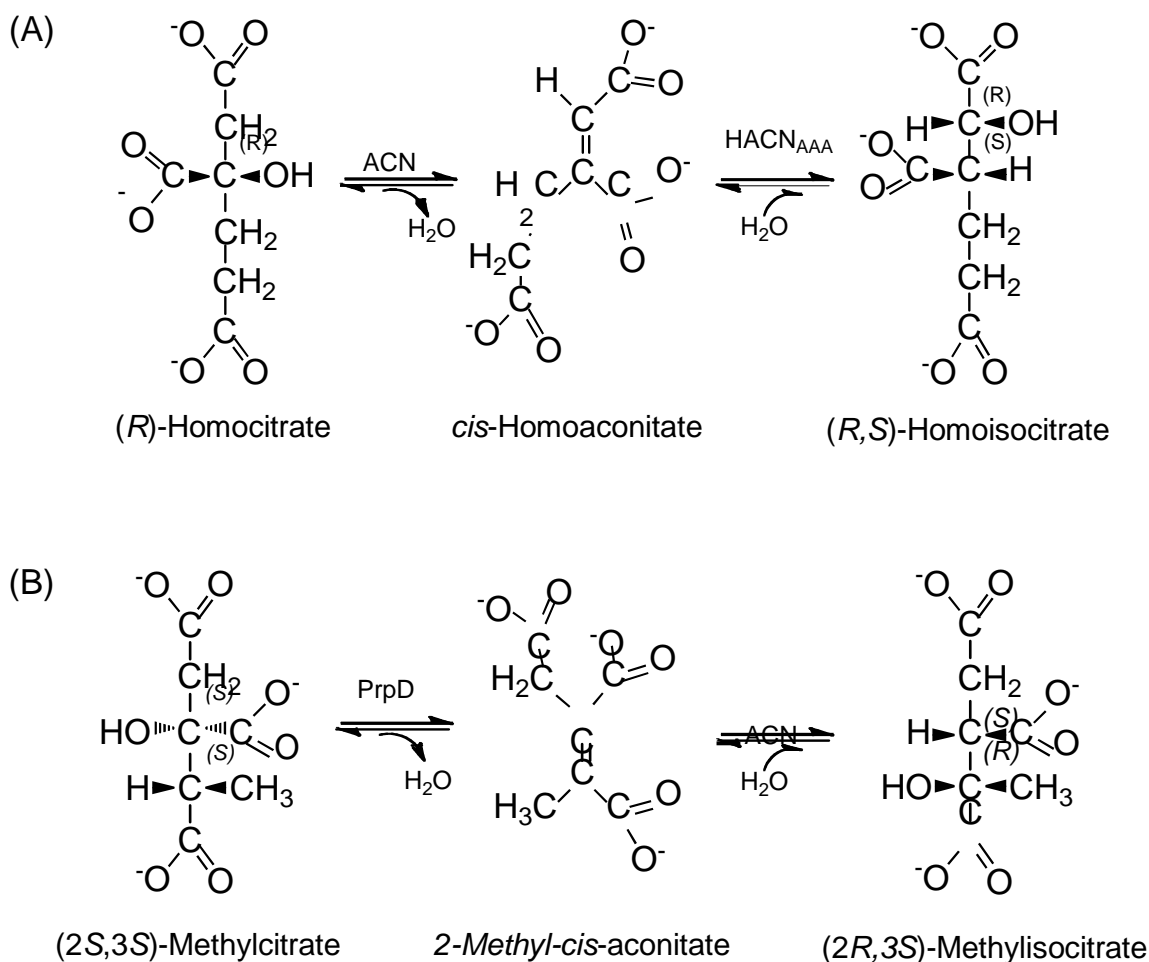


**Figure 3.2. Reactions involved in lysine biosynthesis and propionate metabolism.** (A) An aconitase is proposed to catalyze the dehydration of (*R*)-homocitrate to *cis*-homoaconitate. The  $\alpha$ -aminoadipate HACN ( $\text{HACN}_{\text{AAA}}$ ) catalyzes the second reaction, the hydration of *cis*-homoaconitate to (2*R*,3*S*)-homoisocitrate. (B) The *S. enterica* PrpD catalyzes the initial dehydration of (2*S*,3*S*)-methylcitrate for propionate metabolism. The *S. enterica* AcnA or AcnB enzyme catalyzes the hydration of 2-methyl-*cis*-aconitate to form (2*R*,3*S*)-methylisocitrate.

Although the HACN<sub>MJ</sub> was previously unidentified, it was predicted to differ from the  $\alpha$ -aminoadipate HACN because methanogens do not possess an aconitase. Therefore, one enzyme was proposed for the full isomerization of homocitrate, homo<sub>2</sub>citrate, and homo<sub>3</sub>citrate.

Methanogen genomes contain two copies of genes annotated as encoding large and small subunits of [4Fe-4S] dependent isopropylmalate isomerases (IPMIs). The large subunits (MJ0499 and MJ1003), homologous to domains 1, 2, and 3 of mitochondrial aconitase (mACN), and small subunits (MJ1271 and MJ1277), homologous to mACN domain 4, were predicted to interact to form the functional IPMI and HACN. To identify and characterize the genes encoding methanogen HACN, the four combinations of large and small subunits were heterologously expressed in *E. coli*. The MJ0499/MJ1277 pair of proteins was identified as the IPMI required for leucine and isoleucine biosynthesis (Chapter 2) [48].

In this study, the MJ1003/MJ1271 pair of proteins was identified as the HACN involved in CoB biosynthesis [49]. Direct assays showed that this reconstituted Fe<sub>4</sub>-S<sub>4</sub> enzyme catalyzed the hydration of *cis*-aconitate, *cis*-homoaconitate, *cis*-homo<sub>2</sub>aconitate, *cis*-homo<sub>3</sub>aconitate, and *cis*-homo<sub>4</sub>aconitate. The enzyme was also able to catalyze the production of D-malate from the minimal substrate maleic acid. In a coupled reaction with HICDH<sub>MJ</sub>, the homoaconitate analogs were converted to their corresponding 2-oxoacids, demonstrating that the homoisocitrate products are substrates for HICDH<sub>MJ</sub>. In contrast to previously studied HACN proteins, the methanogen enzyme catalyzed both dehydration of (*R*)-homocitrate to form *cis*-homoaconitate and the subsequent hydration reaction that forms homoisocitrate. Although (*S*)-homocitrate and *trans*-homoaconitate were initially identified as intermediates in the production of 2-oxoadipate, these compounds served as inhibitors of HACN<sub>MJ</sub>. Therefore, methanogen HACN cannot

catalyze all of the predicted dehydratase reactions in the originally proposed pathway for CoB biosynthesis.

## **3.2. MATERIALS AND METHODS**

### **3.2.1. Chemicals and Reagents**

(*R*)-Homocitrate (*S*)-homocitrate, and (2*R*,3*S*)-Homoisocitrate were synthesized by Yunhua Jia and Dr. David Palmer (University of Saskatchewan). *cis*-Homoaconitate, and the *cis*-homoaconitate analogs were chemically synthesized by Dr. David Graham.

### **3.2.2. Protein Expression and Purification**

The MJ1003 and MJ1271 proteins were coexpressed in an *E. coli* BL21(DE3) (pDG141 pDG163) strain described previously (Chapter 2). The cells were grown at 37°C with shaking at 250 rpm until the culture reached an optical density at 600 nm of 0.6-0.8. Expression was then induced by the addition of 50  $\mu$ M isopropyl-1-thio- $\beta$ -D-galactopyranoside, and the culture was transferred to a 16°C water bath and shaken continuously for 15-20 h. The MJ1003 and MJ1271 proteins were purified by heat treatment of the cell lysate, followed by anion exchange chromatography, dialysis, and concentration. The protein was further concentrated using a stirred ultrafiltration cell (Amicon) under N<sub>2</sub> with a 10-kDa molecular mass cut-off filter (Pall). The untagged MJ1596 HICDH protein was expressed in an *E. coli* Arctic Express (DE3)-RIL (pDG131) strain. The cells were grown in medium containing streptomycin (50  $\mu$ g ml<sup>-1</sup>), tetracycline (50  $\mu$ g ml<sup>-1</sup>), and getamycin (50  $\mu$ g ml<sup>-1</sup>) at 16°C with shaking at 250 rpm. HICDH protein expression, extraction, purification, and concentration were performed as described for the MJ1003/MJ1271 proteins.

### 3.2.3. Reconstitution of the Iron-Sulfur Center

In a typical reconstitution reaction, copurified MJ1003 and MJ1271 proteins (1 mg ml<sup>-1</sup> apoenzyme) were mixed with  $\text{Fe}(\text{NH}_4)_2(\text{SO}_4)_2$  and sodium sulfide as described previously (Chapter 2) [48]. The reconstitution mixture was stirred under argon at 0-4°C until maximum activity was observed (typically 3-4 h). Hydrolyase activity was monitored in a standard assay with 0.2 mM *cis*-homoaconitate as described below. A mock reconstitution control consisted of the above mixture without protein.

### 3.2.4. Determination of Iron-Sulfur Content

The holoenzyme was reconstituted using concentrated MJ1003/MJ1271 apoprotein (2.5 mg ml<sup>-1</sup>), and desalted using a PD-10 column (GE Healthcare) equilibrated with an anoxic solution of 50 mM Tris-HCl (pH 8.0). Desalting was performed at room temperature in an anaerobic chamber (Coy Laboratory Products) with an atmosphere of N<sub>2</sub>:CO<sub>2</sub>:H<sub>2</sub> (75:20:5 by volume). Fractions containing the desalted protein were combined, and aliquots were removed for iron and sulfide analysis. Total iron analysis was performed using the colorimetric bathophenanthrolinedisulfonate assay with a standard curve prepared from ferric chloride [95]. The labile sulfide concentration was determined using the methylene blue assay with the standard addition of sodium sulfide [96]. The total protein concentration was determined by the Bradford dye binding method (Thermo-Pierce) using bovine serum albumin as a standard. The standard errors calculated for each assay were propagated to estimate the error associated with each analysis.

### 3.2.5. Measurement of Hydrolyase Activities

Reactions (1 ml) were conducted in quartz semimicrocells with screw cap septa (Starna) containing 50 mM CHES-KOH (pH 9.0), 200 mM KCl, 20  $\mu\text{g ml}^{-1}$  holoenzyme, and various substrate concentrations. The sealed quartz cell containing buffer and substrate was degassed under argon for 10 min and equilibrated at 60°C for 10 min. The reactions were initiated by the addition of holoenzyme, and the decrease in UV absorbance was monitored at 60°C. Initial rates were measured from the linear portion of the reaction progress curve at 235 nm for *cis*-homoaconitate ( $\epsilon_{235} = 4580 \text{ M}^{-1} \text{ cm}^{-1}$ ), 235 nm for *cis*-homoaconitate ( $\epsilon_{235} = 4420 \text{ M}^{-1} \text{ cm}^{-1}$ ), 240 nm for *cis*-homo<sub>3</sub>aconitate ( $\epsilon_{240} = 3180 \text{ M}^{-1} \text{ cm}^{-1}$ ), and 240 nm and 250 nm for *cis*-homoaconitate ( $\epsilon_{240} = 3140 \text{ M}^{-1} \text{ cm}^{-1}$ ,  $\epsilon_{250} = 1370 \text{ M}^{-1} \text{ cm}^{-1}$ ). All of the molar absorption coefficients were determined in the reaction buffer at 60°C. One unit of hydrolyase activity catalyzed the conversion of 1  $\mu\text{mol}$  of substrate to product per min. Steady-state kinetic constants were estimated by nonlinear regression of initial rate data fit to the Michaelis-Menten-Henri equation [48]. The inhibitors were screened in direct assays containing buffer, 20  $\mu\text{g ml}^{-1}$  HACN, and various concentrations of substrate analogs; these reactions were initiated by the anaerobic addition of 100  $\mu\text{M}$  *cis*-homoaconitate, and hydrolyase activity was monitored at 240 nm. The stereochemistry of maleate hydration products was determined enzymatically using tartrate dehydrogenase and L-malate dehydrogenase enzymes as described previously (Chapter 2) [48].

### 3.2.6. Coupled Assay of Hydratase Activity

The hydration of unsaturated intermediates in the forward direction was measured by a coupled reaction with HICDH by monitoring the reduction of  $\text{NAD}^+$  to NADH at 340 nm [93]. Reaction mixtures containing 50 mM TAPS-KOH (pH 8.5), 50 mM KCl, 5

mM  $\text{MgCl}_2$ , 20 mM  $\beta$ -mercaptoethanol, 1 mM  $\text{NAD}^+$ , and 30  $\mu\text{g ml}^{-1}$  HICDH were degassed as described above, after which MJ1003/MJ1271 holoenzyme was added to a final concentration of 10  $\mu\text{g ml}^{-1}$ . The reaction mixtures were equilibrated to 60°C, and the reactions were initiated with 5  $\mu\text{l}$  of substrate. The initial rates were measured using the linear portion of the reaction progress curve. One unit of enzymatic activity catalyzed the reduction of 1  $\mu\text{mol NAD}^+ \text{min}^{-1}$ . The apparent kinetic constants were estimated as described above.

### 3.2.7. HPLC Analysis of Reaction Products

Standard reactions containing 10 mM *cis*-homoaconitate analogs and HACN holoenzyme (40  $\mu\text{g ml}^{-1}$ ) were incubated for 20 h at 60°C. A portion of the reaction product was analyzed by reversed phase HPLC using a Synergi Hydro-RP column (Phenomenex; 250 by 4.6 mm) with a guard column (4 by 3 mm). Chromatography was performed at 35°C with an isocratic elution with 20 mM potassium phosphate (pH 2.5) and 5% (v/v) acetonitrile in water at a flow rate of 1  $\text{ml min}^{-1}$ . Retention factors for standard compounds ( $t_0 = 2.5$  min) were 0.4 (homocitrate), 1.0 (homocitrate), 1.1 (*cis*-homoaconitate), and 2.2 (*cis*-homo<sub>2</sub>aconitate). Reaction products from incubations with *cis*-homo<sub>3</sub>aconitate and *cis*-homo<sub>4</sub>aconitate were analyzed using mobile phase containing buffer and 15% (v/v) acetonitrile in water. The retention factors were 1.5 (*cis*-homo<sub>3</sub>aconitate) and 3.5 (*cis*-homo<sub>4</sub>aconitate). A photodiode array detector was used to identify analytes; *cis*-homoaconitate analogs had absorption maxima near 215 nm, whereas hydroxyacid products absorbed maximally near 205 nm.

### 3.2.8. LC-MS Analysis of Enzyme Reaction Products

Standard reactions (1 ml) containing 250  $\mu\text{M}$  homoaconitate (or analog), and MJ1003/MJ1271 holoenzyme were incubated at 60°C for 20 h under argon. The reaction mixture was adjusted to pH 1 with HCl and extracted twice with ethyl acetate and once with diethyl ether. The combined organic phases were dried under  $\text{N}_2$  at 60°C. The residue was dissolved in water and analyzed by LC-MS using a Thermo LTQ-XL instrument. The sample was applied to a reversed phase column (Macro Bullet 3  $\mu\text{M}$  200 Å Magic C18AQ; Michrom Bioresources; 25 x 4 to 1 mm tapered) and eluted with a gradient from 5 to 95% acetonitrile with 0.1 % formic acid in water at a flow rate of 0.5 ml min<sup>-1</sup>. Electrospray ionization mass spectrometry was performed in the negative ion mode.

For the analysis of coupled reaction products, 1 mM  $\text{NAD}^+$  and HICDH were added to the reaction mixture. To form the methoxime derivatives of 2-oxoacid products, the pH was adjusted to 13-14 with sodium hydroxide and 0.25 ml of 10% O-methylhydroxylamine hydrochloride was added. The mixtures were incubated at room temperature for 1 h and then adjusted to pH 1 with HCl and saturated with NaCl. The acidic solution was extracted as described above. The concentrated sample was applied to a reversed phase column (Hypersil Gold; Thermo; 50 x 2.1 mm) and eluted with a gradient from 95-20% acetonitrile in aqueous 0.1% formic acid at a flow rate of 0.5 ml min<sup>-1</sup>. Electrospray ionization mass spectrometry was performed in the positive ion mode.



### **3.3. RESULTS**

#### **3.3.1. Protein Purification and Subunit Interaction**

Previously, the MJ0499/MJ1277 interacting pair of proteins was identified as the IPMI involved in methanogen leucine and isoleucine biosynthesis [48]. To identify the HACN<sub>MJ</sub>, the MJ1003 and MJ1271 pair of proteins was coexpressed in *E. coli* and the soluble proteins were copurified to approximately 90% homogeneity by heat treatment and anion-exchange chromatography, as analyzed by SDS-PAGE and densitometry (Figure 3.3). The apparent mass of MJ1003 was 46-kDa, matching the theoretical mass of 46.1-kDa. Likewise, the apparent mass of MJ1271 correlated well with its theoretical mass (18-kDa and 18.6-kDa, respectively). The large and small subunits coeluted during analytical size exclusion chromatography with a Stokes radius of 42 Å, corresponding to a 143-kDa protein (Figure 3.4). Therefore, the MJ1003/MJ1271 pair probably associates as a heterotetramer of two large and two small subunits, consistent with the association of MJ0499 and MJ1277.

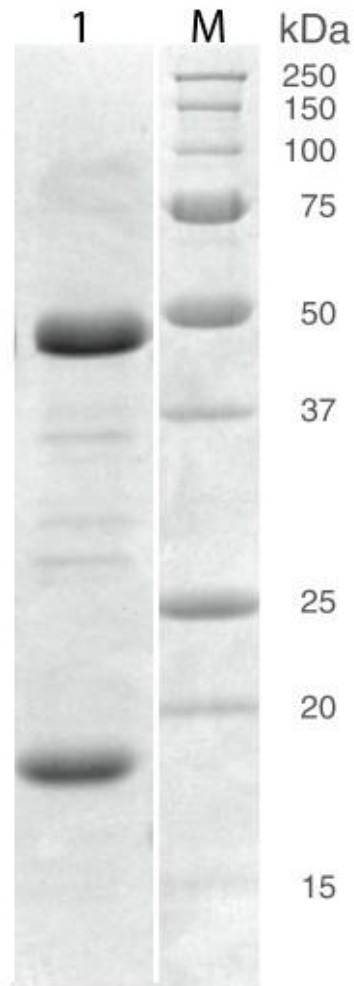


**Figure 3.3. Purified HACN<sub>MJ</sub>.** Lane 1, 10  $\mu$ g MJ1003-MJ1271; lane M, protein size markers (Biorad). Proteins were separated by SDS-PAGE on a 15% acrylamide gel and stained with Coomassie blue.

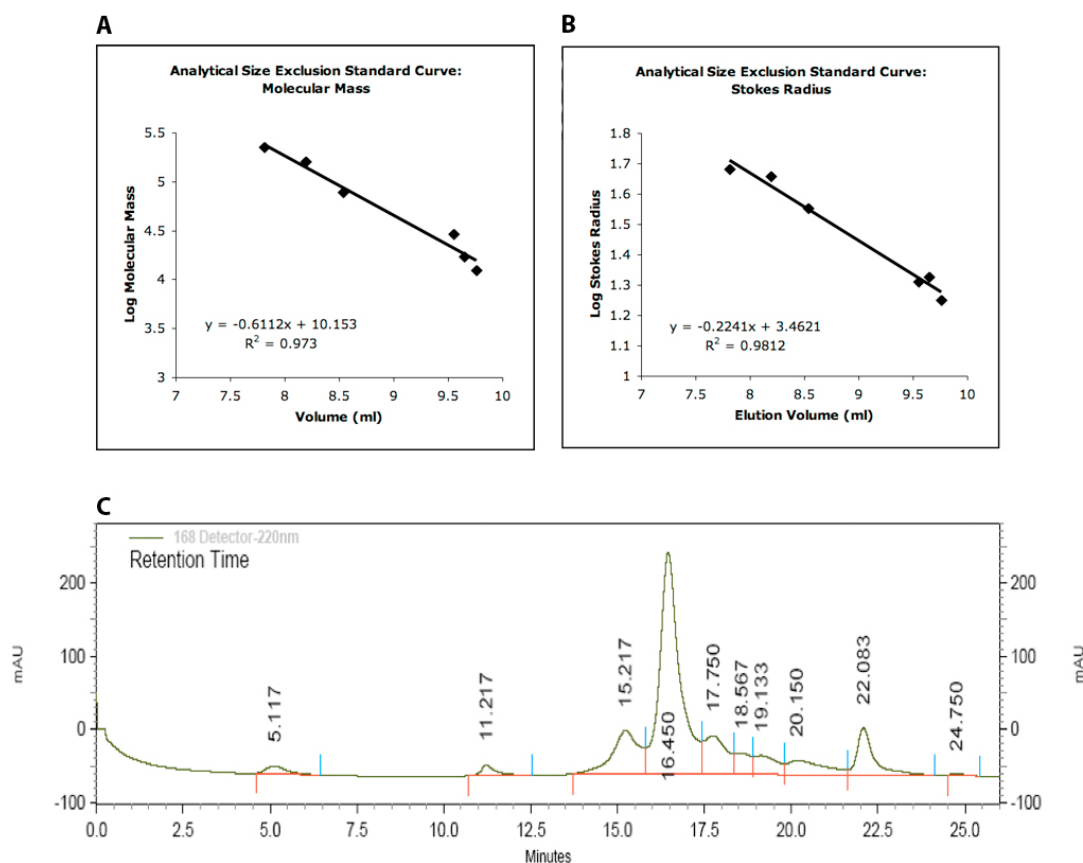


**Figure 3.4. MJ1003-MJ1271 Subunit Interaction.** Proteins were separated by analytical size exclusion chromatography HPLC with UV absorbance detection at 220nm in milli-absorbance units (mAU). Standard curves based on elution volume with respect to (A) molecular mass and (B) Stokes radius of the following standards: cytochrome c, myoglobin, carbonic anhydrase, conalbumin, alcohol dehydrogenase, aldolase, and  $\beta$ -amylase. (C) Chromatogram of  $1 \mu\text{g ml}^{-1}$  purified MJ1003-MJ1271. The peak at 16.450 min corresponds to MJ1003-MJ1271, confirmed by SDS-PAGE.

### 3.3.2. Hydrolyase Activity of the MJ1003/MJ1271 Proteins

HACN and IPMI belong to the aconitase family of proteins. These hydrolyases possess an oxygen sensitive [4Fe-4S] cluster responsible for coordinating the C $\alpha$  or C $\beta$  substrate hydroxyl and carboxyl groups [69]. Exposure to air or other oxidants, such as superoxide and hydrogen peroxide, results in a loss of the non-cysteine bound Fe and ultimately degradation of the cluster [97]. Therefore, the MJ1003/MJ1271 apoprotein was chemically reconstituted to the holoenzyme after incubation with iron (II) and sulfide under anaerobic conditions. The reconstituted protein contained  $5.1 \pm 0.2$  moles of iron and  $5.1 \pm 0.8$  moles of sulfide per mole of MJ1003/MJ1271 dimer after anaerobic desalting to remove excess buffer salts. Therefore, the holoenzyme appears to possess a single Fe<sub>4</sub>-S<sub>4</sub> cluster per dimer, consistent with other members of the aconitase family. Although no activity was observed above background ( $0.029 \text{ s}^{-1}$ ) with citraconate, citramalate, or 3-isopropylmalate, the reconstituted MJ1003/MJ1271 catalyzed the hydration of the chemically synthesized *cis*-homoaconitate.

The activity of MJ1003/MJ1271 was measured in a direct assay consisting of the holoenzyme, substrate, and buffer salts. Assay conditions were optimized based on the MJ1003/MJ1271 catalyzed hydration of *cis*-homoaconitate (Figure 3.5). The holoenzyme was active between pH 8.0 and 10, with maximal activity in CHES-KOH at pH 9.0. Although the enzyme was active in the absence of any salt, the highest activity was observed in the presence of 200 mM KCl (60% increase in activity compared to 0 mM KCl). The presence of divalent metal cations had no effect on activity. Consistent with the thermal stability results of MJ0499/MJ1277, the activity of MJ1003/MJ1271 was maximal at 60°C. The interacting MJ1003/MJ1277 pair of proteins displayed no activity with *cis*-homoaconitate.

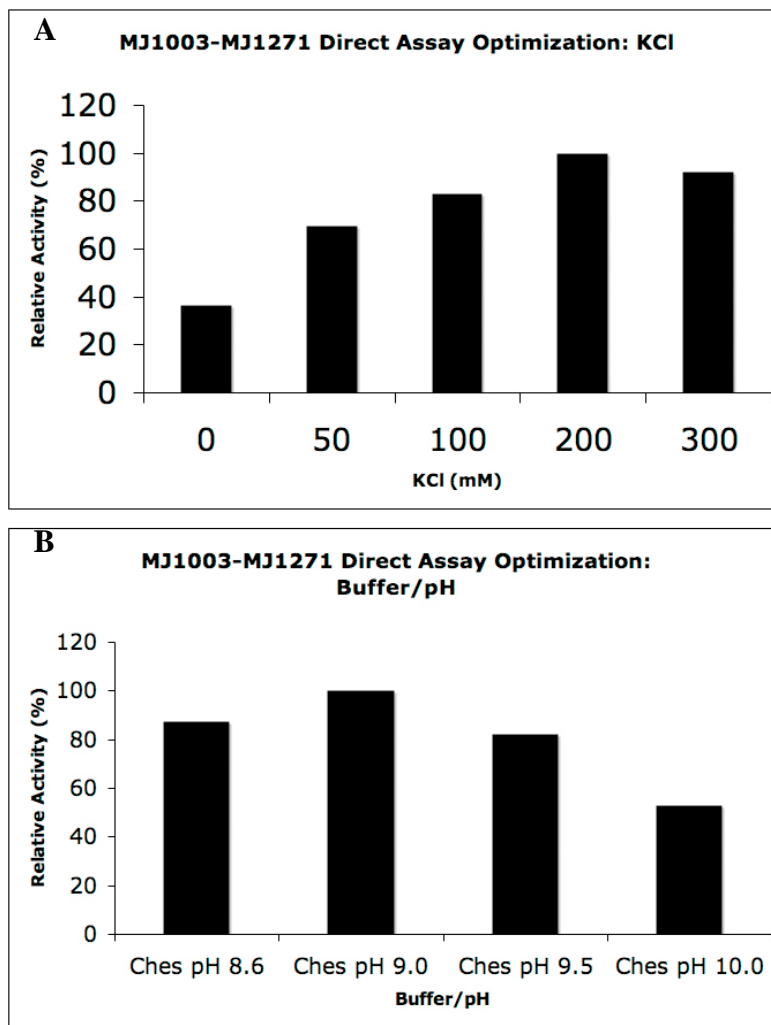


**Figure 3.5. MJ1003-MJ1271 Direct Assay Optimization.** The direct assay was optimized based on the specific activity of  $20 \mu\text{g ml}^{-1}$  reconstituted MJ1003-MJ1271 with  $200 \mu\text{M}$  *cis*-homoaconitate at  $60^\circ\text{C}$ . Each optimization was conducted in duplicate and the results are the average of two data sets. *A*, optimization of KCl concentration. *B*, optimization of buffer and pH.

Methanogen HCS and HICDH are required for the synthesis of 2-oxosuberate from 2-oxoglutarate [39]. Therefore, HACN<sub>MJ</sub> was predicted to exhibit similar broad substrate specificity, catalyzing the isomerization of homocitrate, homo<sub>2</sub>citrate, and homo<sub>3</sub>citrate. To test the predicted substrate specificity of HACN<sub>MJ</sub>, the hydration of *cis*-homoaconitate, *cis*-homo<sub>2</sub>aconitate, and *cis*-homo<sub>3</sub>aconitate by MJ1003/MJ1271 was measured in the direct assay described above and the steady state kinetics for each reaction was determined (Figure 3.6). MJ1003/MJ1271 catalyzed the hydration of the three *cis*-unsaturated intermediates with similar  $K_m$  and  $k_{cat}$  values, indicating that the enzyme does not discriminate between the three intermediates (Table 3.1). The broad substrate specificity of HACN<sub>MJ</sub> was further tested in direct assays with maleic acid, *cis*-aconitate, and non-physiological *cis*-homo<sub>4</sub>aconitate. (Table 3.1). MJ1003/MJ1271 catalyzed the hydration of the minimal substrate maleic acid with a similar  $K_m$  to MJ0499/MJ1277 (400  $\mu$ M) but a seven-fold lower  $k_{cat}$  (5.5 s<sup>-1</sup> and 34 s<sup>-1</sup> for MJ1003/MJ1271 and MJ0499/MJ1277, respectively). *cis*-Aconitate, a substrate for ACN that has a carbon backbone one methylene shorter than *cis*-homoaconitate, also served as a substrate with a similar  $K_m$  to the hydration of maleic acid and a  $k_{cat}$  on the order of *cis*-homoaconitate. The substrate specificity of MJ1003/MJ1271 was extended to *cis*-homo<sub>4</sub>aconitate, a *cis*-unsaturated intermediate that has not previously been isolated as a natural product. Although MJ1003/MJ1271 catalyzed the hydration of this compound with a six-fold greater  $K_m$  than *cis*-homo<sub>3</sub>aconitate, the turnover also increased by approximately 2.5.

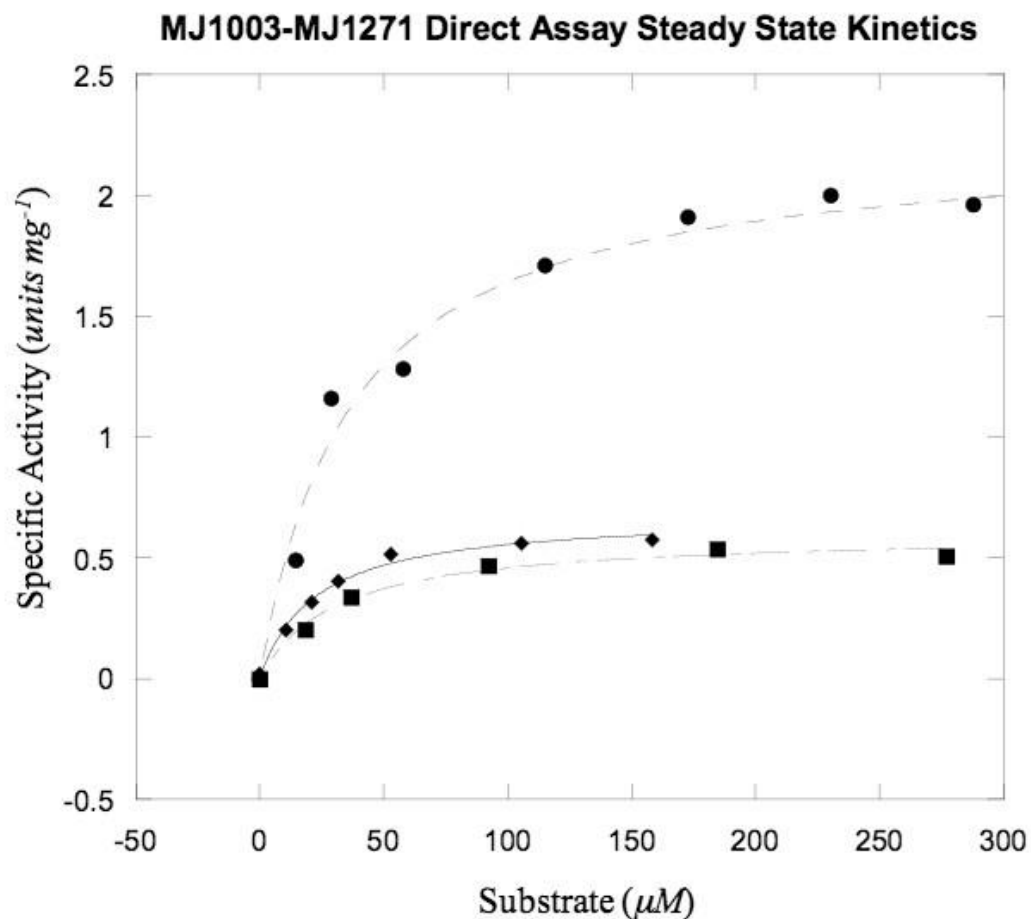


**Figure 3.6. Steady – state kinetics of MJ1003-MJ1271.** Steady – state kinetic constants for MJ1003-MJ1271 were estimated by nonlinear regression of initial rate data fit to the Michaelis-Menten-Henri equation, as described in the text. *Closed diamonds*, kinetics for *cis*-homo<sub>1</sub>aconitate. *Closed squares*, kinetics for *cis*-homo<sub>2</sub>aconitate. *Closed circles*, kinetics for *cis*-homo<sub>3</sub>aconitate.

**Table 3.1. Steady-state kinetic parameters for the direct assay of hydrolyase activity.** Reactions containing substrate and buffer salts were preincubated at 60°C before the addition of reconstituted MJ1003/MJ1271 protein to initiate the reaction. Hydrolase activity was determined by measuring the rate of decrease in UV absorbance caused by the unsaturated substrate, as described under “Experimental Procedures.”

<b>Substrate</b>	<b><math>K_m</math> (<math>\mu M</math>)</b>	<b><math>V_{max}</math> (units <math>mg^{-1}</math>)</b>	<b><math>k_{cat}</math> (<math>s^{-1}</math>)</b>	<b><math>k_{cat}/K_m</math> (<math>M^{-1} s^{-1}</math>)</b>
<b><i>cis</i>-aconitate</b>	300 $\pm$ 90	0.69 $\pm$ 0.07	0.76	2.5 $\times 10^3$
<b><i>cis</i>-Homoaconitate</b>	22 $\pm$ 3	0.68 $\pm$ 0.03	0.75	3.4 $\times 10^4$
<b><i>cis</i>-Homo<sub>2</sub>aconitate</b>	30 $\pm$ 5	0.60 $\pm$ 0.03	0.66	2.2 $\times 10^4$
<b><i>cis</i>-Homo<sub>3</sub>aconitate</b>	36 $\pm$ 6	2.2 $\pm$ 0.09	2.5	6.8 $\times 10^4$
<b><i>cis</i>-Homo<sub>4</sub>aconitate</b>	175 $\pm$ 39	5.1 $\pm$ 0.3	5.6	3.2 $\times 10^4$
<b>Maleate</b>	330 $\pm$ 50	5.5 $\pm$ 0.3	6	1.8 $\times 10^4$
<b>(<i>R</i>)-Homocitrate<sup>a</sup></b>	1500 $\pm$ 200	0.59 $\pm$ 0.03	0.37	2.5 $\times 10^2$

<sup>a</sup>Dehydratase activity was determined by measuring the rate of increase in UV absorbance caused by homoaconitate formation.

The reaction products of MJ1003/MJ1271 direct assay were analyzed by reversed phase HPLC (Figure 3.7). Incubation of the holoenzyme with *cis*-homoaconitate produced a single product peak corresponding to homocitrate and no homoisocitrate was observed. The reaction product was also analyzed by LC-MS and peaks were identified at 187 m/z, corresponding to the  $[M-H]^-$  ion of homoaconitate, and 205 m/z, corresponding to the  $[M-H]^-$  ion of homocitrate or homoisocitrate. No activity was observed in the direct assay or product analysis for *cis*-homoaconitate incubated with either the apoenzyme or a mock reconstitution, indicating that the iron-sulfur cluster is essential for activity.



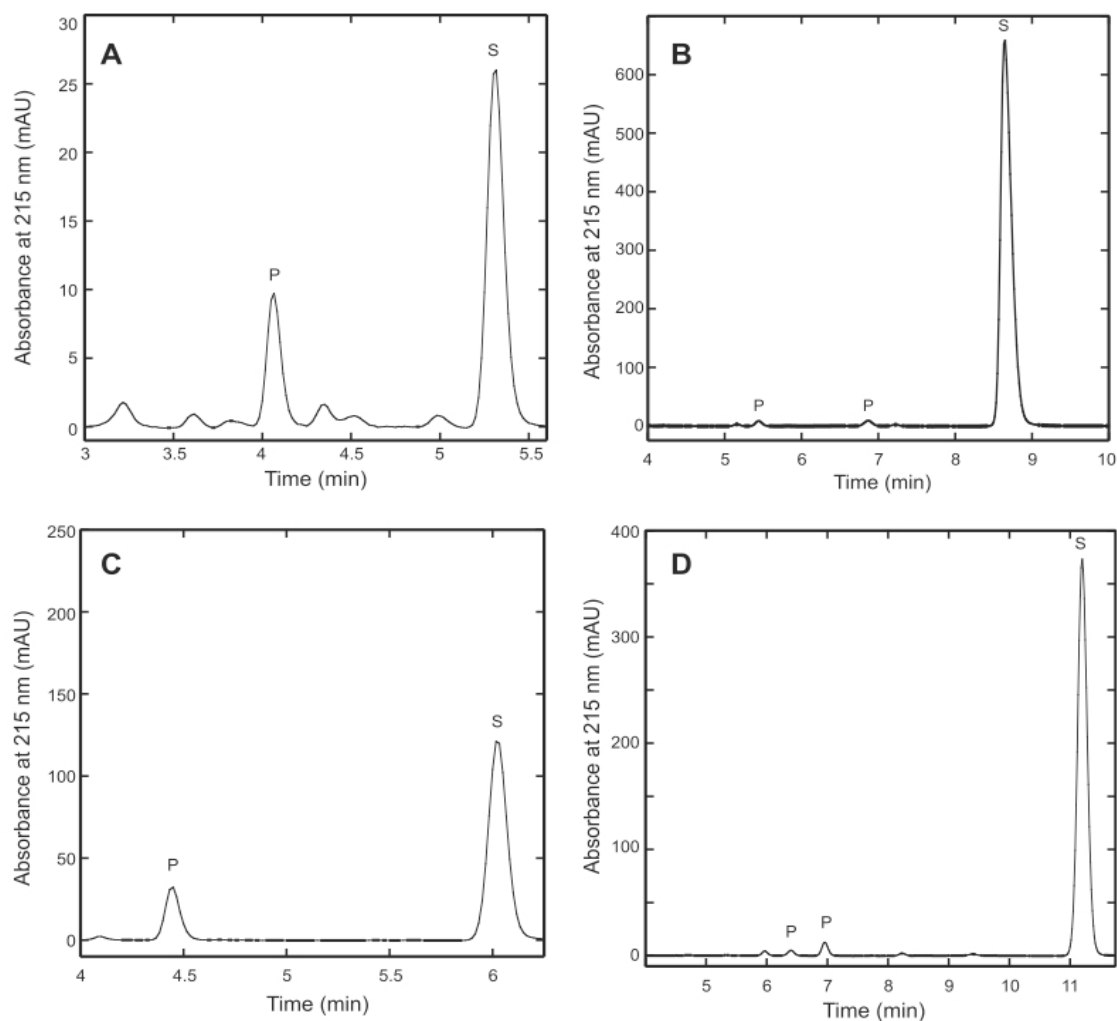


**Figure 3.7. HACN catalyzed the hydration of *cis*-unsaturated tricarboxylic acids to produce hydroxyacids.** Holoenzyme was incubated with *cis*-homoaconitate analogs for 20 h at 60°C. The reaction products were separated by reversed phase HPLC with UV absorbance detection in mAU as described in the text. Substrate peaks (S) were identified by their retention times compared with external standards. Product peaks (P) had absorbance maxima near 205 nm, and they were not observed in control reactions. The unlabeled peaks were also observed in control reactions without enzyme, so they are considered to be contaminants. A, incubation with *cis*-homoaconitate (S) produced homocitrate (P) that was confirmed by coinjection with (*R*)-homocitrate. No homoisocitrate was detected in this experiment. B, incubation with *cis*-homo<sub>2</sub>aconitate produced two product peaks. C, incubation with *cis*-homo<sub>3</sub>aconitate produced a single product peak. D, incubation with *cis*-homo<sub>4</sub>aconitate produced two product peaks. The homoaconitate analogs have significantly higher molar absorptivities than their corresponding hydroxy-acids, which preclude direct comparisons of their concentrations by peak area integration.

The reaction products of the MJ1003/MJ1271 catalyzed hydration of maleic acid was analyzed as previously described (Chapter 2). Incubation of HACN<sub>MJ</sub> with 5 mM maleic acid produced 5 mM D-malate and no L-malate was measured above background (<10  $\mu$ M). MJ0499-MJ1277 also catalyzed the production of D-malate from maleic acid, indicating similar binding modes at the active site for the two enzymes that are consistent with the stereochemistry of their physiological reactions [48].

### 3.3.3. Coupled Activity of HACN with HICDH

The methanogen HICDH was previously purified and the steady state kinetic parameters were established for the oxidative decarboxylation of homoisocitrate, homo<sub>2</sub>isocitrate, and homo<sub>3</sub>isocitrate [44]. To measure only the forward hydration of the *cis*-unsaturated intermediates of the chain elongation reactions, a coupled assay was established with HACN<sub>MJ</sub> in the presence excess HICDH<sub>MJ</sub> and NAD<sup>+</sup>. The rate of hydration was measured as the rate of NAD<sup>+</sup> reduction to NADH in the determined optimal assay conditions: 5 mM MgCl<sub>2</sub>, 100 mM KCl, and 2-mercaptoethanol, at 60°C in TAPS-KOH (pH 8.5) (Figure 3.8). Compared to direct assay results, similar Michaelis constants were observed for the forward hydration of *cis*-homoaconitate, *cis*-homo<sub>2</sub>aconitate, and *cis*-homo<sub>3</sub>aconitate, although an increase in turnover was observed for each substrate due to product removal by HICDH<sub>MJ</sub> (Figure 3.9 and Table 3.2). The products of these coupled reactions were identified as their methoxime derivative by LC-MS based on chemically synthesized standards (Figure 3.10). 2-Oxadipate, 2-oxopimelate, and 2-oxosuberate were detected from homoaconitate, homo<sub>2</sub>aconitate, and homo<sub>3</sub>aconitate, respectively. HICDH<sub>MJ</sub> was also demonstrated to oxidatively decarboxylate homo<sub>4</sub>isocitrate to 2-oxoazelate via *cis*-homo<sub>4</sub>aconitate in a coupled assay.

Therefore, methanogen HACN and HICDH share similar broad substrate specificities by recognizing tricarboxylates with  $\gamma$ -chains extending up to five methylenes long.

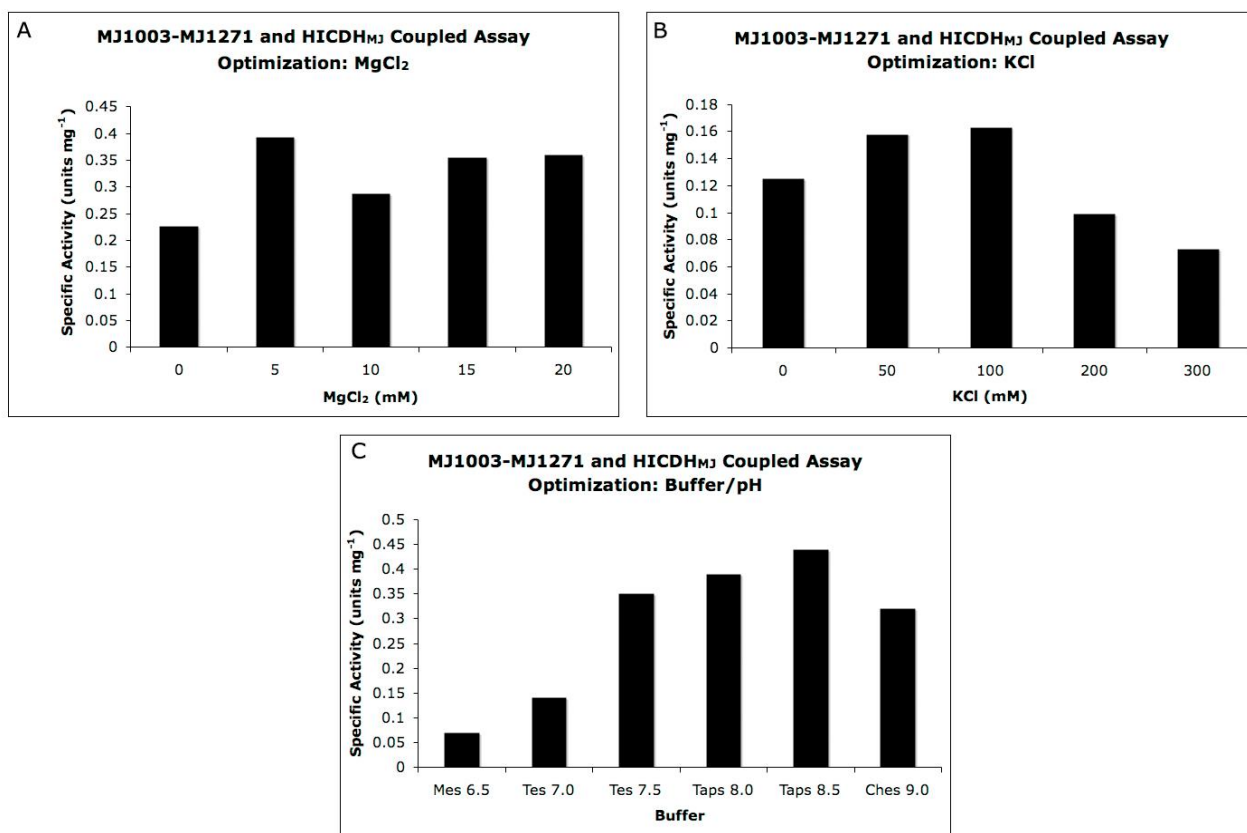


**Figure 3.8. MJ1003-MJ1271 and HICDH<sub>MJ</sub> Coupled Assay Optimization.** The coupled assay was optimized based on the specific activity of 20  $\mu\text{g ml}^{-1}$  reconstituted MJ1003-MJ1271 with 30  $\mu\text{g ml}^{-1}$  HICDH<sub>MJ</sub> and 200  $\mu\text{M}$  *cis*-homoaconitate at 60°C. *A*, optimization of  $\text{Mg}^{2+}$  concentration. *B*, optimization of KCl concentration. *C*, Optimization of buffer and pH.

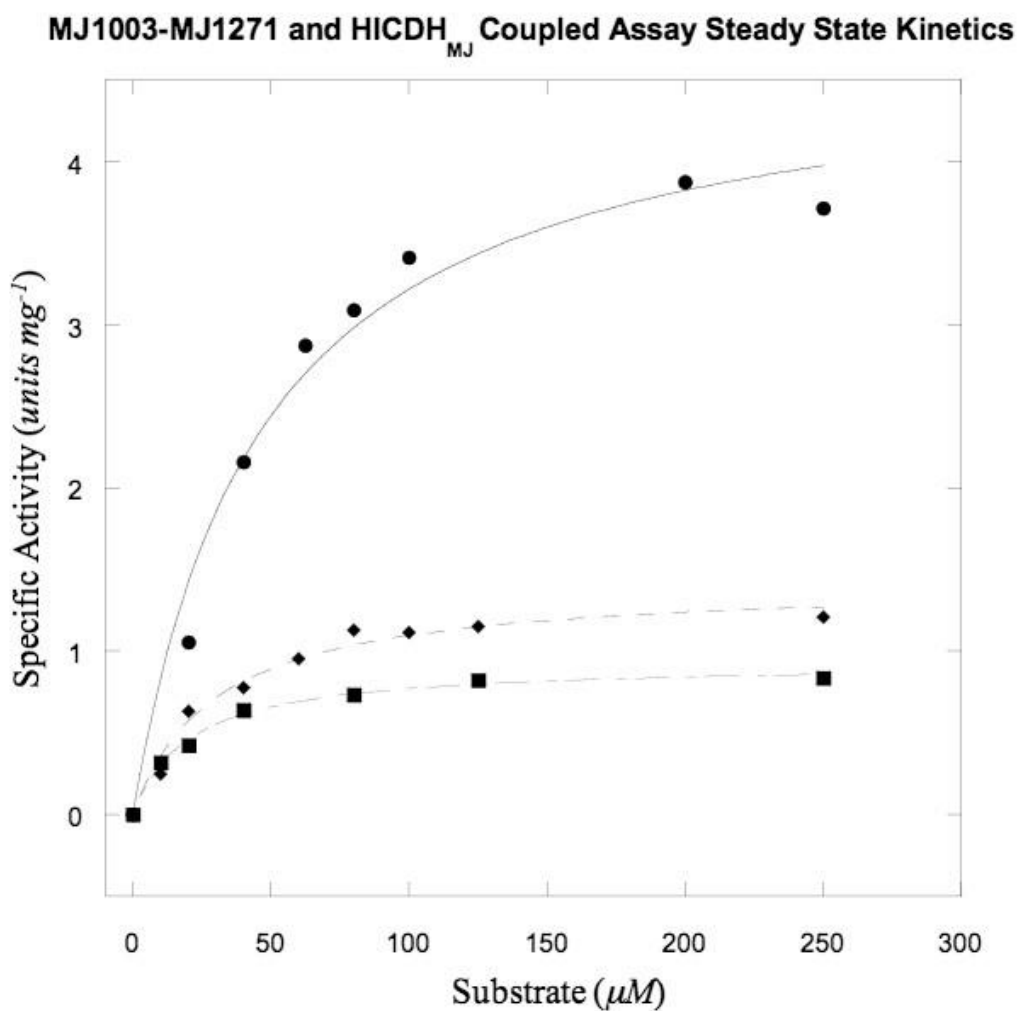


**Figure 3.9. Steady – state kinetics of the MJ1003-MJ1271 and HICDH<sub>MJ</sub> coupled assay.** Steady – state kinetic constants for the direct assay were estimated by nonlinear regression of initial rate data fit to the Michaelis-Menten-Henri equation, as described in the text. *Closed diamonds*, kinetics for *cis*-homoaconitate. *Closed squares*, kinetics for *cis*-homo<sub>2</sub>aconitate. *Closed circles*, kinetics for *cis*-homo<sub>3</sub>aconitate.

**Table 3.2. Kinetic parameters for the coupled assay of HACN hydrolyase activity with HICDH.** Reactions containing 10  $\mu\text{g ml}^{-1}$  HICDH, 30  $\mu\text{g ml}^{-1}$  HACN holoenzyme, 1 mM  $\text{NAD}^+$ , and buffer salts were preincubated at 60°C before the addition of substrate to initiate the reaction. Hydrolase activity was determined by measuring the rate of increase in UV absorbance at 340 nm caused by the reduction of  $\text{NAD}^+$ , as described under “Experimental procedures.”

Substrate	$K_m$ ( $\mu\text{M}$ )	$V_{\text{max}}$ (units $\text{mg}^{-1}$ )	$k_{\text{cat}}$ ( $\text{s}^{-1}$ )	$k_{\text{cat}}/K_m$ ( $\text{M}^{-1} \text{s}^{-1}$ )
<i>cis</i> -Homoaconitate	$25 \pm 3$	$1.4 \pm 0.04$	1.5	$5.9 \times 10^4$
<i>cis</i> -Homo <sub>2</sub> aconitate	$20 \pm 2$	$0.93 \pm 0.02$	1	$5.0 \times 10^4$
<i>cis</i> -Homo <sub>3</sub> aconitate	$46 \pm 9$	$4.7 \pm 0.3$	5.1	$1.1 \times 10^5$
<i>cis</i> -Homo <sub>4</sub> aconitate	N.D. <sup>a</sup>	$5.1^b$	N.D.	N.D.

<sup>a</sup>ND, not determined.

<sup>b</sup>Specific activity determined with 0.78 mM *cis*-homo aconitate.

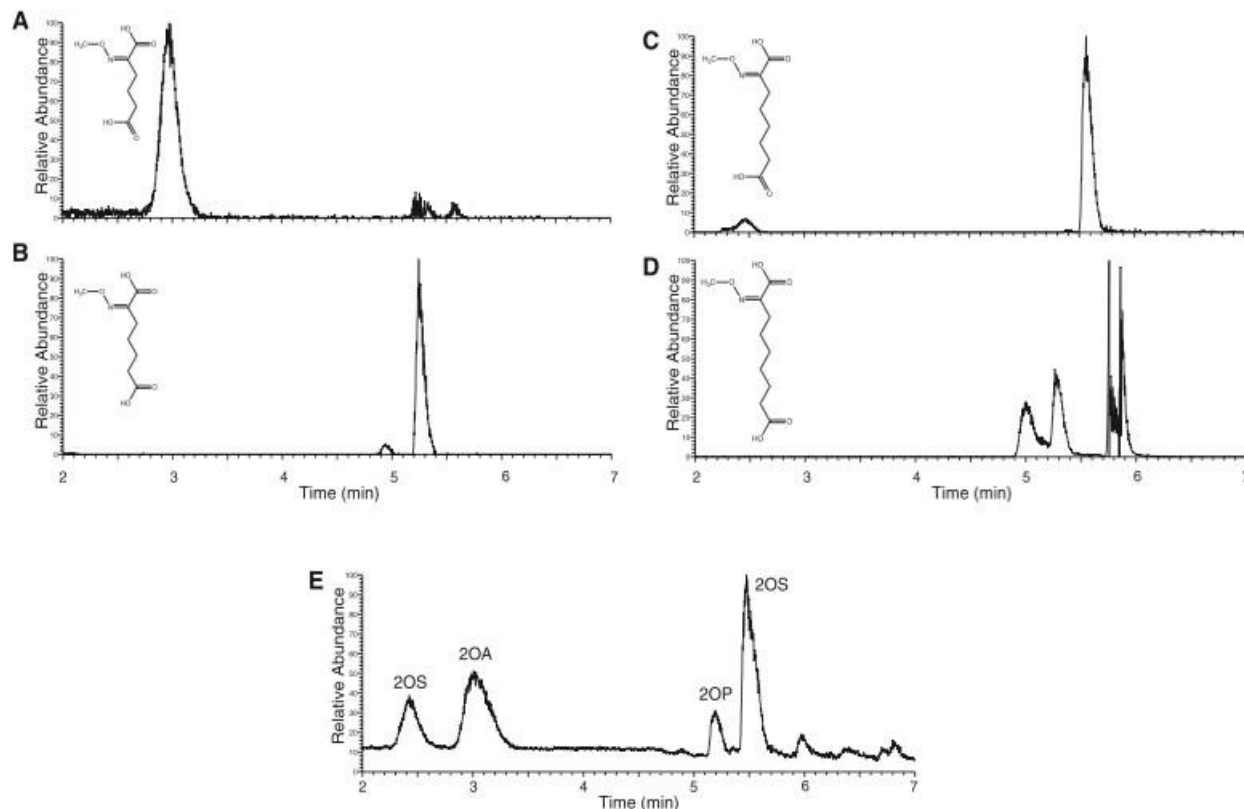


**Figure 3.10. HACN and HICDH hydrated *cis*-homoaconitate analogs and catalyzed their oxidative decarboxylation to produce the corresponding 2-oxoacids.** Methoxime derivatives extracted from the reaction products were analyzed by LC-MS. *A-D* show mass chromatograms for the  $MH^+$  ions of the methoxime-derivatized 2-oxoacids depicted in the inset. Similar plots were obtained for the sodium adducts of each acid. *A*, reactions with *cis*-homoaconitate produced 2-oxoadipate indicated by the  $m/z$  190 peak. *B*, reactions containing *cis*-homo<sub>2</sub>aconitate produced 2-oxopimelate identified by the  $m/z$  204 peak. *C*, reactions containing *cis*-homo<sub>3</sub>aconitate produced 2-oxosuberate identified by the  $m/z$  218 peak. *D*, reactions containing *cis*-homo<sub>4</sub>aconitate produced 2-oxoazellate identified by the  $m/z$  232 peak. This derivative formed several noncovalent complexes producing multiple peaks. *E* contains a chromatogram of 2-methoxime dicarboxylic acid standards showing the reconstructed total ion current. The standards included 2-oxoadipic acid (2OA), 2-oxopimelic acid (2OP), and 2-oxosuberic acid (2OS).

### 3.3.4. Dehydration Reaction and Stereospecificity of HACN

Product analysis from the direct and coupled assays indicates that HACN<sub>MJ</sub> is capable of catalyzing the full isomerization of homocitrate. However, the stereochemistry of this substrate was not determined from those experiments. Previously, (*S*)-homocitrate was observed from the reaction of HCS<sub>MJ</sub> with 2-oxoglutarate [39]. However, HCS<sub>MJ</sub> was also observed to produce (*R*)-homo<sub>2</sub>citrate and (*R*)-homo<sub>3</sub>citrate. (*R*)-Homocitrate and (*S*)-homocitrate were tested in the coupled assay with MJ1003/MJ1271 and HICDH<sub>MJ</sub> to identify the correct homocitrate enantiomer required by HACN<sub>MJ</sub> (Figure 3.11). No activity was observed in the presence of 1 mM (*S*)-homocitrate. However, 1 mM (*R*)-homocitrate was effectively isomerized and oxidatively decarboxylated to 2-oxoadipate with a specific activity of 0.3 U mg<sup>-1</sup> (0.3 s<sup>-1</sup>). The dehydration of (*R*)-homocitrate to *cis*-homoaconitate was measured in a direct assay with HACN<sub>MJ</sub>. A K<sub>m</sub> of 1500 μM and a rate of 0.37 s<sup>-1</sup> was observed for the dehydration reaction (Table 3.1), which is consistent with the kinetics of MJ0499/MJ1277 for (*R*)-citramalate and α-isopropylmalate and aconitase with citrate.

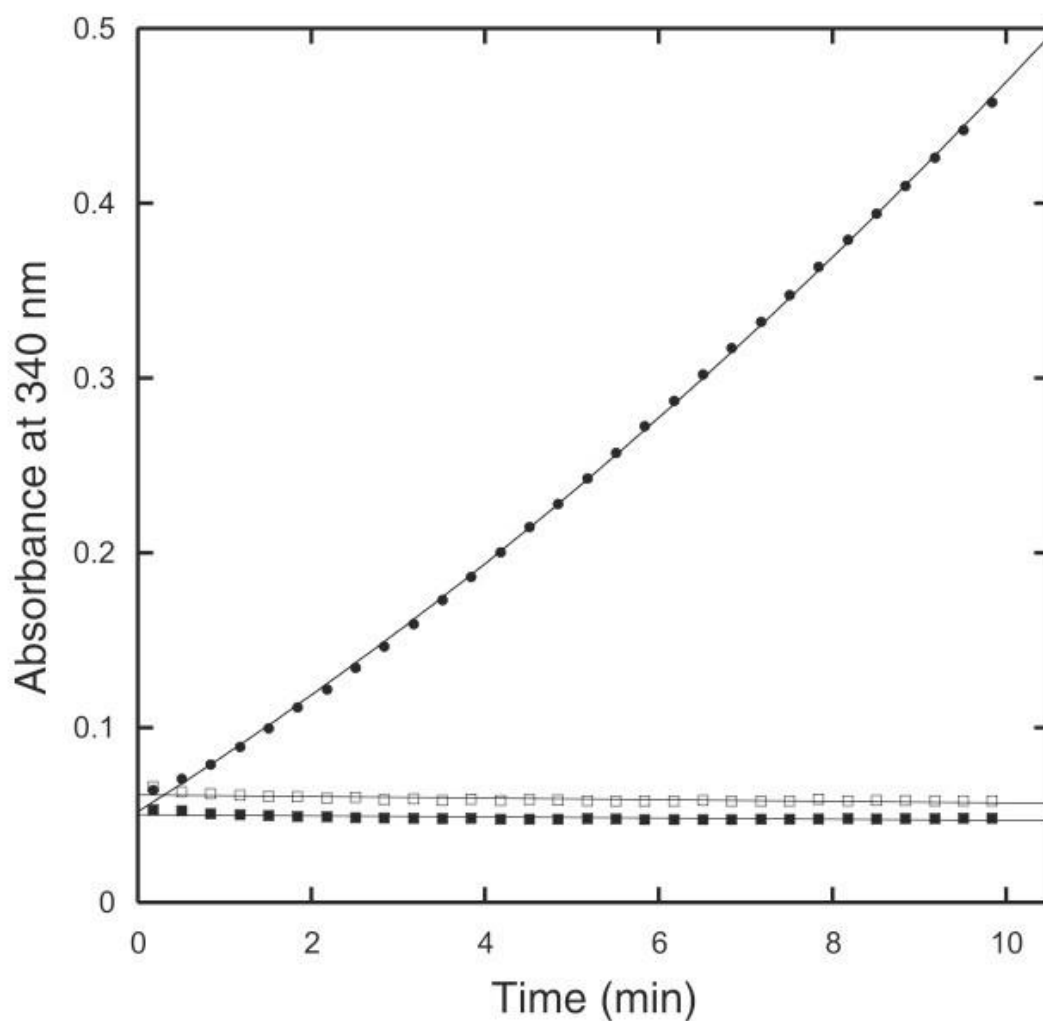


**Figure 3.11. Homoaconitase and homoisocitrate dehydrogenase specifically converted (*R*)-homocitrate to 2-oxoadipate in a coupled reaction.** The reaction progress curves show the NADH absorbance in reactions containing 0.5 mM (*R*)-homocitrate (*solid circles*), 0.5 mM (*S*)-homocitrate (*open squares*), or no substrate (*solid squares*). A control reaction without homoaconitase also showed no NADH production.



### 3.3.5. Inhibitors of HACN

Inhibition of HACN<sub>MJ</sub> was tested in direct assays containing MJ1003/MJ1271 and 100  $\mu$ M *cis*-homoaconitate. Hydrolyase activity was inhibited by 50% in the presence of 100  $\mu$ M *trans*-aconitate and 400  $\mu$ M *trans*-homo<sub>3</sub>aconitate and no activity was observed when 100  $\mu$ M (*S*)-homocitrate was added. No inhibition was detected in the presence of up to 200  $\mu$ M citraconate.

## 3.4. DISCUSSION

Methanogens use three enzymes in succession to extend the carbon chain of 2-oxoglutarate by three methylenes, producing the 2-oxosuberate required for CoB synthesis. Based on sequence homology to mACN, HACN<sub>MJ</sub> was proposed to catalyze each hydration and dehydration reaction in the isomerizations of *cis*-homoaconitate, *cis*-homo<sub>2</sub>aconitate, and *cis*-homo<sub>3</sub>aconitate. However, HACN homologs from the  $\alpha$ -aminoadipate pathway have only been identified to catalyze the hydration of *cis*-homoaconitate to (2*R*,3*S*)-homoisocitrate [93]. The initial dehydration of (*R*)-homocitrate to *cis*-homoaconitate had previously gone undetected, despite the homology between HACN and mACN. This work describes the first characterized HACN to catalyze both dehydration and hydration reactions for the full isomerization of homocitrate to homoisocitrate. Steady-state kinetic constants were established in direct assays for the dehydration of homocitrate, as well as the hydration of *cis*-homoaconitate. A coupled assay with HICDH<sub>MJ</sub> was also used to define the kinetics for the hydration of *cis*-homoaconitate to homoisocitrate. Finally, the production of 2-oxoadipate was observed from the coupled assay with (*R*)-homocitrate as the substrate. Therefore, the methanogen HACN catalyzes both partial reactions in the isomerization of the three  $\alpha$ -hydroxy acid substrates required for 2-oxosuberate production.

The steady state kinetic values for the hydration of *cis*-homoaconitate by HACN<sub>MJ</sub> were similar to the previously characterized *T. thermophilus* HACN. The HACN<sub>TT</sub> catalyzed the hydration of *cis*-homoaconitate with a  $k_{\text{cat}}$  of 1.3 s<sup>-1</sup> but a lower  $K_m$  than HACN<sub>MJ</sub> (8  $\mu$ M) [93]. However, the HACN<sub>TT</sub> did not recognize *cis*-aconitate as a substrate, despite only differing from *cis*-homoaconitate by one methylene in the  $\gamma$ -chain. HACN<sub>MJ</sub> was observed to catalyze the hydration of *cis*-aconitate with a similar turnover to *cis*-homoaconitate although the  $K_m$  was approximately 20 times greater. *cis*-Aconitate can spontaneously convert to the more stable *trans*-isomer, which is a potent inhibitor of both mACN and HACN<sub>MJ</sub>. Initial attempts to define *cis*-aconitate as a substrate for HACN<sub>MJ</sub> were unsuccessful due to a 30% conversion (non-enzymatic) of the stock *cis*-aconitate to *trans*-aconitate (Drevland and Graham, unpublished results). Therefore, because of the relatively low turnover and high  $K_m$ , the hydration of *cis*-aconitate by HACN<sub>TT</sub> may have gone undetected because of *trans*-aconitate in the reaction mixture.

The broad substrate specificity of HACN<sub>MJ</sub> was observed in direct assays with *cis*-unsaturated intermediates containing one to five methylenes in the  $\gamma$ -chain. The enzyme also catalyzed the stereospecific hydration of maleic acid to (*R*)-malate, indicating similar binding modes for all of the substrates. The HACN<sub>TT</sub> was not tested with maleic acid or longer homoaconitate analogs. Thus, it is unknown if this broad specificity is unique to methanogen HACN.

Initial studies to elucidate the pathway to 2-oxosuberate identified *trans*-homoaconitate and (*S*)-homocitrate from the first HCS catalyzed reaction [39]. However, only the conversion of (*R*)-homocitrate to 2-oxoadipate was observed in the coupled assay with HICDH<sub>MJ</sub>. Also, (*S*)-homocitrate and *trans*-homoaconitate are inhibitors of HACN<sub>MJ</sub>. Therefore, these compounds are probably not intermediates in the CoB

biosynthetic pathway. The chain elongation reactions are proposed to follow a more evolutionarily conserved pathway involving (*R*)-homocitrate (Figure 3.12). Further studies are required using purified HCS<sub>MJ</sub> to analyze the stereochemistry of the reaction products.

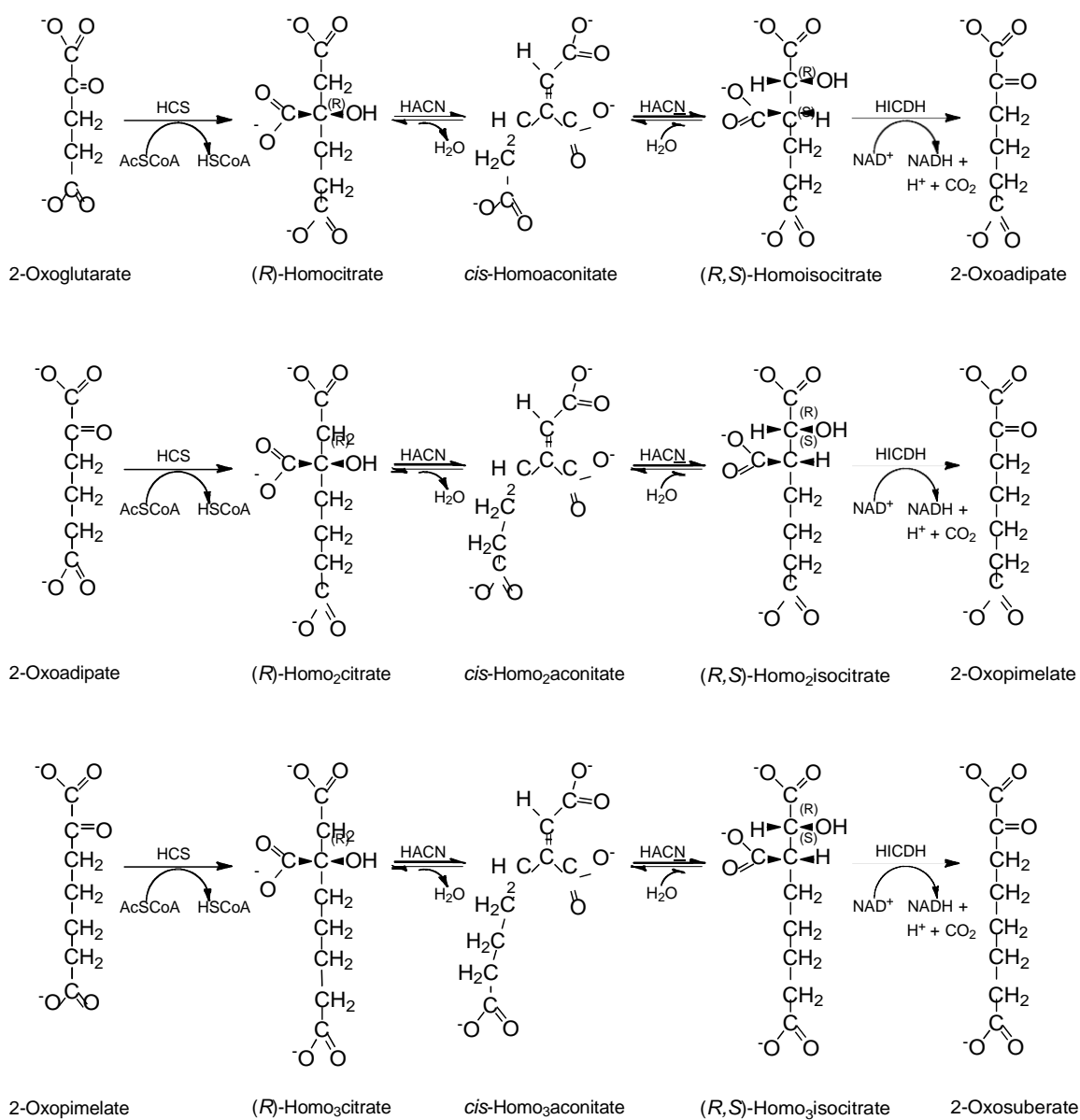


**Figure 3.12. The proposed 2-oxoacid chain elongation pathway for methanogen coenzyme B biosynthesis.**

Although HACN<sub>MJ</sub> was able to catalyze the dehydration of (*R*)-homocitrate to *cis*-homoaconitate, it did so at half the rate of the hydration of the *cis*-unsaturated intermediates and with a  $K_m$  approximately 70 times greater than that for *cis*-homoaconitate. The resulting specificity constant for HACN<sub>MJ</sub> with (*R*)-homocitrate was two orders of magnitude lower than the hydration of the intermediates. However, these results are consistent with the specificity constants for IPMI<sub>MJ</sub> with (*R*)-citramalate and  $\alpha$ -isopropylmalate which were also two orders of magnitude lower than the hydration of citraconate [48]. Future studies will be required to measure the equilibrium constant for this reaction.

## **Chapter 4: Crystallography and Mutational Analysis of the *Methanocaldococcus jannaschii* Homoaconitase Small Subunit-Insight into Structural Determinants for Substrate Recognition**

### **4.1. INTRODUCTION**

The aconitase (ACN) superfamily consists of five phylogenetic groups: (i) mitochondrial aconitases (mACN); (ii) cytoplasmic aconitases (cACN) and iron regulatory proteins (IRP1 and IRP2); (iii) bacterial aconitases (AcnB); (iv) isopropylmalate isomerases (IPMI); (v) homoaconitases (HACN) [69]. The mACN has served as the archetype for this superfamily, having been extensively studied both kinetically and structurally for over five decades. Mitochondrial aconitase uses an iron-sulfur cluster [4Fe-4S] to catalyze the reversible anti-elimination of water from citrate and the subsequent hydration of the unsaturated intermediate, *cis*-aconitate, producing isocitrate in the citric acid cycle (Figure 4.1) [98]. The majority of the ACN family literature is dedicated to the first three phylogenetic groups, with more recent interest in regulatory roles of IRP1 and IRP2. Thus, most of the information regarding the reaction mechanism of IPMI and HACN has been inferred from these previous aconitase studies.



methylnmalate in the pyruvate pathway for isoleucine biosynthesis, an alternative to the more common pathway requiring a threonine dehydratase (Chapter 2) [48]. HACN has been characterized in the  $\alpha$ -aminoadipate pathway for lysine biosynthesis in some bacteria and fungi, as well as coenzyme B biosynthesis in methanogenic archaea [93,49]. In the  $\alpha$ -aminoadipate pathways of *Thermus thermophilus*, *Saccharomyces cerevisiae*, and *Aspergillus nidulans*, HACN has been shown to catalyze only the second half reaction in the isomerization of (*R*)-homocitrate: the hydration of *cis*-homoaconitate to (2*R*,3*S*)-isohomocitrate [93,84,89]. A second enzyme, predicted to be an ACN, was proposed to catalyze the initial dehydration of (*R*)-homocitrate to *cis*-aconitate [93]. However, HACN from *Methanocaldococcus jannaschii* has recently been shown to catalyze the full conversion of (*R*)-homocitrate to isohomocitrate, as well as the full isomerizations of (*R*)-homo<sub>2</sub>citrate and (*R*)-homo<sub>3</sub>citrate, in the chain elongation reactions of coenzyme B biosynthesis (Chapter 3) [49].

Sequence alignments of archaeal HACNs, and IPMIs indicate that the majority of the 21 active site residues elucidated through mACN studies are highly conserved, implying similar structural organization and catalytic mechanisms. The large subunit of these archaeal proteins (~48 kDa) is homologous to domains 1, 2, and 3 of the monomeric mACN, including the CX<sub>63</sub>CXXC motif responsible for ligating the [4Fe-4S] cluster. The large subunit interacts with a small subunit (~18 kDa) homologous to domain 4 of the mACN, forming the functional enzyme (Figure 4.2). Structural and mutational analysis of the pig heart mACN indicates Arg580 from domain 4 is the key residue responsible for recognition of citrate, *cis*-aconitate, and isocitrate in the aconitase mechanism [74,100]. The guanidinium nitrogens of Arg580 hydrogen bond to the substrate  $\gamma$ -carboxylate; replacing Arg580 with lysine results in a 30-fold increase in  $K_m$ . However, bioinformatics indicates that this arginine does not align with an arginine in



archaeal IPMIs or HACNs, rendering functional assignment of uncharacterized proteins problematic by sequence alignment alone. The crystal structure of the proposed HACN small subunit from the euryarchaeal *Pyrococcus horikoshii* shows that the loop region between  $\alpha$ -helices 1 and 2 corresponds to the flexible loop region of the pig heart mACN [101]. However, sequence alignment of the mACN and *P. horikoshii* HACN shows that Arg580 is replaced with a polar threonine residue in the loop region. Unfortunately, the *P. horikoshii* putative HACN subunit has not been purified and characterized. Therefore, deriving information about residues responsible for substrate recognition from a protein of unknown biochemical function proves challenging.

MJ1271	-----MIIK	AH	F	---	DDVDTDAIIPGPYLRTT	28
MJ1277	-----MRSIIK	VW	F	---	NNVDTDAILPARYLVYT	30
PhHACN-s	-----MITT	VW	F	---	DDISTDEITPGRYNLT	28
mACN domain 4	DLEDLQILIKVKGKCTTDHISAA	WL	F	GHLDNISNNLLIGAINVENG	600	
MJ1271	DPYELASHCMAGIDEN-----	FPKKVKEGDVIVAGE	F	C	SRE AVIA	73
MJ1277	KPEELAQFVMTGADPD-----	FPKKVKPGDIIVGGK	F	C	SRE APLG	75
PhHACN-s	DPKELAKIAFIEVRPD-----	FARNVRPGDVVAGK	F	I	SRE AALA	73
mACN domain 4	KANSVRNAVQTQEFGPVPDTARYYKKHGIRWVVGDE	Y	E		SRE AALE	650
MJ1271	IKYCGIKAVIAKSFARIFYRNAINVGLIPIIAN----	TDEIKDGD	DIVEID	119		
MJ1277	LKGAGISCVIAESFARIFYRNAINVGLPLIECKG--	ISEKVN	EGDELEV	123		
PhHACN-s	LKALGIAGVIAESFGRIIFYRNAINIGIPLLLGK----	TEGLKD	GLD	119		
mACN domain 4	PRHLGGRAIITKSFARIHETNLLKKQGLLPLTFADPADYNKIHPVDKLT	IK	700			
MJ1271	LDKEEIVITNKNKTIKCE--	TPKGLEREILAAGGLVNYLKKRKL	IQSKKG	167		
MJ1277	LETGEIKNLTTGEVLKGQ--	KLPEFMMEILEAGGLMPYLKK-KMAESQ--	168			
PhHACN-s	WETGEVR--	KGDEILMFE--	PLEDFLLEIVREGGILEYIRRRGDL	163		
mACN domain 4	GLKDFAPGKPLTCIIKHPNGTQETILLNHTFNETQIEWFRAGSALNRMKE	750				
MJ1271	VKT	170				
MJ1277	---					
PhHACN-s	---					
mACN domain 4	LQK	203				

**Figure 4.2. A multiple sequence alignment of proteins homologous to the *Methanocaldococcus jannaschii* HACN small subunit, MJ1271, using the ClustalW program (version 1.83).** The sequences are *M. jannaschii* MJ1271 (Swiss-Prot accession no. Q58667), *M. jannaschii* MJ1277 (Swiss-Prot accession no. Q58673), *Pyrococcus horikoshii* HACN (PhHACN-s; Swiss-Prot 059393), domain four of pig heart mACN (UniPro reference P16276). Conserved amino acid residues are shown in white on a black background. Similar residues are shown in black on a gray background. An asterisks above the sequences indicates the position of the pig heart mACN Arg580. The MJ1271 and MJ1277 sequences proposed for substrate specificity are boxed.

The small subunits of the *M. jannaschii* IPMI (MJ1277) and HACN (MJ1271) underscore the importance of defining the consensus sequence responsible for substrate recognition. These proteins are more than 50% identical to each other and were both previously annotated as IPMI proteins based on primary sequence alone. To assign protein function, the small subunits were overexpressed, purified, and characterized with their respective large subunits (Chapters 2 and 3) [48,49]. The interacting MJ0499-MJ1277 pair functions as the IPMI in methanogen leucine and isoleucine biosynthesis and the MJ1003-MJ1271 pair was identified as the HACN in coenzyme B biosynthesis.(4,5) The predicted loop regions of these enzymes, as indicated by homology models and sequence alignments, are potentially the best indicators of substrate specificity. The HACN<sub>MJ</sub> small subunit has a consensus sequence of Y<sup>24</sup>LRT while the homologous IPMI<sub>MJ</sub> has the sequence Y<sup>26</sup>LVY. The polar Arg26 and Thr27 of HACN<sub>MJ</sub> could potentially form hydrogen bonds with the  $\gamma$ -carboxylates of *cis*-homoaconitate, *cis*-homo<sub>2</sub>aconitate, and *cis*-homo<sub>3</sub>aconitate. The hydrophobic Val28 and Tyr29 residues of the IPMI<sub>MJ</sub> loop region may be the structural determinants for recognizing the substrates hydrophobic  $\gamma$ -chains. These consensus sequences are conserved in most of the Euryarchaeota. Thus, defining their role in the IPMI and HACN mechanisms would allow for assigning gene function for uncharacterized IPMI and HACNs.

In this work, we present the first structural study of a characterized homoaconitase [50]. The *M. jannaschii* HACN small subunit, MJ1271, was crystallized by Yokoyama and colleagues and refined to 2.1Å (PDB 2PKP) [50]. Site directed mutagenesis of the proposed flexible loop region of MJ1271 (in combination with wild type MJ1003), predicted from the structural model and multiple sequence alignments, revealed residues affecting substrate specificity. Mutating residues Arg26 and Thr27 in

the Y<sup>24</sup>LRT loop region of MJ1271 to the homologous Y<sup>26</sup>LVY region in the *M. jannaschii* IPMI small subunit (MJ1277) identified Arg26 as a key amino acid in substrate recognition. We propose that Arg26 is the equivalent of Arg580 of the pig heart mACN, coordinating the  $\gamma$ -carboxylate of the HACN substrates. The results of this study aid in predicting uncharacterized HACNs and IPMIs that were previously indistinguishable through bioinformatics alone.

## **4.2. MATERIALS AND METHODS**

### **4.2.1. Cloning and Molecular Biology**

The *E. coli* BL21(DE3) strains carrying plasmids pDG141 (expressing MJ1003) and pDG163 (expressing MJ1277) were described previously (Table 4.1) [48]. Splicing overlap extension (SOE) PCR was used to construct two chimeric genes [102]. The MJ1271-MJ1277 chimeric gene contained codons 1 to 29 from MJ1277 fused to codons 28 to 170 from MJ1271. T7 promoter and MJ1271Rev-overlap primers (Table 4.2) were used to amplify the 5'-fragment of this chimeric gene from pDG163, and MJ1271Fwd-overlap and T7 terminator primers were used to amplify the 3'-fragment from pDG160. The purified fragments were joined by SOE-PCR. The chimeric product was purified and digested with NcoI and BamHI restriction enzymes, and then ligated into the same sites of vector pET-19b to create vector pDG476. The MJ1271-LysU chimera replaced codons 23 to 30 of MJ1271 with codons 18 to 23 from the *Thermus thermophilus* lysU gene promoter and 3MJ1271-LysU1 primers were used to amplify the 5'-fragment from pDG163, and 5MJ1271-LysU and T7-terminator primers were used to amplify the 3'-fragment pDG163 [93]. SOE-PCR produced a full-length chimeric gene that was ligated into the NcoI and BamHI sites of pET-19b to form vector pDG476. For crystallography

experiments, the MJ1271 gene was amplified from *Methanocaldococcus jannaschii* chromosomal DNA and ligated into vector pET-21a (Novagen) to produce plasmid pMJ1271.

Plasmid pDG160, encoding the wild-type MJ1271 gene, was mutated using the QuikChange II Site-Directed Mutagenesis Kit (Stratagene) and the mutagenic primers listed in Table 4.2 (together with their reverse complements). The resulting mutations were confirmed by DNA sequence of the plasmids listed in Table 1. Plasmid pRD03 was used as a template to generate the double mutation in pRD17 by the same strategy. Electroporation transformed *E. coli* BL21 (DE3) pDG141 cells with the new plasmids encoding small subunit proteins (Table 4.1).

**Table 4.1. List of plasmids and microorganisms**

Strain or plasmid (parent plasmid)	Description	Source and/or reference
<i>Escherichia coli</i>		
BL21(DE3)	Protein expression host	Novagen
BL21 CodonPlus-RIL	Expression host with additional tRNAs	Stratagene
XL-1 Blue	General cloning host	Stratagene
Plasmids		
pMJ1271 (pET-21a)	MJ1271	This work
pDG141 (pCDF-Duet1)	MJ1003	[48]
pDG160 (pET-19b)	MJ1271	[48]
pDG163 (pET-19b)	MJ1277	[48]
pDG476 (pET-19b)	MJ1271-MJ1277 chimera	This work
pDG625 (pET-19b)	MJ1271-LysU	This work
pRD03 (pDG160)	MJ1271 Arg26Val	This work
pRD06 (pDG160)	MJ1271 Arg26Lys	This work
pRD09 (pDG160)	MJ1271 Thr27Ala	This work
pRD17 (pRD03)	MJ1271 Arg26Val Thr27Tyr	This work

**Table 4.2. Oligonucleotide primers used to construct MJ1271 mutations.**

Primer name	Sequence (5' to 3')
T7	TAATACGACTCACTATAGGG
MJ1277Rev-overlap	GCTAACTCGTAAGGGTCTGTATAAACTAAATACCTTGCTGG
MJ1277Fwd-overlap	CCAGCAAGGTATTTAGTTTATACAGACCCTTACGAGTTAGC
T7-terminator	GCTAGTTATTGCTCAGCGG
3MJ1271-LysU1	CCAACCATGAACGGAGCGTATTTTCCTGGAATTATTGCGTC
5MJ1271-LysU1	CGCTCCGTTTCATGGTTGGTGAATACGAGTTAGCTTCACACTG
Arg26Val <sup>1</sup>	CCAGGACCTTACTTAGT <u>G</u> ACTACAGACCCTTACGAG
Arg26Lys <sup>1</sup>	CCAGGACCTTACTTA <u>AAG</u> ACTACAGACCCTTACGAG
Thr27Ala <sup>1</sup>	CCAGGACCTTACTTAAGGG <u>C</u> TACAGACCCTTACGAG
Arg26Val/Thr27Tyr <sup>1</sup>	CCAGGACCTTACTTAGTGTATACAGACCCTTACGAG

<sup>1</sup> Mutations are underlined in these sequences.

#### 4.2.2. Protein Expression and Purification

The plasmids carrying the mutant MJ1271 genes were individually coexpressed with the WT MJ1003 (pDG141) in *E. coli* BL21 (DE3) as described previously (Chapter 2) [49]. The cells were grown at 37°C with shaking at 250 rpm until the culture reached an optical density at 600 nm of 0.6-0.8. Expression was then induced by the addition of 50  $\mu$ M isopropyl-1- $\beta$ -D-galactopyranoside, and the culture resumed shaking for 3-4 hours. The MJ1003 and mutant MJ1271 proteins were purified by heat treatment of the cell lysate, followed by anion exchange chromatography, dialysis and concentration [49].

#### **4.2.3. Analytical Size Exclusion Chromatography**

Interactions between MJ1003 and MJ1271 variants were tested by measuring apparent masses of protein pairs using size exclusion chromatography, as described previously (Chapter 2) [62].

#### **4.2.4. Reconstitution of the Iron-Sulfur Center**

Copurified MJ1003 and MJ1271 mutants (1-2 mg ml<sup>-1</sup> apoenzyme) were reconstituted in the presence of DTT, Fe(NH<sub>4</sub>)<sub>2</sub>(SO<sub>4</sub>)<sub>2</sub>, and Na<sub>2</sub>S as described previously (Chapter 3) [49]. A mock reconstitution control consisted of the above mixture without protein.

#### **4.2.5. Measurement of Hydrolyase Activities**

Reactions (1 ml) were conducted in quartz semi microcells with screw cap septa (Starna) containing 50 mM CHES-KOH (pH 9.0), 200 mM KCl, 10-100 µg ml<sup>-1</sup> holoenzyme, and various substrate concentrations, as described previously (Chapter 3) [49].

#### **4.2.6. Homology modeling and Structure Representation**

The Swiss model automated comparative protein modeling server was used to construct the MJ1277 homology using pdb 2PKP as the template (21). The MJ1003 model was constructed using the Swiss-Pdb Viewer Deep View (v4.0) and pdb 1ACO as the template [103]. Figures were prepared using the PYMOL program (DeLano Scientific LLC).

## 4.3. RESULTS

### 4.3.1. Structure of MJ1277 Homology Model

The *M. jannaschii* IPMI small subunit, MJ1277, shares more than 50% sequence identity with MJ1271. Therefore, a homology model of MJ1277 was built using pdb 2PKP as a template, resulting in a structural alignment with an rmsd of 0.1 Å (Figure 4.3). The model of MJ1277 has an N- to C-terminus arrangement of  $\beta$ 1- $\alpha$ 2- $\alpha$ 3- $\alpha$ 4- $\beta$ 5- $\alpha$ 6- $\beta$ 7- $\alpha$ 8- $\beta$ 9- $\beta$ 10- $\beta$ 11- $\alpha$ 12- $\alpha$ 13, with a similar partition of  $\alpha$ -helices and  $\beta$ -strands. The GS<sup>67</sup>SRE sequence is located in the loop region between  $\beta$ 6 and  $\alpha$ 7, parallel to the Y<sup>26</sup>LVY sequence between  $\alpha$ 3 and  $\alpha$ 4.



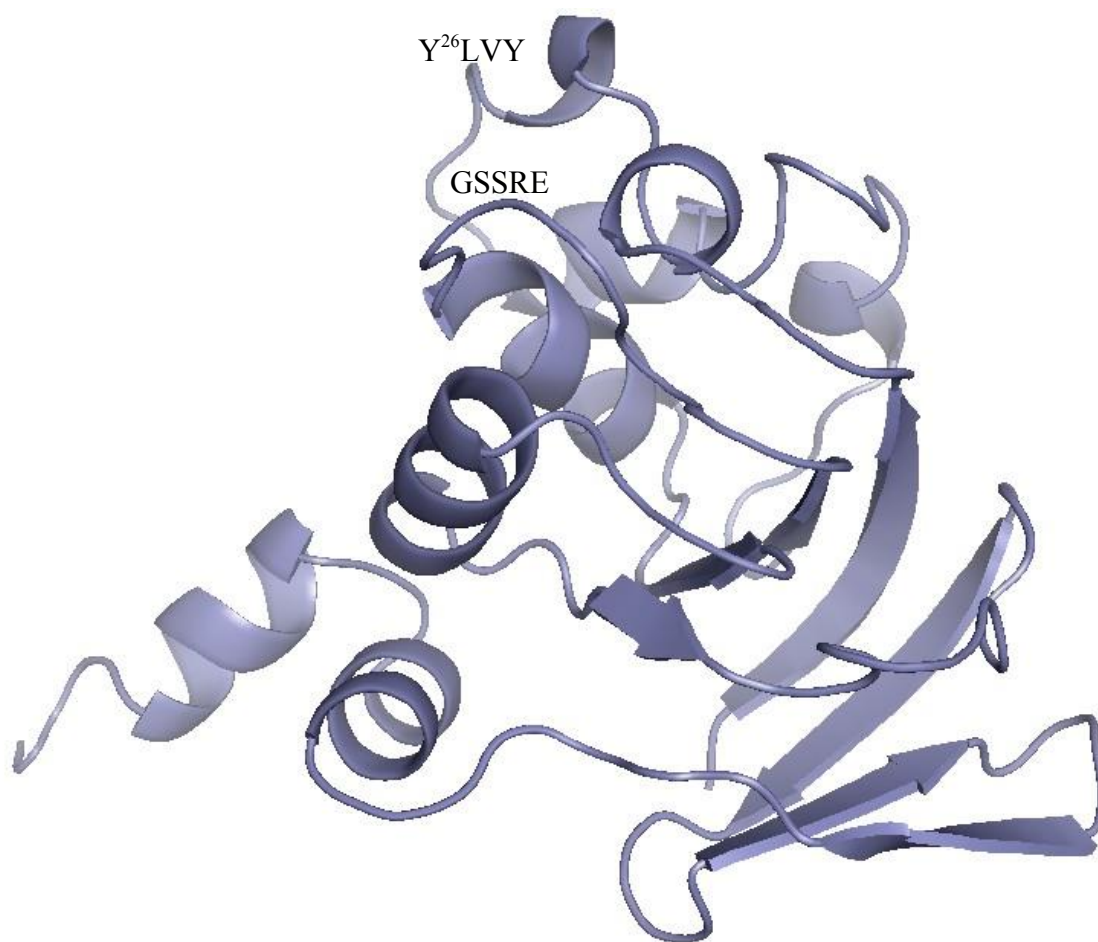


**Figure 4.3. Homology model of the *M. jannaschii* IPMI small subunit, MJ1277.** The MJ1271 homology model was constructed with the Swiss model automated comparative protein modeling server using the MJ1277 structure (PDB 2PKP) as a template. Sequences indicate the loop regions proposed to function in IPMI<sub>MJ</sub> substrate specificity and catalysis,

### 4.3.2 Expression and Subunit interaction of MJ1003 and the MJ1271 Variants

To confirm that the Y<sup>24</sup>LRT sequence of MJ1271 confers substrate specificity for the HACN<sub>MJ</sub>, six variant forms of the *MJ1271* gene were constructed (Table-mutations and primers) and coexpressed with the wild type (WT) *MJ1003*, as described previously (Chapter 3) [49]. The soluble proteins were aerobically purified by heating at 70°C followed by anion exchange chromatography and subunit interaction was analyzed by analytical size exclusion chromatography. The six HACN<sub>MJ</sub> variants eluted as complexes with molecular masses of 144-155 kDa. The large and small subunits are approximately 46 kDa and 18 kDa, respectively. Therefore, these mutant forms of HACN<sub>MJ</sub> are probably forming heterotetramers consisting of two large and two small subunits, which is consistent with WT HACN<sub>MJ</sub>, which eluted with a molecular mass of 143 kDa.

### 4.3.3. MJ1003 – MJ1271 Arg26Val and Arg26Lys

Arg26 in the Y<sup>24</sup>LRT sequence of MJ1271 was predicted to be analogous to Arg580 of pig heart mACN. Mutation of Arg580 to lysine resulted in a 30-fold increase in  $K_m$  for aconitase with isocitrate, a decrease in activity, and a loss of tight substrate binding [74]. Replacing the MJ1271 Arg26 to lysine resulted in a 6-fold increase in  $K_m$  for *cis*-homoaconitate. However, activity with citraconate and 3-isopropylmalate was observed. Arg26 has to accommodate substrates with varying  $\gamma$ -chain lengths. Therefore, mutating Arg26 to the smaller, polar lysine residue probably does not interfere with the hydrophobic  $\gamma$ -chains of the smaller citraconate and 3-isopropylmalate. This is apparent when comparing the  $K_m$  and  $k_{cat}$  values for citraconate (315  $\mu$ M, 8.4 s<sup>-1</sup>) and maleic acid (310  $\mu$ M, 8.1 s<sup>-1</sup>), which are virtually identical. Replacing Arg26 to valine, the analogous residue in MJ1277, has a more obvious effect on substrate recognition. Although similar  $K_m$  values are observed for maleic acid and citraconate, the activity with

respect to 3-isopropylmalate was comparable to the WT IPMI<sub>MJ</sub>. Compared to the WT IPMI<sub>MJ</sub>, the MJ1271 R26V mutant resulted in a less than 2-fold increase in  $K_m$  for 3-isopropylmalate (39  $\mu$ M and 68  $\mu$ M, respectively) and similar turnover (1.9 s<sup>-1</sup> and 1.1 s<sup>-1</sup>, respectively). Although activity was not completely abolished with the WT HACN<sub>MJ</sub> substrates, the  $K_m$  values for *cis*-homoaconitate, *cis*-homo<sub>2</sub>aconitate, and *cis*-homo<sub>3</sub>aconitate increased between 10-30 fold. Therefore, Arg26 of MJ1271 plays a key role in HACN<sub>MJ</sub> substrate recognition while the corresponding valine residue of IPMI<sub>MJ</sub> accommodates the hydrophobic methyl or isopropyl  $\gamma$ -chain chains of citraconate and 3-isopropylmalate.

**Table 4.3. Steady-state kinetic values for the MJ1003-MJ1271 variant enzymes compared to WT IPMI<sub>MJ</sub>**

Enzyme	<u>Maleic acid</u>		<u>Citraconate</u>		<u><math>\beta</math>-Isopropylmalate</u>	
	$K_m$ ( $\mu$ M)	$k_{cat}$ (s <sup>-1</sup> )	$K_m$ ( $\mu$ M)	$k_{cat}$ (s <sup>-1</sup> )	$K_m$ ( $\mu$ M)	$k_{cat}$ (s <sup>-1</sup> )
IPMI <sub>MJ</sub>	400 $\pm$ 50	36	80 $\pm$ 20	14	39 $\pm$ 7	1.9
R26V	230 $\pm$ 10	9.9	190 $\pm$ 20	5.5	68 $\pm$ 5	1.1
R26K	310 $\pm$ 32	8.1	315 $\pm$ 71	8.36	180 $\pm$ 30	0.8
T27A	3400 $\pm$ 200	24.2	920 $\pm$ 230	4.1	ND <sup>a</sup>	ND
R26V T27Y	489 $\pm$ 86	23.1	290 $\pm$ 70	9.8	133 $\pm$ 37	1.6

<sup>a</sup> Not detected.

**Table 4.4. Steady-state kinetic values for the MJ1003-MJ1271 variant enzymes compared to WT HACN<sub>MJ</sub>**

	<b><u>Maleic acid</u></b>		<b><u>Homoaconitate</u></b>		<b><u>Homo<sub>2</sub>aconitate</u></b>		<b><u>Homo<sub>3</sub>aconitate</u></b>	
Enzyme	K <sub>m</sub> (μM)	k <sub>cat</sub> (s <sup>-1</sup> )	K <sub>m</sub> (μM)	k <sub>cat</sub> (s <sup>-1</sup> )	K <sub>m</sub> (μM)	k <sub>cat</sub> (s <sup>-1</sup> )	K <sub>m</sub> (μM)	k <sub>cat</sub> (s <sup>-1</sup> )
HACN <sub>MJ</sub>	330 ± 50	6	22 ± 3	0.75	30 ± 5	0.66	36 ± 6	2.5
R26V	230 ± 10	9.9	220 ± 30	0.48	870 ± 150	5.8	660 ± 170	2.8
R26K	310 ± 32	8.1	135 ± 27	1.43	- <sup>a</sup>	-	-	-
T27A	3400 ± 200	24.2	220 ± 20	2.5	269 ± 68	2.2	650 ± 80	4.1
R26V/T27Y	489 ± 86	23.1	460 ± 80	1.7	1600 ± 500	6.6	640 ± 90	1.9

<sup>a</sup> Dash indicates that the substrate was not tested.

#### 4.3.4. MJ1003 – MJ1271 Thr27Ala

In the conserved YLRT and YLVY sequences of HACN<sub>MJ</sub> and IPMI<sub>MJ</sub>, respectively, the residue adjacent to the critical arginine and valine differ. In the loop region of the pig heart mACN, adjacent to Arg580 is a glycine residue that is not known to function in the active site. To analyze whether Thr27 of HACN<sub>MJ</sub> plays a catalytic role, the MJ1271 Thr27Ala variant was constructed. While the MJ1271 Arg26Val and Arg26Lys mutants maintained similar K<sub>m</sub> values for maleic acid, the Thr27Ala mutant resulted in an almost 10-fold increase in K<sub>m</sub> compared to WT IPMI<sub>MJ</sub>. Although 3-isopropylmalate was not detected as a substrate, most likely because of electrostatic interactions of the Arg26 guanadinium group with the nonpolar isopropyl γ-chain of the compound, activity with citraconate was observed. Although the resulting K<sub>m</sub> with citraconate was approximately 1 mM, the mutant enzyme had appreciable turnover, resulting in a specificity constant of 3.4 x 10<sup>4</sup> M<sup>-1</sup> s<sup>-1</sup>. Compared to the WT HACN<sub>MJ</sub> substrates, the K<sub>m</sub> values for *cis*-homoaconitate, *cis*-homo<sub>2</sub>aconitate, and *cis*-homo<sub>3</sub>aconitate increased 10-20 fold for the Thr27Ala mutant while the specificity constants decreased 2-10 fold.

#### 4.3.5. MJ1003 – MJ1271 Arg26Val/Thr27Tyr

Comparing the loop regions predicted to be responsible for HACN<sub>MJ</sub> and IPMI<sub>MJ</sub> recognition, Y<sup>24</sup>LRT and Y<sup>26</sup>LVY, respectively, the Arg-Val and Thr-Tyr residues comprise the structural difference in these regions. Therefore, the MJ1271 Arg26Val/Thr27Tyr variant was constructed in an effort to alter the loop region of MJ1271 to more structurally resemble the loop region of MJ1277. Exchanging the Arg26 and Thr27 residues resulted in a  $K_m$  of 489  $\mu$ M for maleic acid, similar to WT HACN<sub>MJ</sub> and IPMI<sub>MJ</sub>, and a turnover that was on the order of the Thr27Ala variant and WT IPMI<sub>MJ</sub>. However, compared to the Arg26Val variant, the  $K_m$  and  $k_{cat}$  values for both citraconate and 3-isopropylmalate increased slightly. The  $K_m$  values for *cis*-homoaconitate, *cis*-homo<sub>2</sub>aconitate, and *cis*-homo<sub>3</sub>aconitate increased 20-50 fold compared to WT HACN<sub>MJ</sub>. Although the double mutation did result in an increase in  $k_{cat}$  for *cis*-homoaconitate and *cis*-homo<sub>2</sub>aconitate, all three substrates had specificity constants that were an order of magnitude lower than the wild type enzyme. The discrepancy between the kinetics for citraconate and 3-isopropylmalate, when compared with the Arg26Val variant, probably results from structural changes in the loop region with the threonine to tyrosine mutation, as discussed for MJ1271 Thr27Ala above.

#### 4.3.6. MJ1003-MJ1271/1277 Chimera

A chimeric MJ1271 protein was constructed which replaced the first 28 amino acids with the first 28 amino acids of MJ1277 to test whether the substrate specificity could be completely altered from HACN<sub>MJ</sub> to IPMI<sub>MJ</sub>. Although the chimera interacted with MJ1003 as a heterotetramer, no activity was detected for any of the tested substrates

after reconstitution. The failure to detect activity is consistent with expressing MJ1003 with MJ1277. The HACN<sub>MJ</sub> large subunit and IPMI<sub>MJ</sub> small subunit interact but no activity was observed for any tested compound.

#### 4.3.7. Loop replacement: MJ1003-MJ1271/LysU

In previous studies of HACNs involved in lysine biosynthesis, the reversible hydration of *cis*-homoaconitate to (2*R*,3*S*)-homoisocitrate has been observed while the initial dehydration of (*R*)-homocitrate has gone undetected [93]. Sequence alignments and homology models of the *T. thermophilus* LysU protein reveals a loop region with the sequence Y<sup>21</sup>APFMV. However, this sequence does not provide insight into the mechanism discrepancy. A chimeric form of MJ1271 was created, replacing the loop region containing the Y<sup>24</sup>LRT region with the corresponding region of the *T. thermophilus* LysU protein, in an effort to alter the reactions catalyzed by the HACN<sub>MJ</sub> to that of the  $\alpha$ -aminoadipate HACNs. Although the chimeric protein still interacted with MJ1003 and maintained relatively low activity with maleic acid ( $K_m$  350  $\mu$ M;  $k_{cat}$  0.45 s<sup>-1</sup>;  $k_{cat}/K_m$  1.4 x 10<sup>3</sup> M<sup>-1</sup> s<sup>-1</sup>), no activity was detected for *cis*-homoaconitate or any other tested substrates.

### 4.3 DISCUSSION

The structure of the *M. jannaschii* HACN small subunit, MJ1271, was solved by molecular replacement using the *P. horikoshii* HACN small subunit (PhIPMI-s; pdb 1V7L) and the structure was refined to 2.1Å. MJ1271 consists of 16  $\beta$ -strands and  $\alpha$ -helices with an N- to C-terminus arrangement of  $\beta$ 1- $\alpha$ 2- $\alpha$ 3- $\alpha$ 4- $\beta$ 5- $\alpha$ 6- $\beta$ 7- $\alpha$ 8- $\beta$ 9- $\alpha$ 10- $\beta$ 11- $\beta$ 12- $\alpha$ 13- $\beta$ 14- $\alpha$ 15- $\alpha$ 16 (Figure 4.4) [50].  $\alpha$ -Helices 2-4, 6, 8, 15 and 16 are

concentrated next to a  $\beta$ -barrel type structure that is interrupted by  $\alpha 10$  and  $\alpha 13$ . The conserved GS<sup>65</sup>SRE sequence, in which Ser65 is analogous to the catalytic Ser642 of the pig heart mACN, is located in a loop region positioned between  $\beta 5$  and  $\alpha 6$ . This loop is spatially adjacent to a loop region between  $\alpha 2$  and  $\alpha 3$  containing the Y<sup>24</sup>LRT sequence predicted to function in substrate recognition. Tyr24 and Leu25 of this sequence reside in  $\alpha 2$ , while Arg26 and Thr27 are positioned in the loop region between helices.

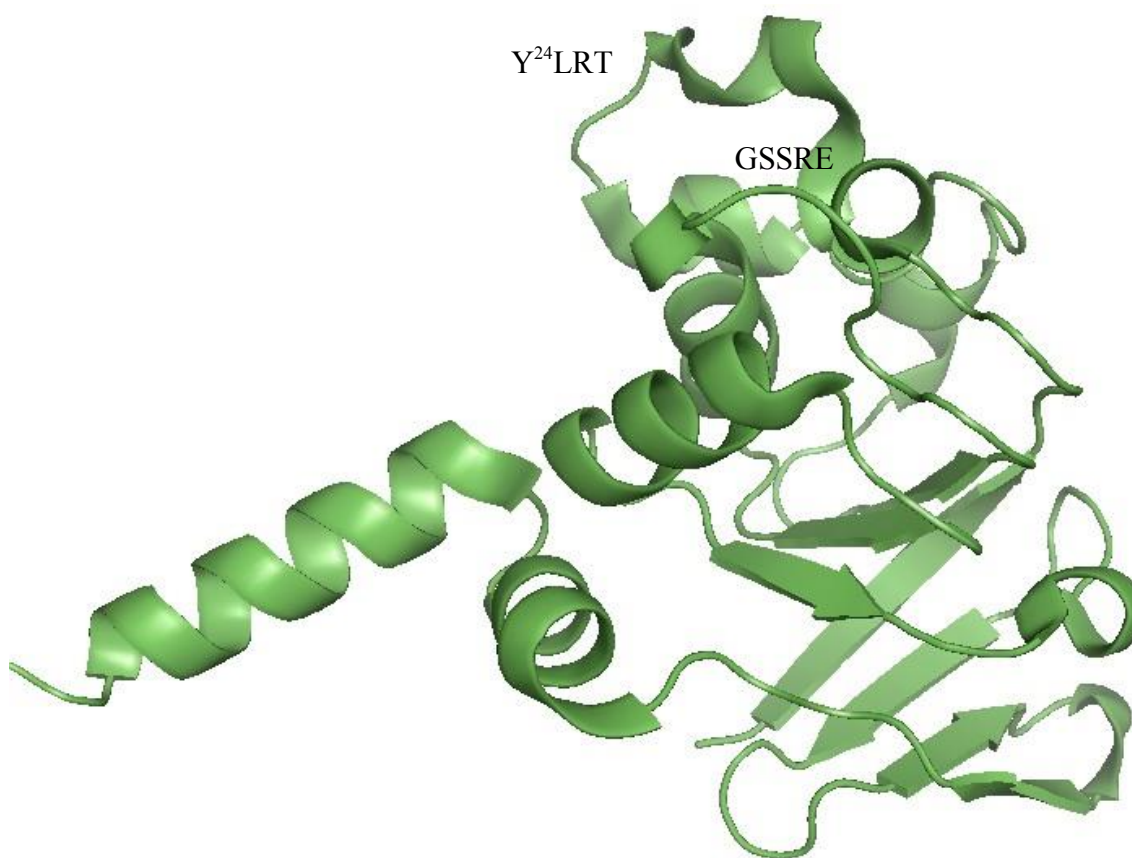


**Figure 4.4. Structure of the *M. jannaschii* HACN small subunit, MJ1271 (PDB 2PKP).** Sequences indicate the loop regions proposed to function in HACN<sub>MJ</sub> substrate specificity and catalysis,

The MJ1271 protein is clearly a homolog of the fourth domain of mACN and the *P. horikosii* HACN, as evident in both sequence (Figures 4.2 and 4.5) and structural alignment. These three structures consist of an N-terminal network of  $\alpha$ -helices adjacent to a C-terminal  $\beta$ -barrel type structure. Structural alignment of MJ1271 with the relaxed (without substrate) or tense (substrate bound) structures of pig heart mACN results in an rmsd of 1.9 Å (Z scores between 19.0 – 19.2), as indicated by the DALI server. Therefore, structural information, including the elucidation of active site residues, can be



inferred from the extensive structural and mechanistic studies of mACN, despite the lack of interacting large subunit, MJ1003.

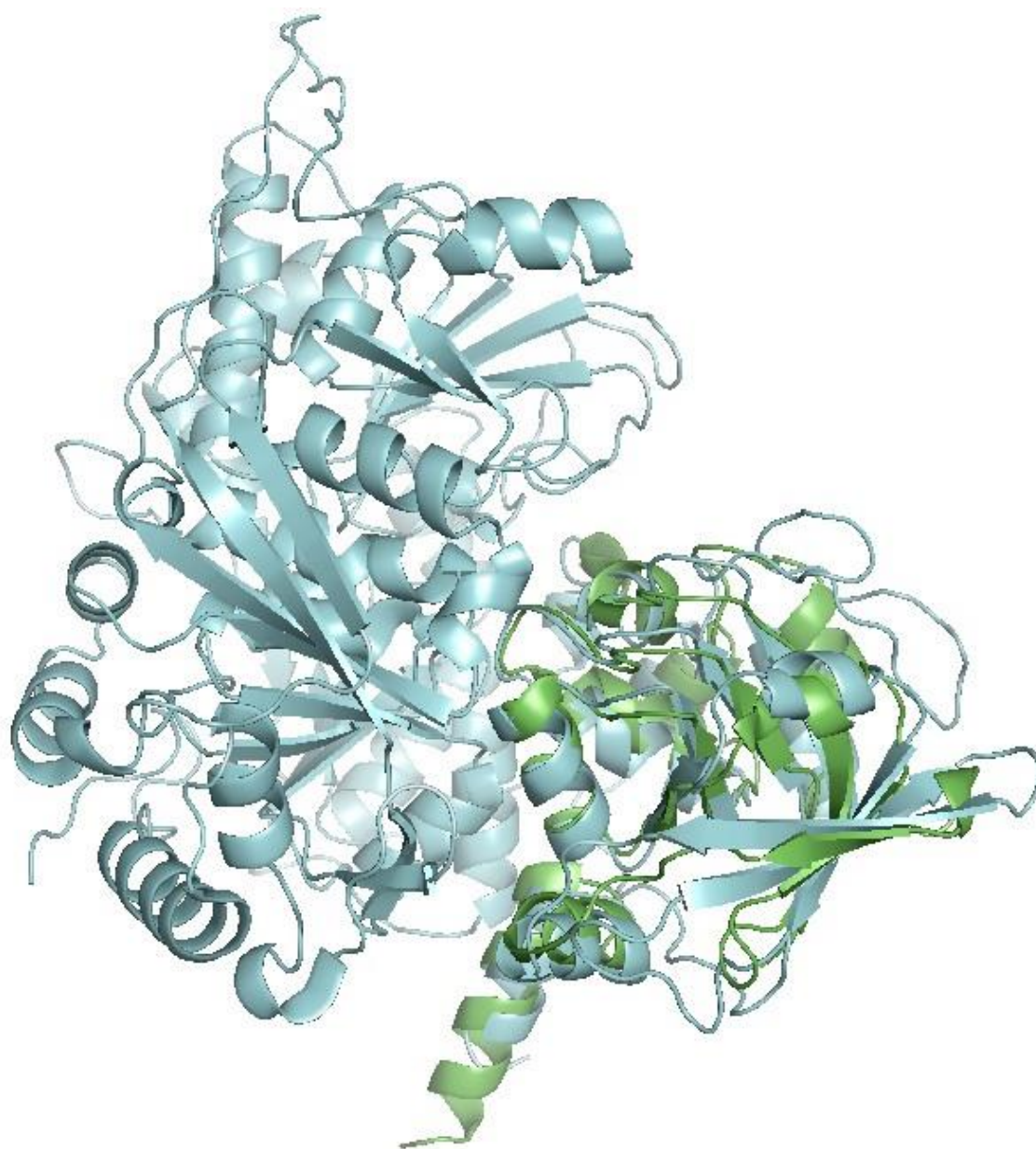


**Figure 4.5.** Structural alignment of the mACN domain 4 (blue; PDB 1AMJ) and *M. jannaschii* HACN small subunit, MJ1271 (green; 2PKP).

In the relaxed and tense states of mACN, the  $\alpha$ -helices of domain four are packed at the interface with domains 1, 2, and 3, forming the active site cleft [104]. The GS<sup>642</sup>SRE and Arg580 residues, located within the loop regions of these  $\alpha$ -helices, comprise most of the active site residues found in this domain. Therefore, it is predicted that the  $\alpha$ -helices of the MJ1271 structure (and the MJ1277 homology model) are at the interface between the large and small subunit and are the location of critical active site residues. In a structural alignment of MJ1271 with substrate free mACN (pdb 1AMJ), the conserved C $\alpha$  backbone of the GSSRE sequence align fairly well and the catalytic serine residues (Ser642 and Ser65 for mACN and MJ1271, respectively) have side chains with similar orientation (Figure 4.6A). The remaining residues in the sequence, most notably the Arg644 in mACN (Arg67 in MJ1271), the residue that stabilizes the Ser642 alkoxide in the mACN mechanism, have side chains that show significant differences in orientation. Also, the GSSRE sequence of mACN resides completely in a loop region, where the GSSRE sequence of MJ1271 is located at the interface of the loop and  $\alpha$ 6. Aligning MJ1271 with substrate bound mACN (PDB 1AMI) shows a similar alignment of C $\alpha$  backbones and side chain residues of the GSSRE sequence. However, a difference in the alignment of S642 of mACN and Ser65 of MJ1271 is observed, indicating an almost 180° rotation of the mACN side chain, which is consistent with the alignment of the relaxed state (pdb 1AMJ) with the tense (pdb 1AMI) state of mACN (Figure 4.6C).

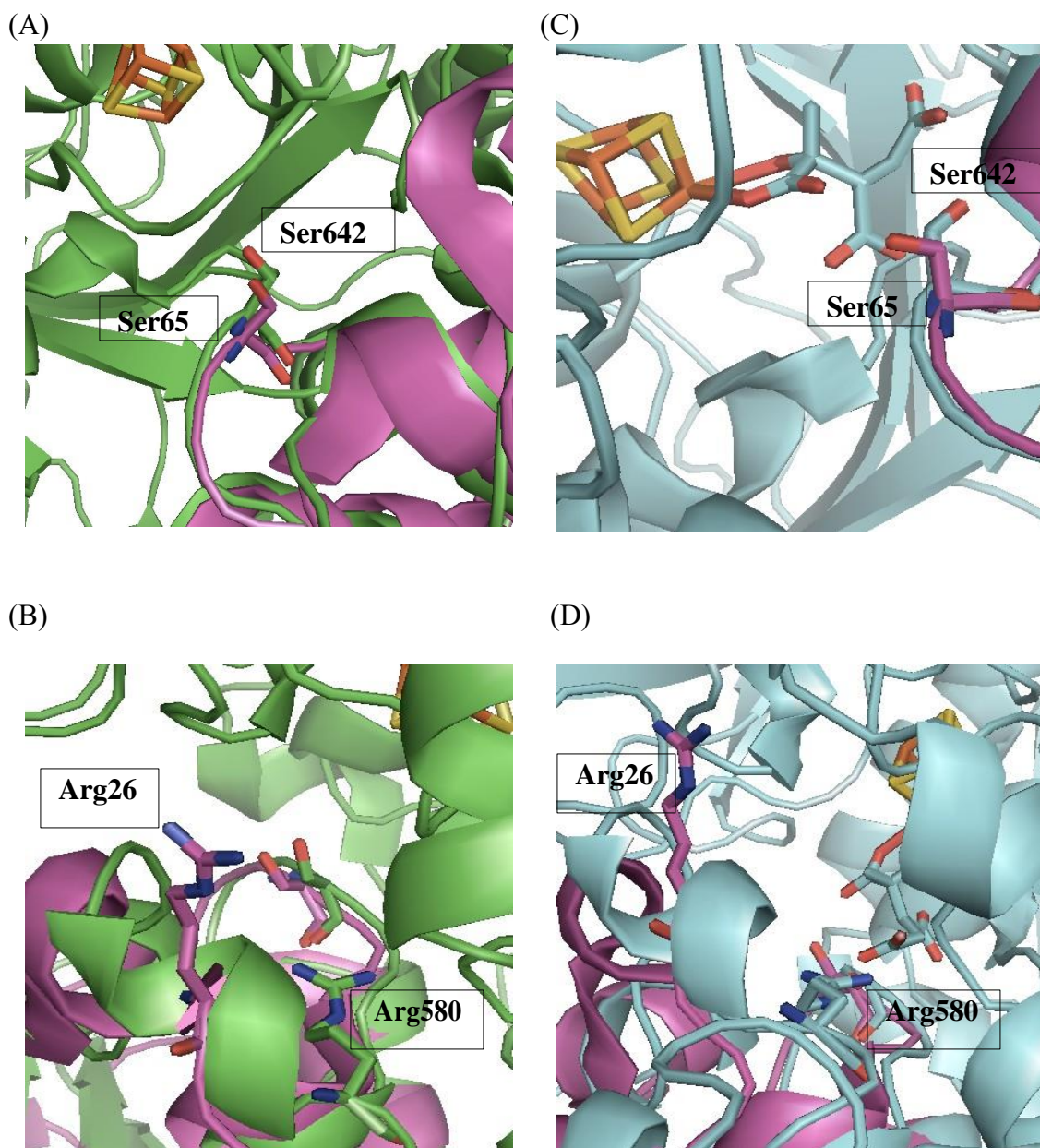


**Figure 4.6. Structural alignment of MJ1271 (PDB 2PKP) with domain 4 of mACN in the relaxed (PDB 1AMI) and tense states (PDB 1AMJ).** (A) Alignment of MJ1271 Ser65 (magenta) with the mACN Ser642 (green) in the relaxed state; (B) alignment of MJ1271 Arg 26 (magenta) with the mACN Arg580 (blue) in the relaxed state; (C) alignment of MJ1271 Ser65 (magenta) with the mACN Ser642 (blue) in the tense state; (D) alignment of MJ1271 Arg26 (magenta) with the mACN Arg580 (blue) in the tense state.

The position of the MJ1271 Y<sup>24</sup>LRT sequence with respect to the conserved GS<sup>65</sup>SRE loop region indicates that this sequence is aligned to interact with the  $\gamma$ -carboxylates of the HACN substrates. However, the Y<sup>24</sup>LRT sequence aligns poorly with the corresponding loop region of pig heart mACN, which is the site of Arg580 (Figure 4.7). The Arg26 of MJ1271 aligns with Leu577 of mACN, instead of Arg580, and there is an approximately 120° difference in the orientation of the two arginine residues. Arg26 is also oriented perpendicular to the GS<sup>65</sup>SRE sequence and does not appear to be in line to contact the substrate  $\gamma$ -carboxylate as Arg580 is with respect to the mACN GSSRE sequence. However, structural alignment of MJ1271 with both relaxed and tense structures of aconitase suggest that MJ1271 may be in the relaxed state (Figure 4.6). The binding of substrate at the active site of mACN results in conformational changes 30 Å from the active site [104]. Therefore, conformational changes resulting from substrate binding may change the position of this residue. The orientation of the Y<sup>24</sup>LRT loop region may also be influenced by interaction with MJ1003. A crystal structure of the interaction MJ1003-MJ1271 proteins in the presence and absence of protein will be required to accurately assess the orientation of Arg26 of MJ1271.

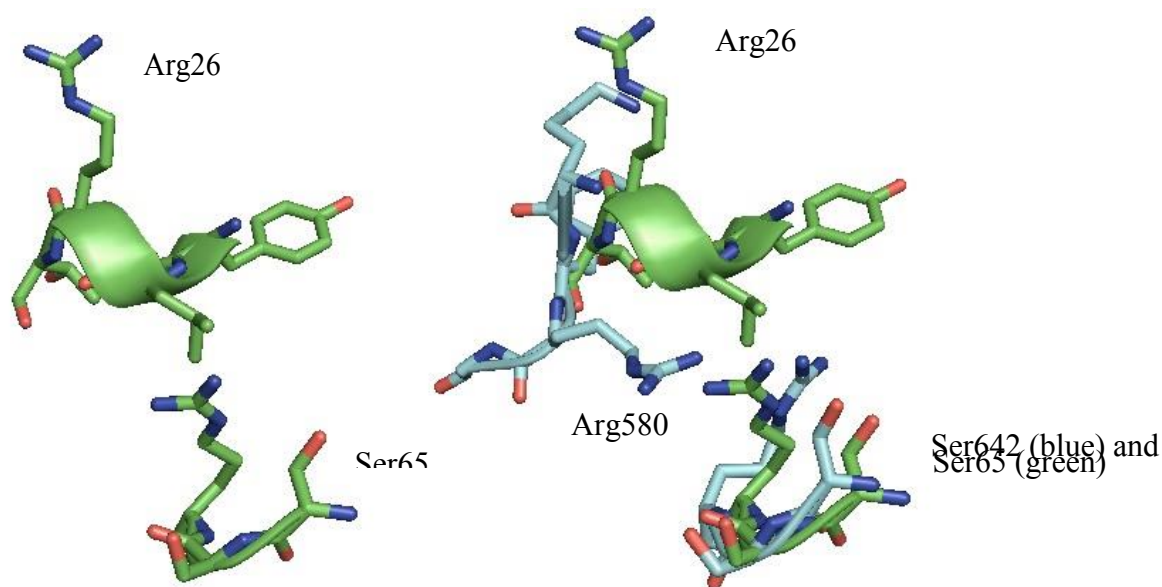


**Figure 4.7. Structural alignment of the MJ1271 loop regions proposed to function in substrate specificity and catalysis with the corresponding loop regions of mACN.** *Left*, Y<sup>24</sup>LRT and S<sup>65</sup>SR sequence of MJ1271 (green); *Right*, structural alignment of MJ1271 (green) with the loop containing Arg580 and S<sup>642</sup>SR (blue; PDB 1AMJ).

The results of the site directed mutagenesis of MJ1271 suggests that Arg26 is a critical residue in the substrate specificity of HACN<sub>MJ</sub>. Mutation of this residue to the valine or lysine dramatically increased the Michaelis constants for *cis*-homoaconitate, *cis*-homo<sub>2</sub>aconitate, and *cis*-homo<sub>3</sub>aconitate compared to the WT HACN<sub>MJ</sub>. The HACN<sub>MJ</sub> variants were also active with the substrates of IPMI<sub>MJ</sub>. The Arg26Val mutation resulted in  $K_m$  and  $k_{cat}$  values comparable to IPMI<sub>MJ</sub>, suggesting that Val28 of the MJ1277 Y<sup>26</sup>LVY sequence is necessary to accommodate the hydrophobic  $\gamma$ -chain of citraconate and dimethylcitraconate.

The residue adjacent to Arg580 of pig heart mACN has not been shown to function in the mechanism of aconitase. The adjacent residue to the MJ1271 Arg26 is a threonine, which corresponds to Tyr29 of MJ1277. Replacing Thr27 with alanine

disrupted the activity of HACN<sub>MJ</sub> for all substrates, most notably by increasing the  $K_m$  of maleic acid 10 fold compared to WT HACN<sub>MJ</sub>. The MJ1271 structure indicates that the Thr27 side chain is oriented away from the predicted active site of HACN<sub>MJ</sub>. Based on the structural and kinetic data, Thr27 probably plays a structural role in the flexibility of the loop region, potentially making contacts with other active site amino acids, but does not appear to interact directly with the substrate.

In an attempt to completely alter the substrate specificity of HACN<sub>MJ</sub> to mimic IPMI<sub>MJ</sub>, a chimeric protein was constructed where the first 28 amino acids of MJ1271 were replaced with the corresponding residues of MJ1277. Although these proteins interacted as a heterotetramer and bound an iron-sulfur cluster, no activity was observed above background with any of the tested substrates. The inability to observe activity with maleic acid, the minimal substrate, indicates that, although the proteins interact, they may interact in a way where the catalytic residues of MJ1277 do not align with the active site of MJ1003. Similar results were observed after coexpressing and reconstituting MJ1003 with MJ1277.

Although the substrate specificity of the HACN<sub>MJ</sub> protein was altered to accommodate the substrates of IPMI<sub>MJ</sub>, activity was not completely lost for HACN<sub>MJ</sub> substrates. Thus, it is likely that the interacting large subunits of these proteins, MJ1003 and MJ0499, respectively, also play a role in substrate specificity. However, the characterizations of HACN<sub>MJ</sub> and IPMI<sub>MJ</sub>, the crystallography and homology modeling of MJ1271 and MJ1277, and the site directed mutagenesis of MJ1271 all indicate that the conserved Y<sup>24</sup>LRT and Y<sup>26</sup>LVY sequences are sufficient indicators of protein function in archaea. Therefore, uncharacterized proteins with the Y<sup>24</sup>LRT sequence are likely HACNs, while proteins with the YLV(Y/I/M) sequence are IPMIs. These studies should allow for the proper annotation of these uncharacterized proteins.

The HACN<sub>MJ</sub>, IPMI<sub>MJ</sub>, and mACN catalyze the dehydration of their respective  $\alpha$ -hydroxyacid substrates and subsequent rehydration of the resulting *cis*-unsaturated intermediates, forming a  $\beta$ -hydroxyacid. Given the homology of the  $\alpha$ -aminoadipate HACN to these enzymes, it is surprising the initial dehydration of (*R*)-homocitrate has not been observed. We replaced the region of MJ1271 containing the Y<sup>24</sup>LRT sequence with the corresponding sequence from the *T. thermophilus* HACN in an attempt to alter the catalytic mechanism to accommodate only the hydration of *cis*-homoaconitate to (2*R*, 3*S*)-homoisocitrate. Although the MJ1003-MJ1271/LysU variant interacted as a heterotetramer and was active with maleic acid as a substrate, no activity was observed with any of the other HACN<sub>MJ</sub> or IPMI<sub>MJ</sub> substrates. Therefore, a crystal structure of an  $\alpha$ -aminoadipate HACN with bound substrate as well as mutagenesis of active site amino acids will be required to resolve this difference in overall mechanism.

Although most crenarchaea use both the  $\alpha$ -aminoadipate and isopropylmalate pathways for lysine and leucine biosynthesis, respectively, they appear to only have one HACN/IPMI homolog with a conserved YL(K/V)Y sequence. These putative enzymes are expected to accept a broad pool of hydroxyacid substrates. While these crenarchaeal proteins have yet to be purified and characterized, the results of the MJ1271 mutagenesis show that mutating Arg26 of YLRT to either lysine or valine allows for the recognition of both HACN<sub>MJ</sub> and IPMI<sub>MJ</sub> substrates. However, the WT HACN<sub>MJ</sub> did not accept the substrates of IPMI<sub>MJ</sub> and, similarly, IPMI<sub>MJ</sub> did not accept HACN substrates. Therefore, future studies will involve the characterization, crystallization, and mutagenesis of these crenarchaeal proteins to evaluate more closely how these ancestral proteins recognize their substrates.



## Chapter 5: Archaeal Iron-Sulfur Cluster Biosynthesis

### 5.1. INTRODUCTION

Iron-sulfur clusters are versatile inorganic cofactors involved in oxidation-reduction (redox), non-redox, and radical chemistry, as well as serving as biological sensors for the regulation of gene expression [105]. Proteins requiring these clusters have been identified in all known organisms. Although these protein-bound iron-sulfur clusters are readily synthesized in vitro, intricate mechanisms for cluster biosynthesis and transfer are required in vivo to prevent toxicity from free iron and sulfur.

Three main systems have been identified for iron-sulfur cluster biosynthesis in bacteria and eukaryotes: NIF, ISC, and SUF [106,107]. The NIF system is required for maturation of nitrogenase in bacteria while ISC plays a general “house-keeping” role in bacteria and eukaryotes. The SUF system, present in bacteria, archaea, and plants is expressed under oxidative stress or iron starvation. These three systems involve proteins with common functions. NifS, IscS, and SufS are cysteine desulfurases, producing sulfane sulfur and alanine from cysteine. IscU, IscA, NifU, SufU, and SufA function as scaffolding proteins for the synthesis of iron-sulfur clusters and transfer to target apoproteins [106,107]. The SUF system also possess the proteins SufB, a persulfide acceptor, and SufC, an ABC-type ATPase, which form a complex that may potentially serve as a scaffold for cluster synthesis and transfer [108].

Recently, the *apbC* locus from *Salmonella enterica* serovar Typhimurium LT2 was identified to encode for an iron-sulfur scaffold protein [109]. Strains with lesions at this locus were conditional thiamine auxotrophs, similar to *S. enterica* strains with disruptions in the *isc* operon, blocking thiazole synthesis [110,111]. A role for ApbC in



iron-sulfur cluster biosynthesis was suggested when *apbC* mutations resulted in decreased aconitase and succinate dehydrogenase activity, two enzymes requiring these clusters for catalysis [111]. Lesions in the *apbC* locus of *S. enterica* also prevented growth when tricarballoylate was the sole carbon source. Tricarballoylate, a citrate analogue, is metabolized via the FAD-dependent tricarballoylate dehydrogenase (TcuA), which converts the substrate to *cis*-aconitate for the TCA cycle [112]. The FAD of TcuA is regenerated by the membrane bound TcuB protein, which uses two [4Fe-4S] clusters and heme to transfer electrons from FADH<sub>2</sub> to the cytoplasmic membrane quinone pool [113]. The dependence of ApbC for growth on tricarballoylate and not the Isc or Suf analogues suggests that this protein functions in iron-sulfur cluster formation on TcuB. Indeed, the activity of TcuB in *S. enterica* strains lacking *apbC* was diminished compared to wild type [109].

The *S. enterica* ApbC is a 40-kDa cytosolic protein homologous to the P-loop NTPases Cfd1 and Nbp34. These two NTPases have been implicated as iron-sulfur scaffold components of the yeast CIA machinery, binding and transferring their clusters to target proteins in the cytosol [114,115]. Cfd1 possesses a C-terminal CX<sub>18</sub>CPXCX<sub>n</sub>C motif and binds four moles of iron and sulfur while Nbp35 has an N-terminal ferredoxin-like CX<sub>13</sub>CX<sub>2</sub>CX<sub>5</sub>C motif in addition to the conserved C-terminal motif of Cfd1, and binds 8 moles of iron and sulfur [114,115]. Although Cfd1 and Nbp35 have been shown to function independently *in vitro*, the two proteins form a complex that binds 12 moles of iron and 12 moles of sulfur per mole of dimeric complex [114]. These two proteins also have conserved Walker A box motifs for binding and hydrolyzing ATP.

Similar to the Cfd1 and Nbp35 proteins, ApbC is also a member of the P-loop NTPase family, possessing a Walker A box motif. However, ApbC has two conserved C-terminal cysteine residues, with a consensus sequence of CXXC, and no conserved N-

terminal cysteines [111]. After anaerobic reconstitution, ApbC bound two moles of iron and two moles of sulfur per mole of protein, consistent with a [2Fe-2S] cluster, although a [4Fe-4S] cluster may form at the dimer interface [116]. Consistent with Cfd1 and Nbp35, the reconstituted ApbC effectively transferred its bound cluster to apo-isopropylmalate isomerase (apo-IPMI) [116,114]. Although the *S. enterica* protein exhibits ATPase activity, ATP was not required for transfer of the cluster to apo-IPMI [116,117]. However, a mutation in the Walker A box motif resulted in an inactive protein, suggesting that ATP is required for binding or loading of the iron-sulfur cluster, but not transfer [116,117].

Iron-sulfur cluster dependent proteins have been identified from Archaea, such as the isopropylmalate isomerase and homoaconitase (HACN) (Chapters 2 and 3) [48,49]. However, the genome sequences of many archaea lack homologs of the Nif and Isc systems. Homologs of the *iscS* and *iscU* are present in some euryarchaea while others, such as *Pyrococcus furiosus*, methanogens *Methanocaldococcus jannashii* and *Methanococcus maripaludis*, and the crenarchaeal *Sulfolobus solfataricus* are lacking homologs of these genes [47,118]. Two components of the Suf system, *sufB* and *sufC*, have homologs in archaea but not *sufS* or *sufA*. A cysteine desulfurase may not be required for anaerobic archaea due to their sulfur-rich environments. Instead, inorganic sulfur may be incorporated directly into scaffold proteins for cluster synthesis.

Despite the absence of some Nif, Isc, or Suf components, archaea possess homologs of the *S. enterica* ApbC and *S. cerevisiae* Nbp35 proteins. The *M. maripaludis* MMP0704 protein shares 40% amino acid identity with the two scaffold proteins, including the conserved ATP-binding motif and cysteine motifs for binding iron-sulfur clusters. The MMP0704 protein has an N-terminal ferredoxin-like CX<sub>3</sub>CXXCX<sub>5</sub>C motif



In this study, the *S. solfataricus* SSO0460, *M. jannaschii* MJ0283, and MMP0704 proteins were identified as the first archaeal proteins that form functional Fe-S carrier proteins [51]. These apbC/NBP35 homologs were able to complement an *S. enterica* strain with an *apbC* null mutation for growth on tricarballoyate. Although the Walker A box and C-terminal CXXC motif of MMP0704 were required for in vivo activity, the N-terminal ferredoxin-like domain was not. Purified and reconstituted MMP0704 bound a [4Fe-4S] cluster at its N-terminus and a [2Fe-2S] cluster at the C-terminus.

## **5.2. MATERIALS AND METHODS**

### **5.2.1. Cloning of MJ0283 and MMP0704**

The *M. jannaschii* gene at locus MJ0283 (RefSeq NP\_247256.1) was amplified by PCR using oligonucleotide primers 5MJ0283BN and 3MJ0283B. The product was ligated between the NdeI and BamHI sites of vector pET-11a to produce plasmid pDG499. A PCR product obtained using primers 5MJ0283BN2 and 3MJ0283B lacked codons 1-18, which encode the amino-terminal ferredoxin-like domain of MJ0283. The ligation of this DNA between the NdeI and BamHI sites of vector pET-11a produced pDG530.

The *M. maripaludis* gene at locus MMP0704 (RefSeq NP\_987824.1) was amplified using primers 5MMP0704N and 3MMP0704X. The PCR product was ligated between the NdeI and XhoI sites of vector pET-20b to produce plasmid pDG549. Primers 5MMP0704N2 and 3MMP0704X were used to amplify a truncated sequence that lacked codons 1-19.

### 5.2.2. Protein expression and purification

Expression vectors were transformed into *Escherichia coli* BL21(DE3) cells by electroporation. Grown aerobically at 37°C in LB Miller medium supplemented with ampicillin (100 µg ml<sup>-1</sup>), these cultures were induced with 0.1% D-lactose in mid-logarithmic growth phase. Cells were harvested and lysed as described previously, and the MMP0704 proteins were purified by nickel affinity chromatography using standard methods [48]. Fractions containing the MMP0704-His<sub>6</sub> protein were combined in dialysis tubing (SpectraPor4, 14,000 molecular mass cutoff), and dialyzed for 15 h in 2 L of buffer containing 50 mM KCl and 20 mM Tris-HCl (pH 8.0) at 4°C. Dialysis was continued for 5 h in fresh buffer before the protein inside the dialysis tubing was concentrated by dehydration with polyethylene glycol (20,000 Da). The MJ0283 proteins were purified by heat treatment of cell-free extracts prepared in 50 mM KCl and 20 mM Tris-HCl (pH 8.0) [48]. Total protein concentrations were determined by the Bradford dye-binding method (Thermo-Pierce) using bovine serum albumin as a standard.

### 5.2.3. Reconstitution of the protein iron-sulfur centers and determination of iron-sulfur content.

The purified apoproteins were diluted to a final concentration of 2.5 mg ml<sup>-1</sup> in 625 µl reactions, sealed under argon gas [48]. The reconstitution buffer contained 200 mM KCl, 3 mM dithiothreitol, 0.64 mM ATP, 1.3 mM MgCl<sub>2</sub> and 50 mM Tris-HCl (pH 8.0). A five-fold molar excess of FeCl<sub>3</sub> was added to the stirred reactions at 0°C. After 10 min, a five-fold excess of Na<sub>2</sub>S was added dropwise, and the mixture was stirred under argon for two hours to reconstitute clusters in holoproteins. The MMP0704 holoproteins were desalted using a PD-10 column (GE Healthcare) equilibrated with an anoxic solution of 50 mM Tris-HCl (pH 8.0) in an anaerobic chamber [49]. Iron and sulfide

analyses were performed using standard methods [95,96]. The standard errors for each mean value were calculated by propagating errors from each analysis.

#### **5.2.4. Size exclusion chromatography**

Analytical size exclusion chromatography was performed as described previously [62]. The mobile phase, 50 mM sodium phosphate (pH 6.8), was sparged with helium, although chromatography was performed under aerobic conditions. Absorbances of UV and visible light were recorded using a photodiode array detector, and chromatograms were analyzed using 32 Karat software (ver. 7.0, Beckman-Coulter)

### **5.3. RESULTS**

#### **5.3.1. Expression and purification of methanogen ApbC/Nbp35 proteins**

The full length and truncated forms of MMP0704-His<sub>6</sub> were both expressed as soluble proteins from *E. coli* BL21(DE3). The proteins were substantially pure after nickel affinity chromatography and had molecular masses of 33 kDa for the full length MMP0704-His<sub>6</sub> (expected 32.1 kDa) and 29 kDa for the truncated MMP0704[20-289]-His<sub>6</sub> (expected 30.4 kDa), as analyzed by SDS-PAGE (Figure 5.2). The anaerobically purified proteins did not display the characteristic UV-visible absorption peak around 400nm that is indicative of an Fe→S charge transfer (Figure: 5.3). Therefore, the purified proteins were lacking iron-sulfur clusters.

The MJ0283 proteins were also expressed as soluble proteins in *E. coli*. The thermostable proteins were purified by heat treatment at 70°C and had molecular masses of 31 kDa for the full length MJ0283 (expected 31.2 kDa) and 30 kDa for the truncated MJ0283[19-290], as analyzed by SDS-PAGE (Figure 5.2)

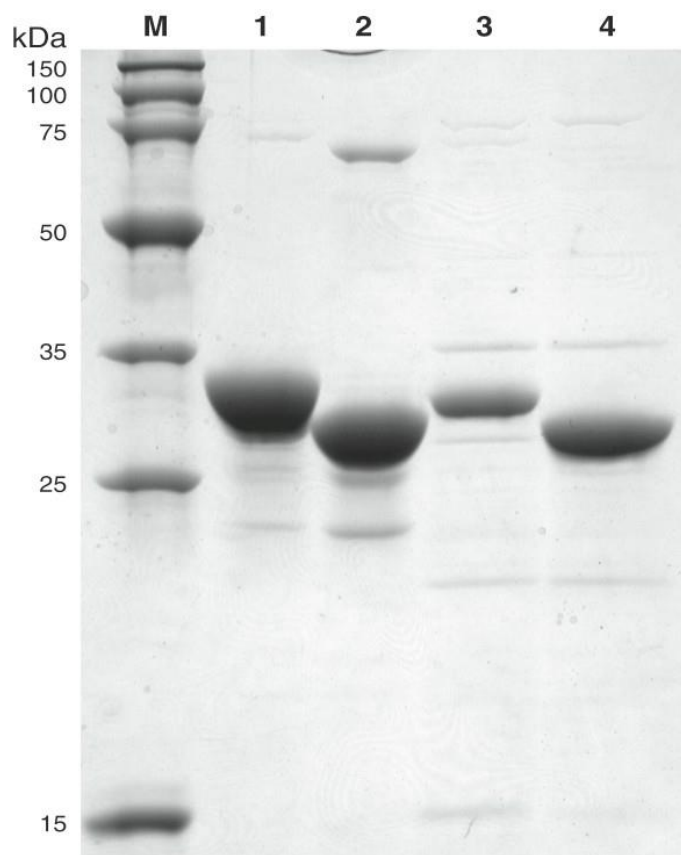


**Figure 5.2. Sodium dodecyl sulfate-polyacrylamide gel electrophoresis analysis of an overloaded, Coomassie blue-stained gel shows the purities and solubilities of heterologously expressed MMP0704 and MJ0283 proteins (10  $\mu$ g each).** Marker proteins, shown in lane M, have the molecular masses indicated to the left. Lane 1 contains affinity purified MMP0704-His<sub>6</sub> protein, with an apparent molecular mass of 33 kDa (calculated mass, 32.1 kDa). Lane 2 contains affinity-purified MMP0704[20-289]-His<sub>6</sub> protein, with an apparent molecular mass of 29 kDa (calculated mass, 30.4 kDa). Lane 3 contains heat-stable, purified MJ0283 protein, with an apparent molecular mass of 32 kDa (calculated mass, 31.2 kDa). Lane 4 contains heat-stable, purified MJ0283[19-290] protein, with an apparent molecular mass of 30 kDa (calculated mass, 29.5 kDa).

### 5.3.2. Reconstitution of the protein iron-sulfur centers

ATP is required for the reconstitution and stability of the MMP0704 proteins. In the absence of ATP, the proteins formed insoluble aggregates in the presence of iron and sulfide. However, the addition of a five fold molar excess of ATP resulted in soluble proteins. After reconstitution, the proteins were anaerobically desalted and analyzed for the presence of iron-sulfur clusters as well as iron and sulfide content. The full length MMP0704-His<sub>6</sub> and truncated MMP0704[20-289]-His<sub>6</sub> holoenzymes displayed broad UV-Vis absorption peaks around 400 nm, characteristic of a protein bound iron-sulfur cluster (Figure 5.3). The truncated MMP0704[20-289]-His<sub>6</sub> holoenzyme bound  $1.7 \pm 1$  moles of iron and  $2.2 \pm 0.3$  moles of sulfide per mole of protein. Therefore, the C-terminal portion of the MMP0704 protein possesses a monomeric [2Fe-2S] cluster. The full length MMP0704-His<sub>6</sub> holoenzyme bound  $7.5 \pm 1.2$  moles of iron and  $7.7 \pm 1.6$  moles of sulfide per mole of protein. Therefore, the full length MMP0704 holoenzyme probably forms a [4Fe-4S] cluster at the N-terminus and a [2Fe-2S] cluster at the C-terminus per monomer.



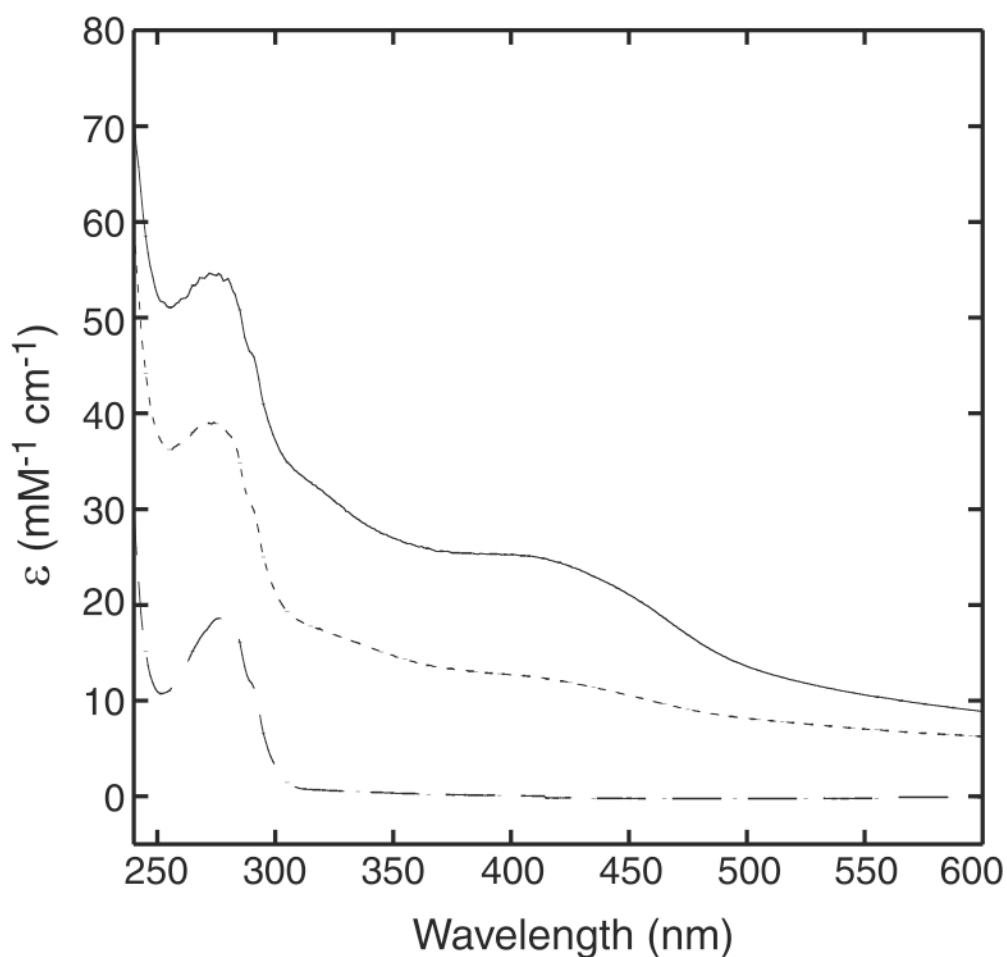


**Figure 5.3. UV-visible absorption spectra of reconstituted MMP0704-His<sub>6</sub> and MMP0704(20-289)-His<sub>6</sub> holoproteins.** The MMP0704-His<sub>6</sub> apoprotein (Broken line, bottom spectrum) was treated with ferric chloride, sulfide, and Mg-ATP and then desalted to reconstitute the holoprotein (solid line, top spectrum). The MMP0704(20-289)-His<sub>6</sub> apoprotein had an absorption spectrum identical to that of the full length apoprotein (data not shown), while the truncated holoprotein had an intermediate absorption spectrum (dashed line, middle spectrum). The millimolar absorption coefficient ( $\epsilon$ ) was calculated from measured absorbance and protein concentration values.

### 5.3.3. MMP0704 proteins interact in a complex dynamic equilibrium

The apparent molecular masses of the MMP0704 proteins were measured by analytical size exclusion chromatography. Reconstitution of the full length and truncated proteins with ferric chloride, sodium sulfide, and Mg-ATP resulted in stable oligomeric forms of MMP0704, consistent with the *S. enterica* ApbC and yeast Nbp35/Cfd1 proteins. The MMP0704[20-289]-His<sub>6</sub> apoprotein eluted as mostly a monomeric protein with an apparent mass of 27 kDa and Stokes radius of 24 Å (Figure 5.4). Approximately 20% of the protein eluted as a dimer with an apparent mass of 68 kDa and Stokes radius of 33 Å. However, after reconstitution, the holoprotein eluted as a mixture of 66% dimer and 33% monomer. An absorbance peak at 410 nm was observed for the dimeric holoprotein, suggesting an iron-sulfur cluster was present. No peak was observed for the apoprotein or the monomeric holoprotein.

The full length MMP0704-His<sub>6</sub> apoprotein eluted from the analytical size exclusion column as a mixture of different oligomeric states (Figure 5.5). Approximately 12% of the protein appeared to elute as an aggregate with a high molecular mass. The major form of the apoprotein was monomeric (35 kDa apparent mass, Stokes radius 26 Å), comprising 50% of the total protein. Approximately 23% of the protein eluted with an apparent mass of 64 kDa (Stokes radius 32 Å), which could be a dimer, and 15% eluted as a trimer with an apparent mass of 94 kDa (Stokes radius 37 Å). After reconstitution, the oligomeric forms of the full length MMP0704-His<sub>6</sub> consisted of a 40% 204 kDa protein (Stokes radius 48 Å), 26% 110 kDa protein (Stokes radius 39 Å) and 33% 64 kDa (Stokes radius 23 Å). A peak at 410 nm was observed for the 62 kDa dimer protein, consistent with the truncated holoprotein, as well as for the 197 kDa protein.

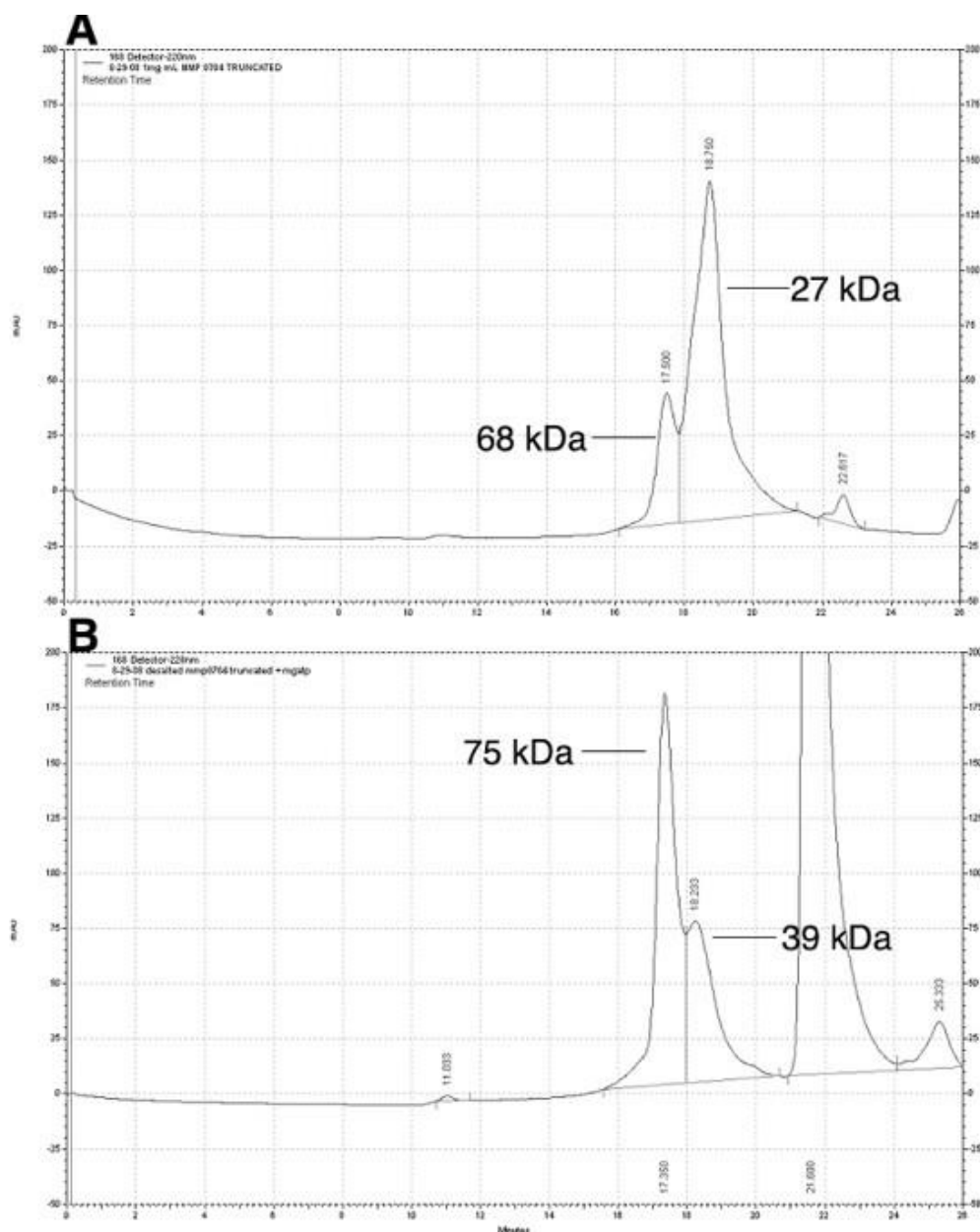


**Figure 5.4. Analytical size exclusion chromatography of the MMP0704[20-289]-His<sub>6</sub> protein.** (A) Chromatogram (detector wavelength of 220 nm) of 1  $\mu\text{g ml}^{-1}$  purified apo-MMP0704[20-289]-His<sub>6</sub> protein. Indicated molecular weights are based on the elution times of standard proteins, as previously described (Chapter 2). (B) Chromatogram (detector wavelength of 220 nm) of 1  $\mu\text{g ml}^{-1}$  purified and reconstituted MMP0704[20-289]-His<sub>6</sub>, as described in the text.

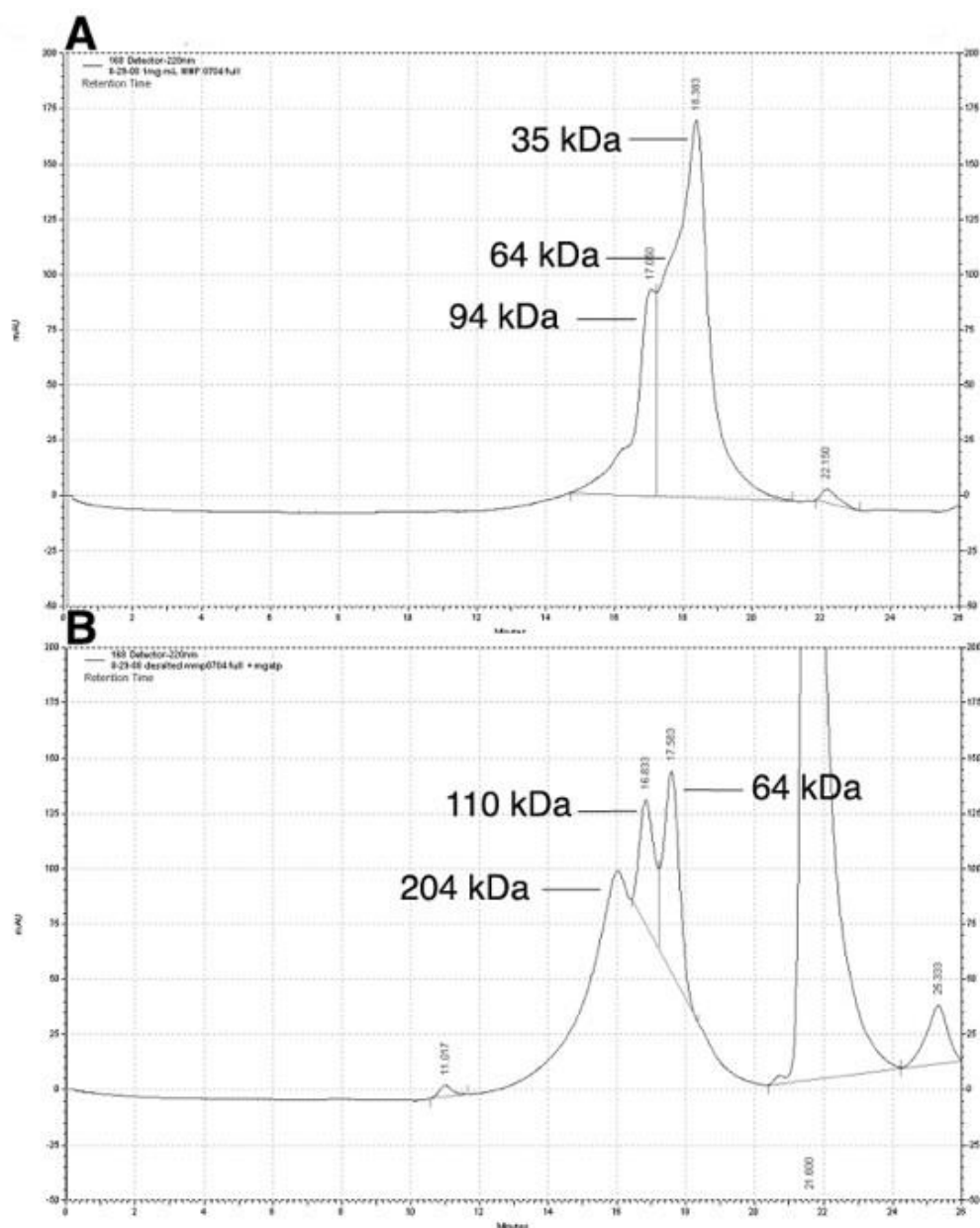


**Figure 5.5. Analytical size exclusion chromatography of the MMP0704-His<sub>6</sub> protein.** (A) Chromatogram (detector wavelength of 220 nm) of 1  $\mu\text{g ml}^{-1}$  purified apo-MMP0704 protein. Indicated molecular weights are based on the elution times of standard proteins, as previously described (Chapter 2). (B) Chromatogram (detector wavelength of 220 nm) of 1  $\mu\text{g ml}^{-1}$  purified and reconstituted MMP0704-His<sub>6</sub> as described in the text.

## 5.4. DISCUSSION

The genome sequence of *M. maripaludis* contains nine paralogs of the MMP0704 protein. However, only MMP0704 possesses the conserved cysteine residues found in ApbC and Nbp35. Homologs were subsequently identified in the euryarchaeal *M. jannaschii* and the crenarchaeal *S. solfataricus* genome sequences. The *S. cerevisiae* Nbp35 contains an N-terminal ferredoxin-like domain with four conserved cysteine residues, a Walker A box for ATP binding and hydrolysis, and four conserved C-terminal cysteine residues. Overexpression and purification of the Nbp35 resulted in an oxygen stable [4Fe-4S] cluster at the N-terminal domain [119]. However, no clusters were observed after heterologous expression and aerobic purification of MMP0704 (Figure 5.2). Incubating the purified protein with ferric iron, sulfide, and DTT under anaerobic conditions resulted in [4Fe-4S] and [2Fe-2S] clusters for the full length MMP0704 in a complex mixture of varying oligomeric states. The truncated holoprotein bound a [2Fe-2S] cluster in a predominantly dimeric form. This is consistent with the hypothesis that the C-terminal cysteine residues are at the interface of the MMP0704 dimer, forming a [4Fe-4S] cluster from the two monomeric [2Fe-2S] clusters. Further studies involving Mössbauer and electron paramagnetic resonance (EPR) will be required to determine the actual structure of the holoprotein Fe-S clusters.

The ApbC protein was required for *S. enterica* growth on tricarballoylate [109]. To test the role of the archaeal homologs in iron-sulfur biosynthesis, Jeffrey Boyd (University of Wisconsin, Madison) transfected an *S. enterica apbC* null mutant strain with plasmids containing *MMP0704*, *MJ0283*, or *SSO0460* [51]. Although all strains were able to grow in the presence of glucose, the archaeal apbC homologs were required for growth on tricarballoylate (Table 5.1) [51]. Removing the N-terminal ferredoxin-like domain of MMP0704 resulted in faster doubling times compared to cells containing the

plasmid expressing the full length MMP0704. Replacing the four N-terminal cysteine residues of the full length MMP0704 to alanine resulted similar doubling times to *S. enterica* cells containing the wild type MMP0704, although the lag time to exponential growth was significantly shorter [51]. The full length MJ0283 protein was unable to complement the *S. enterica apbC* null mutant strain. However, removal of the N-terminal domain resulted in doubling times comparable to the full length MMP0704. Bacterial and most archaeal homologs of the Nbp35 protein lack the N-terminal ferredoxin domain. The complementation studies indicate that this domain is also not required for MMP0704 or MJ0283 function in *S. enterica*. These results are consistent with the *in vitro* reconstitution of the full length and truncated MMP0704 proteins (Figure 5.3). Although the N-terminal domain was shown to possess a [4Fe-4S] cluster after reconstitution, it was not required for reconstituting the C-terminal iron-sulfur cluster. The *in vivo* and *in vitro* results indicate that the *M. maripaludis* and *M. jannaschii* ApbC homologs transfer the C-terminal iron-sulfur cluster for reconstitution of the TcuB protein in *S. enterica*. Further studies will be required to test the role of N-terminal domain in *M. maripaludis* and *M. jannaschii*.

**Table 5.1. Archaeal ApbC/Npb35 homologs can function in place of *S. enterica* ApbC in vivo [51].**

TABLE 3. Archaeal ApbC/Npb35 homologs can function in place of *S. enterica* ApbC in vivo<sup>a</sup>

Vector	Vector insert	Doubling time <sup>b</sup> (h) with:	
		Glucose	Tricarballylate
pJMB100	<i>apbC</i>	1.1 ± 0.0	1.6 ± 0.1
pJMB102	MJ0283	1.1 ± 0.0	NG <sup>c</sup>
pJMB103	Δ1-18 MJ0283	1.1 ± 0.0	3.1 ± 0.2
pJMB104	MMP0704	1.1 ± 0.1	3.0 ± 0.3
pJMB107	MMP0704( <i>Ser55Ala</i> )	1.2 ± 0.0	NG
pJMB108	MMP0704( <i>Cys218Ala</i> )	1.1 ± 0.1	NG
pJMB112	MMP0704( <i>Cys220Ala</i> )	1.1 ± 0.0	NG
pJMB114	MMP0704( <i>Cys218,220Ala</i> )	1.0 ± 0.1	NG
pJMB109	MMPO704( <i>Cys5,9,12,18Ala</i> )	1.1 ± 0.0	2.7 ± 0.3
pJMB105	Δ1-19 MMP0704	1.1 ± 0.0	2.2 ± 0.0
pJMB110	Δ1-19 MMP0704( <i>Ser55Ala</i> )	1.1 ± 0.0	NG
pJMB111	Δ1-19 MMP0704( <i>Cys218Ala</i> )	1.1 ± 0.0	2.2 ± 0.0
pJMB114	Δ1-19 MMP0704( <i>Cys220Ala</i> )	1.1 ± 0.0	2.6 ± 0.1
pJMB115	Δ1-19 MMP0704( <i>Cys218,220Ala</i> )	1.1 ± 0.0	NG
pJMB116	SSO0460	1.2 ± 0.0	2.7 ± 0.1
pJMB106	None	1.1 ± 0.0	NG

<sup>a</sup> Complementation was conducted as outlined [51].

<sup>b</sup> Doubling times were calculated using the following formulas:  $\mu = \ln(X/X_0)/T$ , where  $\mu$  is the growth rate, X is the OD<sub>650</sub> value at a given time point,  $X_0$  is the OD<sub>650</sub> value at time zero, and T is the time between readings X and  $X_0$ , and doubling time (g) =  $(\ln 2)/\mu$ . The numbers shown represent the averages of results for three independent cultures. Minimal media with the indicated carbon sources were used. The media were supplemented with thiamine.

<sup>c</sup> NG, no growth.

The *S. enterica* ApbC protein did not require ATP for *in vitro* transfer of an iron-sulfur cluster. However, mutation of the Walker A motif resulted in an inactive protein, suggesting that the ATPase activity is required for cluster loading but not transfer. Consistent with the ApbC study, an MMP0704 plasmid bearing a mutation of the catalytic serine to alanine failed to complement the *S. enterica apbC* null mutant for tricarballoylate dependent growth [51]. Similarly, *in vitro* reconstitution of the full length or truncated MMP0704 protein in the absence of MgATP resulted in insoluble protein. The addition of MgATP to the reconstitution mixture was required for successful Fe-S cluster reconstitution (Figure 5.3). Thus, ATP is required for loading an Fe-S cluster. Further *in vitro* testing will be required to assess whether ATP is required for cluster transfer from MMP0704 to a target apoprotein.

The C-terminal domain of MMP0704 contains the CXXC motif that binds either a [2Fe-2S] or [4Fe-4S] cluster. Mutation of the cysteine residues in the CXXC motif to serine in the yeast Cfd1 resulted in an inactive protein [115]. Also, mutation of the cysteines in the CXXC motif of the *S. enterica* ApbC protein disrupted the *in vivo* functionality of this protein, although the variant proteins were still able to bind two moles of iron and two moles of sulfide per mole of protein [117]. Mutation of the CXXC motif of the full length MMP0704 also disrupted the *in vivo* functionality of this protein [51]. However, mutation of either cysteine to alanine in the truncated MMP0704 did not affect *S. enterica apbC* null mutant strain complementation compared to the non-mutated truncated protein; a double mutation of Cys218,220Ala of the truncated protein was required to disrupt *in vivo* function [51]. The functional dependency of the MMP0704 protein on the CXXC motif, and not the N-terminal ferredoxin-like motif, suggests that this C-terminal motif is responsible for [Fe-S] cluster transfer to target apo-proteins.



The *S. solfataricus* SSO0460 was able to complement the *S. enterica* abpC mutant strain for growth on tricarballoylate [51]. The N-terminal motif is absent in this protein, which is consistent with most crenarchaeal homologs. Also, the second cysteine residue in the CXXC motif is replaced with an aspartic acid. The activity of this protein, despite the missing cysteine residue, is consistent with mutational studies of the ApbC and MMP0704 CXXC motifs. Aspartic acid has been observed as a ligand for [4Fe-4S] cluster binding of the *Pyrococcus furiosus* ferredoxin [120].

In *E. coli*, SufB interacts with SufC, enhancing the ATPase activity of SufC [121]. The SufBC complex also interacts with the SufES complex, as well as SufD [108]. SufES transfer a persulfide to SufB, which acts as a scaffold for a [4Fe-4S] cluster, potentially for transfer to a target apoprotein [108]. The genome sequence of *M. jannaschii* contains two genes encoding homologs of the SufB and SufC proteins, MJ0034 and MJ0035, respectively. However, *M. jannaschii* does not possess homologs of SufS or SufE, although this methanogen may use inorganic sulfur for iron-sulfur cluster biosynthesis [122]. A role for MJ0283, MJ0034, and MJ0035 proteins is proposed in Figure 5.6.

In Figure 5.6 the MJ0283 homodimer hydrolyzes ATP to assemble a [4Fe-4S] cluster at the proposed C-terminal dimer interface. The *S. enterica* ApbC was previously shown to be required for the *in vivo* assembly of the TcuB [4Fe-4S] cluster as well as the *in vitro* reconstitution of an IPMI [4Fe-4S] cluster [109,116]. Therefore, MJ0283 may transfer the bound cluster to a target apoprotein, such as the *M. jannaschii* IPMI and HACN proteins. However, the MJ0283 protein may also serve as a scaffold for accepting a cluster as well. In Figure 5.7 the MJ0034 and MJ0035 proteins interact, assembling a [2Fe-2S] or [4Fe-4S] cluster on MJ0034 in the presence of ATP. In this hypothetical model, the bound cluster is transferred from the MJ0034-MJ0035 complex to MJ0283 in

an ATP dependent reaction. The [4Fe-4S] cluster of MJ0283 could then be transferred to a target apoprotein. In an alternative model, the MJ0034-MJ0035 complex could transfer an iron-sulfur cluster directly to a target apoprotein. However, this activity has not been demonstrated with the bacterial SufBC complex. Therefore, future work will involve in vivo and in vitro experiments to analyze the role of the MJ0283, MJ0034, and MJ0035 proteins in *M. jannaschii* iron-sulfur cluster biosynthesis.

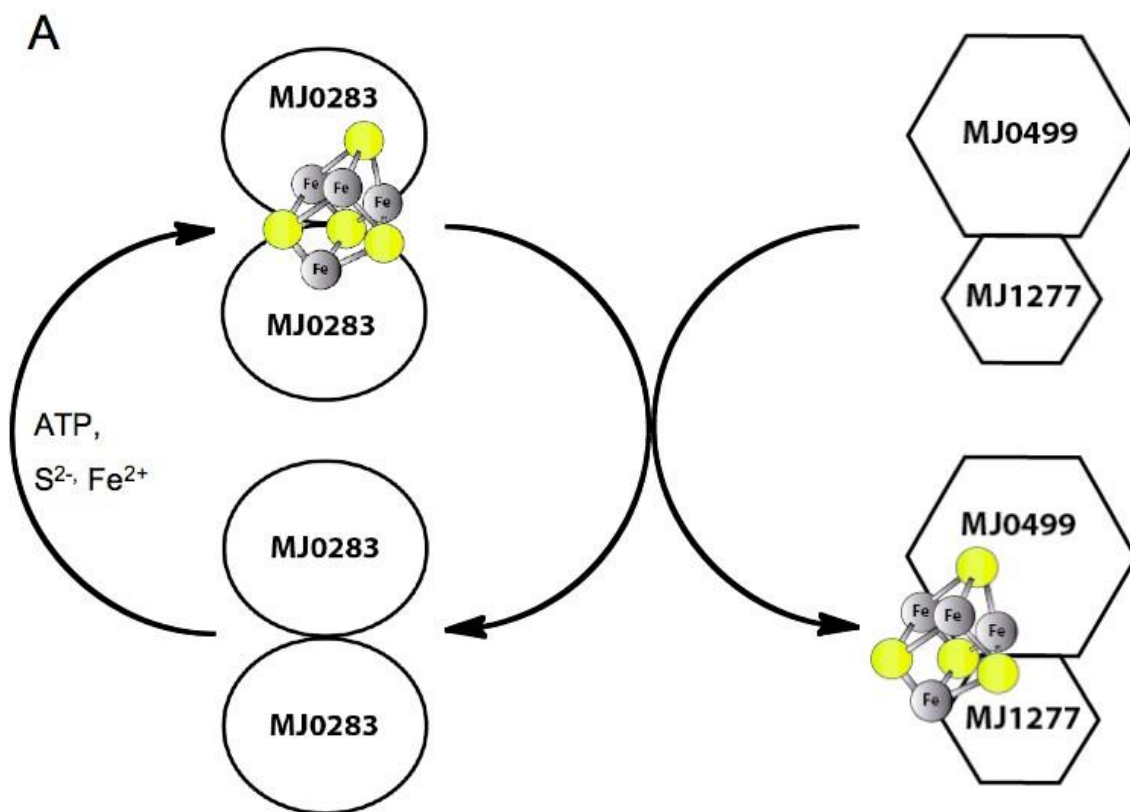


**Figure 5.6. Model for iron-sulfur cluster biosynthesis in *M. jannaschii* with MJ0283.**

The MJ0283 assembles a [4Fe-4S] cluster at the dimer interface using inorganic sulfur, iron from an unknown source, and ATP. The cluster is then transferred to a target apoprotein, such as the IPMI<sub>MJ</sub> (MJ0499-MJ1277)

B

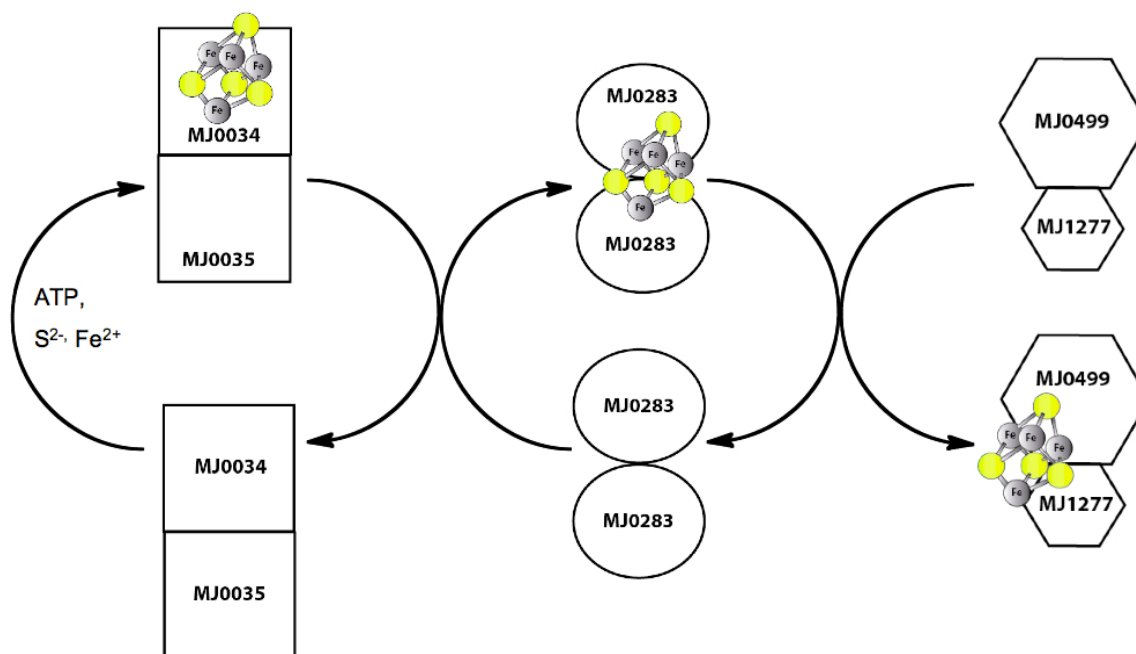


**Figure 5.7. Model for iron-sulfur cluster biosynthesis in *M. jannaschii* with MJ0283 and MJ0034-MJ0035.** The MJ0034-MJ0035 interacting pair uses inorganic sulfur, iron (from an unknown donor), and ATP to assemble a [4Fe-4S] cluster on MJ0034. The cluster is then transferred to the MJ0283 scaffold protein for the subsequent transfer to a target apoprotein, such as the IPMI<sub>MJ</sub> (MJ0499-MJ1277)

## Chapter 6: Summary and Future Directions

### 6.1. OVERVIEW

Methanogenic archaea produce over 1 billion tons of methane each year through methanogenesis from a variety of anaerobic environments, including wetlands, landfills, hydrothermal vents, and animal rumens. Approximately 400 million tons of the methane produced via methanogenesis escapes from these environments to the atmosphere where methane affects tropospheric and stratospheric chemistry [1,2]. Atmospheric methane concentrations have more than doubled since the industrial revolution and the effects of this greenhouse gas on climate change are currently a critical environmental concern [3]. Therefore, identifying methods of controlling methane production from these microorganisms could have a significant impact on slowing or reducing global warming until political and technological institutions are put in place to reduce CO<sub>2</sub> emissions.

Coenzyme B (CoB) is involved in the terminal step of methanogenesis, forming a heterodisulfide bond with methyl-coenzyme M catalyzed by methyl-coenzyme M reductase, a reaction that is common among all methanogens [32]. CoB has only been identified in methanogens and inhibiting the production of this coenzyme would be lethal. Therefore, CoB is an attractive target for developing inhibitors for methanogenesis.

Inhibiting methanogenesis would be useful for controlling the methane output of ruminant animals. Eructation of methane from ruminant animals accounts for more than 10% of the 400 million tons of methane produced each year by these microorganisms [123,124]. Also, these animals lose 2-12% of their ingested energy to methanogenesis.

Thus, producing inhibitors of methanogenesis that are environmentally safe would aid in reducing or eliminating methane output from ruminants and, therefore, aiding in reducing climate change.

Inhibiting methanogenesis would also aid in biofuel production. In organic waste streams used for ethanol and n-butyrate production, methanogens compete with acetate reduction for acetate and hydrogen. The efficiency of mixed cultures to produce these biofuels can be reduced by more than 50% due to the presence of methanogens [9]. Selective inhibition of methanogenesis in these cultures would increase the efficiency of ethanol and n-butyrate, providing alternative energy sources in the move away from fossil fuels.

The research presented herein was centered on further elucidating the biosynthetic pathway of CoB. Only two enzymes had previously been identified from the proposed CoB biosynthetic pathway: homocitrate synthase (HCS) and homoisocitrate dehydrogenase (HICDH). To further understand the pathway for CoB production, this study was centered on the identification and characterization of the *Methanocaldococcus jannaschii* homoaconitase. The homologous isopropylmalate isomerase (IPMI) was also characterized and a structural study involving the two enzymes provided insight into the residues responsible for substrate specificity. Finally, proteins involved in the synthesis of iron-sulfur clusters required for the function of the HACN and IPMI were identified.

## **6.2. METHANOGEN LEUCINE AND ISOLEUCINE BIOSYNTHESIS**

Although Methanogens produce isoleucine, they do not possess a threonine dehydratase for the production 2-oxobutyrate. However, a citramalate synthase from *M. jannaschii* was identified, suggesting methanogens produce isoleucine via the citramalate pathway from pyruvate and acetyl-CoA. To synthesize 2-oxobutyrate from citramalate,

the *M. jannaschii* leucine biosynthetic enzymes, IPMI and IPMDH, were proposed to also function as the citramalate isomerase and  $\beta$ -methylmalate dehydrogenase, respectively. In this study, the MJ0499-MJ1277 pair of proteins was characterized as the IPMI required for methanogen leucine and isoleucine biosynthesis [48]. This iron-sulfur cluster protein catalyzed the isomerization of  $\alpha$ -isopropylmalate to  $\beta$ -isopropylmalate as well as (*R*)-citramalate to  $\beta$ -methylmalate. The minimal substrate maleic acid was also a substrate for MJ0499-MJ1277. Similarly, the isopropylmalate dehydrogenase (IPMDH) catalyzed the oxidative decarboxylation of  $\beta$ -isopropylmalate,  $\beta$ -methylmalate, and D-malate. IPMI<sub>MJ</sub> and IPMDH<sub>MJ</sub> exhibit broad substrate specificity for the biosynthesis of leucine and isoleucine. Only the citramalate synthase (CMS) and isopropylmalate synthase (IPMS) are specific for their respective pathways.

### 6.3. METHANOGEN COENZYME B BIOSYNTHESIS

Methanogens use a 2-oxoacid chain elongation pathway to produce 2-oxosuberate for CoB biosynthesis. This pathway involves three iterations of reactions catalyzed by HCS, HACN, and HICDH. The CoB HACN (MJ1003-MJ1271) described in Chapter 3 was the first HACN identified to catalyze both partial reactions in the isomerization of homocitrate to homoisocitrate [49]. This study also defined the broad substrate specificity of HACN<sub>MJ</sub>, establishing the steady state kinetic parameters for *cis*-unsaturated tricarboxylates with  $\gamma$ -chains ranging from 1 – 5 methylenes in length as well as the minimal substrate maleic acid. The observed specificity of HACN<sub>MJ</sub> for (*R*)-homocitrate and *cis*-unsaturated intermediates is contrary to the initially proposed CoB 2-oxoacid-chain elongation pathway. Previously, (*S*)-homocitrate and *trans*-homoaconitate were observed as intermediates of this pathway [43]. However, these products served as inhibitors of HACN<sub>MJ</sub>. These results, coupled with previous studies involving homologs

of HACN and HCS, suggest that the biosynthesis of 2-oxosuberate involves a simpler, more conserved pathway that does not include (*S*)-homocitrate or *trans*-homoaconitate.(2,3) HCS<sub>MJ</sub> has not been characterized and previous attempts to express and purify this protein were unsuccessful (Drevand and Graham, unpublished results). Therefore, to confirm the proposed CoB 2-oxoacid-chain elongation pathway, future work will involve obtaining purified HCS<sub>MJ</sub> and analyzing the stereochemistry of the reaction products.

Although genes have not been identified for the remaining reactions in the proposed CoB biosynthetic pathway, the homoaconitase is a potential target for developing inhibitors against methanogenesis. The broad substrate specificity of this enzyme could be exploited to produce analogs of the longer chain substrates that have not been isolated from non-methanogenic organisms, such as (*R*)-homo<sub>2</sub>citrate and (*R*)-homo<sub>3</sub>citrate. Flurocitrate and nitro analogs of citrate and isocitrate are known competitive inhibitors of aconitase [125]. Future studies will test longer chain analogs of these aconitase inhibitors for inhibition of HACN<sub>MJ</sub>. It is not currently known whether aconitase or the  $\alpha$ -aminoadipate HACN recognize the longer chain substrates of the CoB HACN, such as *cis*-homo<sub>2</sub>aconitate, *cis*-homo<sub>3</sub>aconitate, or even the non-physiological *cis*-homo<sub>4</sub>aconitate. Therefore, these enzymes will be tested for their substrate specificity with the substrates of the CoB HACN.

### 6.3. HACN<sub>MJ</sub> AND IPMI<sub>MJ</sub> STRUCTURAL STUDY

The small subunits of IPMI<sub>MJ</sub> and HACN<sub>MJ</sub> (MJ1277 and MJ1271, respectively) are homologous to domain 4 of mitochondrial aconitase (mACN). Multiple sequence alignments indicate that the GS<sup>642</sup>SRE sequence of pig heart mACN, containing the catalytic Ser642 responsible for proton abstraction in the aconitase mechanism, is



conserved in these two proteins. However, Arg580 of mACN, responsible for coordinating the aconitase substrate in the active, is not conserved. A structural model of MJ1271 and a homology model of MJ1277 were presented and site directed mutagenesis was used to evaluate residues responsible for substrate specificity [50]. These studies indicate that Arg26 of the MJ1271 Y<sup>24</sup>LRT sequence is critical for substrate specificity of WT HACN<sub>MJ</sub>. Mutation of Arg26 to the corresponding residue in WT IPMI<sub>MJ</sub>, Val28, broadened the specificity of HACN<sub>MJ</sub> to include the substrates of IPMI. Therefore, Val28 of IPMI<sub>MJ</sub> is proposed to be required for recognizing substrates with hydrophobic  $\gamma$ -chains. The Y<sup>24</sup>LRT and Y<sup>26</sup>LVY sequences of MJ1277 and MJ1271, respectively, can serve as indicators of protein function for uncharacterized euryarchaeal genes. However, mutation of Arg26 or Thr27 of MJ1271 did not completely abolish HACN activity, suggesting a role of the interacting large subunits in substrate specificity. A crystal structure of the MJ1003-MJ1271 protein pair with bound substrate will be required to elucidate other residues that might affect substrate recognition.

Although the HACN<sub>MJ</sub> catalyzed both hydration and dehydration reactions in the isomerization of homocitrate, bacterial and fungal HACNs have only been observed to catalyze the hydration of *cis*-homoaconitate to (2*R*, 3*S*)-homoisocitrate [93]. In an attempt to evaluate the difference in mechanism, the loop region of MJ1271 bearing the Y<sup>24</sup>LRT sequence was replaced with the corresponding region of the *Thermus thermophilus* HACN small subunit, LysU. Only activity with maleic acid was observed for the purified and reconstituted protein. Therefore, site direct mutagenesis of the *T. thermophilus* HACN, as well as a crystal model with bound substrate, will be required to determine the structural differences responsible for the mechanistic discrepancy.

#### 6.4. IRON-SULFUR CLUSTER BIOSYNTHESIS IN ARCHAEA

A [4Fe-4S] cluster is required for IPMI<sub>MJ</sub> and HACN<sub>MJ</sub> activity, consistent with previously characterized members of the aconitase superfamily [69]. Three conserved cysteine residues bind the [4Fe-4S] cluster at the enzyme active site where it serves a non-redox function in substrate coordination. To prevent stress from free iron and sulfide, organisms have developed intricate systems for synthesizing and transferring iron-sulfur clusters to target apo proteins. The ISC, SUF, and NIF function as the main biosynthetic machineries in prokaryotes and eukaryotes for iron-sulfur cluster synthesis [106,107]. Recently, the ApbC protein from *Salmonella enterica* and the yeast Nbp35 and Cfd1 proteins were also shown to function in transferring these clusters to target proteins [109,114]. The study of the *Methanococcus maripaludis*, *M. jannaschii*, and *Sulfolobus solfataricus* ApbC/Nbp35 homologs marks the first study of archaeal iron-sulfur cluster biosynthesis [51]. The *M. maripaludis* MMP0704 protein requires MgATP to bind a [4Fe-4S] cluster at the N-terminal domain and a [2Fe-2S] cluster at its C-terminal domain. Upon protein reconstitution, MMP0704 exists in a complex mixture of oligomeric states, although the functional protein is probably a dimer. The Walker A motif, for ATP binding and hydrolysis, and the C-terminal domain were necessary to complement an ApbC deficient *S. enterica* strain. The N-terminal domain was shown to be dispensable. These results indicate that MMP0704 and the homologous proteins of *M. jannaschii* (MJ0283) and *S. solfataricus* (SSO0460) function as scaffolding proteins for the formation and transfer of iron-sulfur clusters. Future studies will require in vivo experiments to confirm the function of MMP0704 in an *M. maripaludis* strain. Also, in vitro experiments will examine the ability of MMP0704 or MJ0283 to transfer an iron-

sulfur cluster to an apoprotein, such as IPMI<sub>MJ</sub>, and the role of ATP in cluster binding and delivery.

The genome of *M. jannaschii* also contains two genes encoding homologs of the prokaryotic SufB and SufC proteins: MJ0034 and MJ0035. Previous studies have indicated that SufC has ATPase activity and SufB can accept a persulfide as well bind a [4Fe-4S]. SufB interacts with SufC, SufD, and the SufES complex and both SufB and SufC are essential for the Suf machinery to function. However, the exact role of SufBC iron-sulfur cluster biosynthesis is not currently known. Future studies will involve testing the ability of MJ0034 and MJ0035 to bind an iron-sulfur cluster and transfer it to either MJ0283 or a target apoprotein.

## Bibliography

- 1 Neue, H. (1993) Methane emissions from rice fields. *Bioscience* **43**, 466-483
- 2 Hansen, J., Sato, M., Ruedy, R., Lacis, A., and Oinas, V. (2000). Global warming in the twenty-first century: an alternative scenario. *Proc. Natl. Acad. Sci. U.S.A.* **97**, 9875-9880
- 3 Houghton, J.T., Ding, Y., Griggs, D.J., Noguer, M., van der Linden, P.J., Dai, X., Maskell, K., and Johnson, C.A. (eds). Climate change 2001: the scientific basis. Cambridge Univ. Press, Cambridge, 2001)
- 4 Cicerone, R.J. (1988) Biogeochemical aspects of atmospheric methane. *Global Biogeo. Cycles* **2**, 299-327
- 5 Hansen, J. and Sato, M. (2004). Greenhouse gas growth rates. *Proc. Natl. Acad. Sci. U.S.A.* **101**, 16109-16114
- 6 Wang, J.S., Logan, J.A., and McElroy, M.B. (2004). A 3-D model analysis of the slowdown and interannual variability in the methane growth rate from 1988 to 1997. *Global Biogeo. Cycles* **18**, 3011-3041
- 7 Claasen, P.A.M., van Lier, J.B., Lopez Contreras, A.M., van Niel, E.W.J., Sitjtsma, L., Stams, A.J.M., de Vries, S.S., and Weusthuis, R.A. (1999). Utilisation of biomass for the supply of energy carriers. *Appl. Microbiol. Biotechnol.* **52**, 741-755
- 8 Antoni, D., Zverlov, V.V., and Schwarz, W.H. (2007). Biofuels from microbes. *Appl. Microbiol. Biotechnol.* **77**, 23-35
- 9 Steinbusch, K.J.J., Arvaniti, E., Hamelers, H.V.M., and Buisman, C.J.N. (2009). Selective inhibition of methanogenesis to enhance ethanol and n-butyrate production through acetate reduction in mixed culture fermentation. *Bioresour. Technol.* **13**, 3261-3267
- 10 Thauer, R.K. (1998). Biochemistry of methanogenesis: a tribute to Marjory Stephenson. *Microbiology* **144**, 2377
- 11 Graham, D.E. and White, R.H. (2002). Elucidation of methanogenic coenzyme biosyntheses: from spectroscopy to genomics. *Nat. Prod. Rep.* **19**, 133-147
- 12 Thauer, R.K., Kaster, A.-K., Seedorf, H., Buckel, W., and Hedderich, R. (2008). Methanogenic archaea: ecologically relevant differences in energy conservations. *Nat. Rev. Microbiol.* **8**, 579-591

- 13 Rouvière, P.E. and Wolfe, R.S. (1988). Novel biochemistry of methanogenesis. *J. Biol. Chem.* **263**, 7913-7916
- 14 Leigh, J.A., Rinehart, K.L., and Wolfe, R.S. (1985). Methanofuran (carbon dioxide reduction factor), a formyl carrier in methane production from carbon dioxide in *Methanobacterium*. *Biochemistry* **24**, 995-999
- 15 Vorholt, J.A. and Thauer, R.K. (1997). The active species of "CO<sub>2</sub>" utilized by formylmethanofuran dehydrogenase from methanogenic Archaea.. *Eur. J. Biochem.* **248**, 919-924
- 16 Donnelly, M.I. and Wolfe, R.S. (1986). The role of formylmethanofuran:tetrahydromethanopterin formyltransferase in methanogenesis from carbon dioxide. *J. Biol. Chem.* **261**, 16653-16659
- 17 Donnelly, M.I., Escalante-Semerena, J.C., Rinehart, K.L.J., and Wolfe, R.S. (1985). Methenyl-tetrahydromethanopterin cyclohydrolase in cell extracts from *Methanobacterium*. *Arch. Biochem. Biophys.* **242**, 430-439
- 18 Hartzell, P.L., Zvilius, G., Escalante-semerena, J.C., and Donnelly, M.I. (1985). Coenzyme F<sub>420</sub> dependence of the methylenetetrahydromethanopterin dehydrogenase of *Methanobacterium thermoautotrophicum*. *Biochem. Biophys. Res. Commun.* **133**, 884-890
- 19 Mukhopadhyay, B. and Daniels, L. (1989). Aerobic purification of N<sup>5</sup>,N<sup>10</sup>-methylenetetrahydromethanopterin dehydrogenase, separated from N<sup>5</sup>,N<sup>10</sup>-methylenetetrahydromethanopterin cyclohydrolase, from *Methanobacterium thermoautotrophicum* strain Marburg. *Can. J. Microbiol.* **35**, 499-507
- 20 Ma, K. and Thauer, R.K. (1990). Purification and properties of N<sup>5</sup>,N<sup>10</sup>-Methylenetetrahydromethanopterin reductase from *Methanosarcina barkeri*. *Eur. J. Biochem.* **191**, 187-193
- 21 Te Brömmelstroet, B.W., Geerts, W.J., Keltjens, J.T., van der Drift, C. and Vogels, G.D. (1991). Purification and properties of 5,10-methylenetetrahydromethanopterin dehydrogenase and 5,10-methylenetetrahydromethanopterin reductase, two coenzyme F<sub>420</sub>-dependent enzymes, from *Methanosarcina barkeri*. *Biochim. Biophys. Acta.* **1079**, 293-302
- 22 Gärtner, P., Ecker, A., Fischer, R., Linder, D., Fuchs, G., and Thauer, R.K. (1993). Purification and properties of N<sup>5</sup>-methyltetrahydromethanopterin:coenzyme M

methyltransferase from *Methanobacterium thermoautotrophicum*. *Eur. J. Biochem.* **213**, 537-545

23 Gunsalus, R.P. and Wolfe, R.S. (1980). Methyl coenzyme M reductase from *Methanobacterium thermoautotrophicum*. Resolution and properties of the components. *J. Biol. Chem.* **255**, 1891-1895

24 Gunsalus, R.P. and Wolfe, R.S. (1979). Chromophoric factors F<sub>342</sub> and F<sub>430</sub> of *Methanobacterium thermoautotrophicum*. *FEMS Microbiol. Lett.* **3**, 191-193

25 Hedderich, R. and Thauer, R.K. (1988). *Methanobacterium thermoautotrophicum* contains a soluble enzyme system that specifically catalyzes the reduction of the heterodisulfide of coenzyme M and 7-mercaptoheptanoylthreonine phosphate with H<sub>2</sub>. *FEBS Lett.* **234**, 223-227

26 Noll, K.M., Rinehart, K.L., Tanner, R.S., and Wolfe, R.S. (1986). Structure of component B (7-mercaptoheptanoylthreonine phosphate) of the methylcoenzyme M methylreductase system of *Methanobacterium thermoautotrophicum*. *Proc. Natl. Acad. Sci. U.S.A.* **83**, 4238-4242

27 Sauer, F.D., Mahadevan, S., and Erfle, J.D. (1984). Methane synthesis by membrane vesicles and a cytoplasmic cofactor isolated from *Methanobacterium thermoautotrophicum*. *Biochem. J.* **221**, 61-69

28 Marsden, B.J., Sauer, F.D., Blackwell, B.A., and Kramer, J.K. (1989). Structure determination of the UDP-disaccharide fragment of cytoplasmic cofactor isolated from *Methanobacterium thermoautotrophicum*. *Biochem. Biophys. Res. Commun.* **159**, 1404-1410

29 Sauer, F.D. and Blackwell, B.A. (1987). Structure of purified cytoplasmic cofactor from *Methanobacterium thermoautotrophicum*. *Biochem. Biophys. Res. Commun.* **147**, 1021-1026

30 Keltjens, J.T., Kraft, H.J., Damen, W.G., van der Drift, C., and Vogels, G.D. (1989). Stimulation of the methylcoenzyme M reduction by uridine-5'-diphospho-sugars in cell-free extracts of *Methanobacterium thermoautotrophicum* (strain ⓧH). *Eur. J. Biochem.* **184**, 395-403

31 Sauer, F.D., Blackwell, B.A., Kramer, J.K., and Marsden, B.J. (1990). Structure of a novel cofactor containing N-(7-Mercaptoheptanoyl)-O-3-phosphothreonine. *Biochemistry* **29**, 7593-7600

- 32 Ermler, U., Grabarse, W., Shima, S., Goubeaud, M, and Thauer, R.K. (1997). Crystal structure of methyl-coenzyme M reductase: the key enzyme of biological methane formation. *Science* **278**, 1457-1462
- 33 Ermler, U. (2005). On the mechanism of methyl-coenzyme M reductase. *Dalton Trans.* **21**, 3451-3458
- 34 Shima, S. and Thauer, R.K. (2005). Methyl-coenzyme M reductase and the anaerobic oxidation of methane in methanotrophic archaea. *Curr. Opin. Microbiol.* **8**, 643-648
- 35 Hinderberger, D., Ebner, S., Mayr, S., Jaun, B., Reiher, M., Goenrich, M., Thauer, R.K., Harmer, J. (2008). Coordination and binding geometry of methyl-coenzyme M in the red1m state of methyl-coenzyme M reductase. *J. Biol. Inorg. Chem.* **13**, 1275-1289
- 36 Sarangi, R., Dey, M., and Ragsdale, S.W. (2009). Geometric and electronic structure of the Ni<sup>I</sup> and methyl-Ni<sup>III</sup> intermediates of methyl-coenzyme M reductase. *Biochemistry* **48**, 3146-3156
- 37 Goenrich, M. and Duin, E.C. (2005). Temperature dependence of methyl-coenzyme M reductase activity and of the formation of the methyl-coenzyme M reductase red2state induced by coenzyme B. *J. Biol. Inorg. Chem.* **10**, 333-345
- 38 White, R.H. (1989). Biosynthesis of the 7-Mercaptoheptanoic acid subunit of component B [(7-mercaptoheptanoyl)threonine phosphate] of methanogenic bacteria. *Biochemistry* **28**, 860-865
- 39 Howell, D.M., Harich, K., Xu, H., and White, R.H. (1998).  $\alpha$ -Keto acid chain elongation reactions involved in the biosynthesis of coenzyme B (7-mercaptoheptanoyl threonine phosphate) in methanogenic archaea. *Biochemistry* **37**, 10108-10117
- 40 White, R.H. (1989). Steps in the conversion of  $\alpha$ -ketosuberate to 7-mercaptoheptanoic acid in methanogenic bacteria. *Biochemistry* **28**, 9417-9423
- 41 Solow, B. and White, R.H. (1997). Biosynthesis of the peptide bond in the coenzyme N-(7-mercaptoheptanoyl)-L-threonine phosphate. *Arch. Biochem. Biophys.* **345**, 299-304
- 42 White, R.H. (1994). Biosynthesis of (7-mercaptoheptanoyl)threonine phosphate. *Biochemistry* **33**, 7077-7081
- 43 Namboori, S.C. and Graham, D.E. (2008). Acetamido sugar biosynthesis in the Euryarchaea. *J. Bacteriol.* **190**, 2987-2996

- 44 Howell, D.M., Graupner, M., Xu, H., and White, R.H. (2000). Identification of enzymes homologous to isocitrate dehydrogenase that are involved in coenzyme B and leucine biosynthesis in methanoarchaea. *J. Bacteriol.* **182**, 5013-5016
- 45 White, R.H. (1989). A novel biosynthesis of medium chain length  $\alpha$ -ketodicarboxylic acids in methanogenic archeobacteria. *Arch. Biochem. Biophys.* **270**, 691-697
- 46 Miyazaki, T., Miyazaki, J., Yamane, H., and Nishiyama, M. (2004).  $\alpha$ -Aminoadipate aminotransferase from an extremely thermophilic bacterium, *Thermus thermophilus*. *Microbiology* **150**, 2327-2334
- 47 Bult, C.J. et al. (1996). Complete genome sequence of the methanogenic archaeon, *Methanococcus jannaschii*. *Science* **273**, 1058-1073
- 48 Drevland, R.M., Waheed, A., and Graham, D.E. (2007). Enzymology and evolution of the pyruvate pathway to 2-oxobutyrates in *Methanocaldococcus jannaschii*. *J. Bacteriol.* **189**, 4391-4400.
- 49 Drevland, R.M., Jia, Y., Palmer, D.R., and Graham, D.E. (2008). Methanogen homoaconitase catalyzes both hydrolyase reactions in coenzyme B biosynthesis. *J. Biol. Chem.* **283**, 28888-28896
- 50 Drevland, R.M., Jeyakanthan, J., Gayathri, D., Velmurugan, D., Agari, Y., Ebihara, A., Kuramitsu, S., Shinkai, A., Shiro, Y., Yokoyama, S., and Graham, D.E. (2009). Crystallography and mutational analysis of the *Methanocaldococcus jannaschii* homoaconitase small subunit: insight into structural determinants for substrate specificity. *[In preparation]*
- 51 Boyd, J.M., Drevland, R.M., Downs, D.M., and Graham, D.E. (2008). Archaeal ApbC/Nbp35 homologs function as iron-sulfur cluster carrier proteins. *J. Bacteriol.* **191**, 1490-1497
- 52 Vollbrecht, D. (1974). Three pathways of isoleucine biosynthesis in mutant strains of *Saccharomyces cerevisiae*. *Biochimica et Biophysica Acta* **362**, 382-389
- 53 Hofmeister, A.E.M., Grabowski, R., Linder, D., and Buckel, W. (1993). L-Serine and L-threonine dehydratase from *Clostridium propionicum*. Two enzymes with different prosthetic groups. *Eur. J. Biochem.* **215**, 341-349
- 54 Eikmanns, B., Jaenchen, R., and Thauer, R. K. (1983). Propionate assimilation by methanogenic bacteria. *Arch. Microbiol.* **136**, 106-110



- 55 Eikmanns, B., Linder, D., and Thauer, R. K. (1983). Unusual pathway of isoleucine biosynthesis in *Methanobacterium thermoautotrophicum*. *Arch. Microbiol.* **136**, 111-113
- 56 Charon, N.W., Johnson, R.C., and Peterson, D. (1974). Amino acid biosynthesis in the spirochete *Leptospira*: evidence for a novel pathway of isoleucine biosynthesis. *J. Bacteriol.* **117**, 203-211
- 57 Howell, D.M., Xu, H., and White, R.H. (1999). (R)-Citramalate synthase in methanogenic archaea. *J. Bacteriol.* **181**, 331-333
- 58 Kohlhaw, G., Leary, T.R., and Umbarger, H.E. (1969).  $\alpha$ -Isopropylmalate synthase from *Salmonella Typhimurium*. Purification and properties. *J. Biol. Chem.* **244**, 2218-2225
- 59 Kohlhaw, G. B. (1988). Isopropylmalate dehydratase from yeast. *Methods Enzymol.* **166**, 423-429
- 60 Xu, H., Zhang, Y., Guo, X., Ren, S., Staempfli, A., Chiao, J., Jiang, W., and Zhao, G. (2004). Isoleucine biosynthesis in *Leptospira interrogans* serotype lai strain 56601 proceeds via a threonine-independent pathway. *J. Bacteriol.* **186**, 5400-5409
- 61 Ma, J., Zhang, P., Zhang, Z., Zhai, M., Xu, H., Zhao, G., and Ding, J. (2008). Molecular basis of the substrate specificity and the catalytic mechanism of citramalate synthase from *Leptospira interrogans*. *Biochem. J.* **415**, 45-56
- 62 Helgadóttir, S., Rosas-Sandoval, G., Söll, D., and Graham, D.E. (2007). Biosynthesis of phosphoserine in the *Methanococcales*. *J. Bacteriol.* **180**, 575-582
- 63 Blank, L., Green, J., and Guest, J.R. (2002). AcnC of *Escherichia coli* is a 2-methylcitrate dehydratase (PrpD) that can use citrate and isocitrate as substrates. *Microbiology* **148**, 133-146
- 64 Liebich, H.M., Gesele, E., Wahl, H.G., Wirth, C., Wöll, and Husek, P. (1992). Identification of side-products formed by derivatization of 2-hydroxycarboxylic acids with methyl and ethyl chloroformate. *J. Chromatogr. A* **626**, 289-293
- 65 Vatankhah, M. and Moini, M. (1994). Characterization of fluorinated ethyl-chloroformate derivatives of protein amino acids using positive and negative chemical ionization gas chromatography/mass spectrometry. *Biol. Mass. Spectrom.* **23**, 277-282
- 66 Karsten, W.E., Tipton, P.A., and Cook, P.F. (2002). Tartrate dehydrogenase catalyzes the stepwise oxidation decarboxylation of D-malate with both NAD and thio-NAD. *Biochemistry* **41**, 12193-12199

- 67 Tipton, P.A., and Beecher, B.S. (1994). Tartrate dehydrogenase, a new member of the family of metal-dependent decarboxylating *R*-hydroxyacid dehydrogenases. *Arch. Biochem. Biophys.* **313**, 15-21
- 68 Graham, D.E., Graupner, M., Xu, H., and White, R.H. (2001). Identification of coenzyme M biosynthetic 2-phosphosulfolactate phosphatase: a member of a new class of  $Mg^{2+}$ -dependent acid phosphatases. *Eur. J. Biochem.* **268**, 5176-5188
- 69 Gruer, M.J., Artymiuk, P.J., and Guest, J.R. (1997). The aconitase family: three structural variations on a common theme. *Trends Biochem. Sci.* **22**, 3-6
- 70 Dreyer, J.-L. (1985). Isolation and biochemical characterization of maleic-acid hydratase, an iron-requiring hydro-lyase. *Eur. J. Biochem.* **150**, 145-154
- 71 Jordan, P.A., Tang, Y., Bradbury, A.J., Thomson, A.J., and Guest, J.R. (1999). Biochemical and spectroscopic characterization of *Escherichia coli* aconitases (AcnA and AcnB). *Biochem. J.* **344**, 739-746
- 72 Suzuki, T., Inoki, Y., Yamagishi, A., Iwasaki, T., Wakagi, T., and Oshima, T. (1997). Molecular and phylogenetic characterization of isopropylmalate dehydrogenase of a thermoacidophilic archaeon, *Sulfolobus* sp. Strain 7. *J. Bacteriol.* **179**, 1174-1179
- 73 Dean, A.M. and Dvorak, L. (1995). The role of glutamate 87 in the kinetic mechanism of *Thermus thermophilus* isopropylmalate dehydrogenase. *Protein Sci.* **4**, 2156-2167
- 74 Zheng, L., Kennedy, M.C., Beinert, H., and Zalkin, H. (1992). Mutational analysis of active site residues in pig heart aconitase. *J. Biol. Chem.* **267**, 7896-7903
- 75 van der Werf, M. J., Van Den Tweel, J. J., and Hartmans, S. (1993). Purification and characterization of maleate hydratase from *Pseudomonas pseudoalcaligenes*. *Appl. Environ. Microbiol.* **59**, 2823 – 2829
- 76 van der Werf, M. J., Van Den Tweel, J. J., and Hartmans, S. (1993). Thermodynamics of the maleate and citraconate hydration reactions catalyzed by malease from *Pseudomonas pseudoalcaligenes*. *Eur. J. Biochem.* **217**, 1011-1017
- 77 Kisumi, M., Komatsubara, S., and Chibata, I. (1977). Pathway for isoleucine formation from pyruvate by leucine biosynthetic enzymes in leucine-accumulating isoleucine revertants of *Serratia marcescens*. *J. Biochem.* **82**, 95-103

- 78 Graham, D.E. and Huse, H.K. (2008). Methanogens with pseudomurein use diaminopimelate aminotransferase in lysine biosynthesis. *FEBS Lett.* **582**, 1369-1375
- 79 Qian, J., West, A.H., and Cook, P.F. (2006). Acid-base chemical mechanism of homocitrate synthase from *Saccharomyces cerevisiae*. *Biochemistry* **45**, 12136-12143
- 80 Li, F., Hagemeyer, C.H., Seedorf, H., Gottschalk, G., and Thauer, R.K. (2007). Re-citrate synthase from *Clostridium kluyveri* is phylogenetically related to homocitrate synthase and isopropylmalate synthase rather than to Si-citrate synthase. *J. Bacteriol.* **189**, 4299-4304
- 81 Curatti, L., Hernandez, J.A., Igarashi, R.Y., Soboh, B., Zhao, D., and Rubio, L.M. (2007). *In vitro* synthesis of the iron-molybdenum cofactor of nitrogenase from iron, sulfur, molybdenum, and homocitrate using purified proteins. *Proc. Natl. Acad. Sci. U.S.A.* **104**, 17626-17631
- 82 Lin, Y., Alguindigue, S.S., Nicholas, K.M., West, A.H., and Cook, P.F. (200). Complete kinetic mechanism of homoisocitrate dehydrogenase from *Saccharomyces cerevisiae*. *Biochemistry* **46**, 890-898
- 83 Yamamoto, T., Miyazaki, and Eguchi, T. (2007). Substrate specificity analysis and inhibitor design of homoisocitrate dehydrogenase. *Bioorg. Med. Chem.* **15**, 1346-1355
- 84 Strassman, M. and Ceci, L.N. (1966). Enzymatic formation of *cis*-homoaconitic acid, an intermediate in lysine biosynthesis in yeast. *J. Biol. Chem.* **241**, 5401-5407
- 85 Maragoudakis, M.E. (1967). Homoaconitic acid accumulation by a lysine-requiring yeast mutant. *J. Bacteriol.* **94**, 1060-1065
- 86 Maragoudakis, M.E. and Strassman, M. (1966). Homocitric acid accumulation by a lysine-requiring yeast mutant. *J. Biol. Chem.* **241**, 695-699
- 87 Strassman, M., Ceci, L.N., and Silverman, B.E. (1964). Enzymatic conversion of homoisocitric acid into alpha-ketoadipic acid. *Biochem. Biophys. Res. Commun.* **14**, 268-271
- 88 Strassman, M. and Ceci, L.N. (1965). Enzymatic formation of alpha-ketoadipic acid from homoisocitric acid. *J. Biol. Chem.* **240**, 4357-4361
- 88 Maragoudakis, M.E. and Strassman, M. (1966). Homocitric acid accumulation by a lysine-requiring yeast mutant. *J. Biol. Chem.* **241**, 695-699

- 89 Weidner, G., Steffan, B., and Brakhage, A.A. (1997). The *Aspergillus nidulans* lysF gene encodes homoaconitase, an enzyme involved in the fungus-specific lysine biosynthesis pathway. *Mol. Gen. Genet.* **255**, 237-247
- 90 Lombo, T., Takaya, N., Miyazaki, H., Gotoh, K., Nishiyama, M., Kosuge, T., Nakamura, A., and Hoshino, T. (2004). Functional analysis of the small subunit of the putative homoaconitase from *Pyrococcus horikoshii* in the Thermus lysine biosynthetic pathway. *FEMS Microbiol. Lett.* **233**, 315-324
- 91 Kosuge, T. and Hoshino, T. (1998). Lysine is synthesized through the alpha-amino adipate pathway in *Thermus thermophilus*. *FEMS Microbiol. Lett.* **169**, 361-367
- 92 Zabriskie, T.M. and Jackson, M.D. (2000). Lysine biosynthesis and metabolism in fungi. *Nat. Prod. Rep.* **17**, 85-97
- 93 Jia, Y., Tomita, T., Yamauchi, K., Nishiyama, M., and Palmer, D.R.J. (2006). Kinetics and product analysis of the reaction catalyzed by recombinant homoaconitase from *Thermus thermophilus*. *Biochem. J.* **396**, 479-485
- 94 Horswill, A.R. and Escalante-Semerena, J.C. (2001). In vitro conversion of propionate to pyruvate by *Salmonella enterica* enzymes: 2-methylcitrate dehydratase (PrpD) and aconitase enzymes catalyze the conversion of 2-methylcitrate to 2-methylisocitrate. *Biochemistry* **40**, 4703-4713
- 95 Wu, S.-P., Wu, G., Surerus, K.K., and Cowan, J.A. (2002). Iron-sulfur cluster biosynthesis. Kinetic analysis of [2Fe-2S] cluster transfer from holo ISU to apo Fe: role of redox chemistry and a conserved aspartate. *Biochemistry* **41**, 8876-8885
- 96 Beinert, H. (1983). Semi-micro methods for analysis of labile sulfide and of labile sulfide plus sulfane sulfur in unusually stable iron-sulfur proteins. *Anal. Biochem.* **131**, 373-378
- 97 Jang, S. and Imlay, J.A. (2007). Micromolar intracellular hydrogen peroxide disrupts metabolism by damaging iron-sulfur enzymes. *J. Biol. Chem.* **282**, 929-937
- 98 Beinert, H., Kennedy, M.C., and Stout, C.D. (1996). Aconitase as iron-sulfur protein, enzyme, and iron-regulatory protein. *Chem. Rev.* **96**, 2335-2374
- 99 Gross, S.R., Burns, R.O., and Umbarger, H.E. (1963). The biosynthesis of leucine. II. The enzymic isomerization of b-carboxy-b-hydroxyisocaproate and a-hydroxy-b-carboxyisocaproate. *Biochemistry* **2**, 1046-1052

- 100 Lauble, H. Kennedy, M.C., Beinert, H., and Stout, C.D. (1992). Crystal structures of aconitase with isocitrate and nitroisocitrate bound. *Biochemistry* **31**, 2735-2748
- 101 Yasytake, Y., Yao, M., Sakai, N., Kirita, T., and Tanaka, I. (2004). Crystal structure of the *Pyrococcus horikoshii* isopropylmalate isomerase small subunit provides insight into the dual substrate specificity of the enzyme. *J. Mol. Biol.* **344**, 325-333
- 102 Horton, R.M., Cai, Z.L., Ho, S.N., and Pease, L.R. (1990). Gene splicing by overlap extension: tailor-made genes using the polymerase chain reaction. *Biotechniques* **8**, 528-535
- 103 Arnold K., Bordoli L., Kopp J., and Schwede T. (2006). The SWISS-MODEL Workspace: A web-based environment for protein structure homology modelling. *Bioinformatics*, **22**, 195-201.
- 104 Lauble, H. and Stout, C.D. (1995). Steric and conformational features of the aconitase mechanism. *Proteins* **22**, 1-11
- 105 Beinert, H. (2000) Iron-sulfur proteins: ancient structures, still full of surprises. *J. Inorg. Biol. Chem.* **5**, 2-15
- 106 Lill, R. and Mühlenhoff, U. (2008). Maturation of iron-sulfur proteins in eukaryotes: mechanisms, connected processes, and diseases. *Annu. Rev. Biochem.* **77**, 669-700
- 107 Ayala-Castro, C., Saini, A., and Outten, F.W. (2008). Fe-S cluster assembly pathways in bacteria. *Microbiol. Mol. Biol. Rev.* **72**, 110-125
- 108 Layer, G., Gaddam, S.A., Ayala-Castro, C.N., Ollagnier-de Choudens, S., Lascoux, D., Fontecave, M., and Outten, F.W. (2007). SufE transfers sulfur from SufS to SufB for iron-sulfur cluster assembly. *J. Biol. Chem.* **282**, 13342-13350
- 109 Boyd, J. M., Lewis, J. A., Escalante-Semerena, J. C., and Downs, D. M. (2008) *Salmonella enterica* requires ApbC function for growth on tricarballoylate: evidence of functional redundancy between ApbC and IscU. *J. Bacteriol.* **190**, 4596-4602
- 110 Skovran, E. and Downs, D. M. (2000) Metabolic defects caused by mutations in the isc gene cluster in *Salmonella enterica* serovar Typhimurium: implications for thiamine synthesis. *J. Bacteriol.* **182**, 3896-3903
- 111 Skovran, E. and Downs, D. M. (2003) Lack of the ApbC or ApbE protein results in a defect in Fe-S cluster metabolism in *Salmonella enterica* serovar Typhimurium. *J. Bacteriol.* **185**, 98-106

- 112 Lewis, J. A. and Escalante-Semerena, J. C. (2006). The FAD-dependent tricarballylate dehydrogenase (TcuA) enzyme of *Salmonella enterica* converts tricarballylate into cis-aconitate. *J. Bacteriol.* **188**, 5479-5486
- 113 Lewis, J. A. and Escalante-Semerena, J. C. (2007) Tricarballylate catabolism in *Salmonella enterica*. The TcuB protein uses 4Fe-4S clusters and heme to transfer electrons from FADH<sub>2</sub> in the tricarballylate dehydrogenase (TcuA) enzyme to electron acceptors in the cell membrane. *Biochemistry* **46**, 9107-9115
- 114 Netz, D. J. A., Pierik, A. J., Stumpfig, M., Muhlenhoff, U., and Lill, R. (2007). The Cfd1-Nbp35 complex acts as a scaffold for iron-sulfur protein assembly in the yeast cytosol. *Nat. Chem. Biol.* **3**, 278-286
- 115 Roy, A., Solodovnikova, N., Nicholson, T., Antholine, W., and Walden, W. E. (2003). A novel eukaryotic factor for cytosolic Fe-S cluster assembly. *EMBO J.* **22**, 4826-4835
- 116 Boyd, J. M., Pierik, A. J., Netz, D. J. A., Lill, R., and Downs, D. M. (2008). Bacterial ApbC can bind and effectively transfer iron-sulfur clusters. *Biochemistry* **47**, 8195-8202
- 117 Boyd, J. M., Sondelski, J. L., and Downs, D. M. (2009). Bacterial Apbc protein has two biochemical activities that are required for in vivo function. *J. Biol. Chem.* **284**, 110-
- 118 Hendrickson, E. L. et al. (2004). Complete genome sequence of the genetically tractable hydrogenotrophic methanogen *Methanococcus maripaludis*. *J. Bacteriol.* **186**, 6956-6969
- 119 Stehling, O., Netz, D. J. A., Niggemeyer, B., Rosser, R., Eisentein, S., Puccio, H., Pierik, A. J., and Lill, R. (2008). Human Nbp35 is essential for both cytosolic iron-sulfur protein assembly and iron homeostasis. *Mol. Cell. Biol.* **28**, 5517-5528
- 120 Brereton, P. S., Verhagen, M. F. J. M., Zhou, Z. H., and Adams, M. W. W. (1998). Effect of the iron-sulfur cluster environment in modulating the thermodynamic properties and biological function of ferredoxin from *Pyrococcus furiosus*. *Biochemistry* **37**, 7351-7362
- 121 Eccleston, J.F., Petrovic, A., Davis, C.T., Rangachari, K., and Wilson, R.J. (2006). The kinetic mechanism of the SufC ATPase: the cleavage step is accelerated by SufB. *J. Biol. Chem.* **281**, 8371-8378

- 122 Tchong, S., Xu, H., and White, R.H. (2005). L-cysteine desulfidase: an [4Fe-4S] enzyme isolated from *Methanocaldococcus jannaschii* that catalyzes the breakdown of L-cysteine into pyruvate, ammonia, and sulfide. *Biochemistry* **44**, 1659-1670
- 123 Johnson, K.A. and Johnson, D.E. (1995). Methane emissions from cattle. *J. Anim. Sci.* **73**, 2483-2492
- 124 Beauchemin, K.A. and McGinn, S.M. (2006). Methane emissions from beef cattle: effects of fumaric acid, essential oil, and canola oil. *J. anim. Sci.* **84**, 1489-1496
- 125 Schloss, J.V., Porter, D.J.T., Bright, H.J., and Cleland, W.W. (1980). Nitro analogues of citrate and isocitrate as transition-state analogues for aconitase. *Biochemistry* **19**, 2358-2362

## **Vita**

Randy Michael Drevland was born May 17, 1981 in Staten Island, NY to Richard and Maria Drevland. Randy attended Marist College in Poughkeepsie, NY where he studied biology for two years before switching to a major in chemistry with a biochemistry option. He conducted undergraduate research under the supervision of Dr. Niel Fitzgerald, studying the bioremediation of polycyclic aromatic hydrocarbons from a contaminated environmental source. In May of 2004 Randy graduated cum laude from Marist College with a bachelors degree in chemistry. He enrolled in the University of Texas at Austin in August of 2004 to pursue a doctoral degree in biochemistry. In the Spring of 2005 Randy joined the research group of Dr. David Graham where he studied the enzymology of iron-sulfur cluster containing proteins from methanogenic archaea.

Permanent address: 11915 Stonehollow Dr. Apt 835, Austin, TX, 78758

This dissertation was typed by Randy Michael Drevland.